UNIVERSITY OF CAPE TOWN

MASTERS THESIS

Characterising the sources of fake leptons from top quarks in same sign W boson scattering with the ATLAS detector at $\sqrt{s} = 13$ TeV

Author:
Ms Xolisile THUSINI

Supervisor:
Dr Andrew HAMILTON
Dr Sahal YACOOB

A thesis submitted in fulfilment of the requirements for the degree of Masters of Science

in the

UCT-CERN ATLAS group
Department of Physics

August 23, 2017

Declaration

I, Ms Xolisile THUSINI, declare that this thesis titled, "Characterising the sources of fake leptons from top quarks in same sign W boson scattering with the ATLAS detector at $\sqrt{s} = 13$ TeV" and the work presented in it are my own. I confirm that:

- Where I have consulted the published work of others, this is always clearly attributed.
- Where I have quoted from the work of others, the source is always given. With the exception of such quotations, this thesis is entirely my own work.
- I have acknowledged all main sources of help.
- Where the thesis is based on work done by myself jointly with others, I have made clear exactly what was done by others and what I have contributed myself.

Signed: Signed by candidate

Xolisile Thusini, 21 August 2017

"All you are is a bag of particles acting out the laws of physics. "

Brian Greene

Abstract

University of Cape Town

Department of Physics

Masters of Science

Characterising the sources of fake leptons from top quarks in same sign W boson scattering with the ATLAS detector at $\sqrt{s} = 13$ TeV

by Ms Xolisile THUSINI

This thesis presents a study of $t\bar{t}$ events, which contribute to the same sign $W^{\pm}W^{\pm}jj$ production cross section in pp collisions with $\sqrt{s} = 13$ TeV data collected by the ATLAS detector. The thesis is aimed at probing jets that fake leptons in $t\bar{t}$ events, the so called non-prompt background, using Monte Carlo (MC) simulated samples. The $t\bar{t}$ leptonic/semileptonic decay channels, faking the two same sign lepton signal, are categorised using MC based classifier tools. Of the events that fake the signal, 75.40% is due to charge flip from electrons and 21.03% is due to non-prompt background. The kinematic distributions of these event classes are compared with the signal to look for regions where the non-prompt class is distinguishable. The sum of $t\bar{t}$ events tends to dominate the forward region of the ATLAS detector, $1.5 < |\eta| < 2.5$, while the signal events are more centralised. However, when comparing each $t\bar{t}$ event class with the signal, non-prompt background can not be easily discriminated because the statistics are low.

Acknowledgements

My sincere gratitudes goes to each individual who made a great contribution towards the completion of this thesis.

Thanks goes to my research supervisor Dr Sahal Yacoob, I am sincerely indebted for his patience, invaluable support and proficient guidance that he has shown throughout my research. For several times I felt like the amount of material (work) that I have grasped since I started my MSc was a bit lesser compared to the hours devoted to this work, but through his words of encouragement I have come to point of realisation that I have now acquired the values and the expertise through this MSc research.

I would like to extend my deepest gratitudes to my co-supervisor, Dr Andrew Hamilton for his guidance and remarkable criticism in the writing process of this thesis. I would also like to thank him for not only being an academic advisor but also for being a parent to me. He has made a great impact in my life here at UCT. His words of encouragement and support kept me going forward with an optimistic academic outlook.

This research would have not been a success without financial support. I would like to thank my previous institution, Stellenbosch University together with African Institute for Mathematical Sciences (AIMS); Nation Research Fund (NRF) and the UCT Department of Physics for funding my research. I wish to extend my appreciation to the Woman in Science program together with TATA Africa for awarding me a scholarship as well. Being selected amongst few South African students to attend CERN summer student program in Switzerland and School of Computing in Greece, were my highlights during this research. For that reason I am so grateful to SA-CERN program and the Department of Science and Technology (DST).

A special acknowledgement goes to my office mates, UCT-CERN ATLAS group, for their assistance, contributions and for being there for me as a family. I also thank them for taking their time to read through some of my thesis chapters and making valuable remarks. I am glad that at last everyone joined the "Nik Nacks" team, hope I will be remembered by this.

It has been a tough journey with the passing of my be loved father, Mr Jikizwe Thusini. Thanks to my strong and courageous mother, Mrs Rejoice F. Thusini for continuously supporting me. To my caring auntie, Mrs S'thembele N. Mpanza, and her family and my siblings, I appreciate their support. Last but not least, special words of thanks goes to Mr. Tlou L. Kubjana for being caring, supportive and for his willingness to help, "Kgotso e be le wena!".

Contents

List of Figures

List of Tables

List of Abbreviations

HEP	**H**igh **E**nergy **P**hysics
ssWW	**s**ame **s**ign $W^{\pm}W^{\pm}$
SM	**S**tandard **M**odel of particle physics
BSM	**B**eyond the **S**tandard **M**odel of particle physics
VBS	**V**ector **B**oson **S**cattering
EWSB	**E**lectro**W**eak **S**ymmetry **B**reaking
QCD	**Q**uantum **C**hromo**D**ynamics
QED	**Q**uantum **E**lectro**D**ynamics
CC	**C**harged **C**urrents
NC	**N**eutral **C**urrents
LHC	**L**arge **H**adron **C**ollider
CMS	**C**ompact **M**uon **S**olenoid
LHCb	**LHC**-**b**eauty
ALICE	**A** **L**arge **I**on **C**ollider **E**xperiment
PS	**P**roton **S**ynchrotron
SPS	**S**uper **P**roton **S**ynchrotron
ID	**I**nner **D**etector
SCT	**S**emi**C**onductor **T**racker
TRT	**T**ransition **R**adiation **T**racker
EM	**E**lectro**M**agnetic
LAr	**L**iquid **Ar**gon
MS	**M**uon **S**pectrometer
CSC	**C**athode **S**trip **C**hambers
MDT	**M**onitored **D**rift **T**ube chambers
TGC	**T**hin **G**ap **C**hambers
RPC	**R**esistive **P**late **C**hambers
SV	**S**econdary **V**ertex
DAQ	**D**ata **A**c**Q**uisition
MC	**M**onte **C**arlo
PDF	**P**robability **D**ensity **F**unction
SHERPA	**S**imulation of **H**igh-**E**nergy **R**eactions of **PA**rticles
LO	**L**eading **O**rder
NLO	**N**ext-to-**L**eading **O**rder
QGC	**Q**uartic **G**auge boson **C**ouplings
TGC	**T**riple **G**auge boson **C**ouplings
EWA	**E**ffective W boson **A**pproximation
SDOs	**S**imulated **D**ata **O**bject**s**
RODs	**R**ead**O**ut **D**rivers
MCP	**M**uon **C**ombined **P**erformance group

Le ncwadi inikezelwe kubaba, Jikizwe Thusini (1952-2016), ohambe engasakwazanga ukuthokoza nokubona intombi yakhe ithola iziqu. Ulale ngokuthula noxolo!

Chapter 1

Introduction

The Standard Model (SM) [1, 2, 3] of particle physics is the theory that describes the properties of fundamental particles and the forces of nature at the smallest scale. It further explains the existence of the electroweak force as a spontaneously broken gauge symmetry [4, 5], an important component in understanding the masses of particles and the behaviour of matter. To test these theoretical predictions, many experiments have been performed.

The SM theory has been repeatedly validated by discoveries and measurements from different particle colliders. The discoveries of the W and the Z bosons [6, 7] are part of the experimental measurements that validated the SM. The nature of SM electroweak symmetry breaking (EWSB) is explained theoretically by the Higgs mechanism, which will be discussed in Section 2.2, but the details of its measurements are still under investigation. These are some of the mysteries that have motivated scientists to build high-energy particle colliders such as Tevatron [8] , Super Proton Synchrotron (SPS) [9], and the Large Hadron Collider (LHC) [9], hoping to get a deeper understanding of nature. The LHC is the world's largest particle collider with four experiments instrumented around it.

The discovery of a spin-0 scalar particle [10, 11], which behaves like a SM Higgs boson, at the LHC has begun to shed some light on the SM picture of EWSB. Nonetheless, it is also possible that there are new particles that play a role in this mechanism. The effect of these particles may also be seen in the proton-proton (pp) collisions at the LHC through the scattering of two massive vector bosons. However, without the SM Higgs boson, the predicted probability for W bosons scattering will exceed unity at higher center-of-mass energies of about 1 TeV [12, 13, 14]. Consequently, by adding the SM Higgs boson, the cross-section of longitudinally polarized gauge boson scattering regain a reasonable behaviour at high experimental energies and the consistency of the SM is preserved. These theoretical implications of W boson scattering cross sections have motivated the search for same sign $W^{\pm}W^{\pm}$ (ssWW) scattering.

In a pp collision at the LHC, the vector boson scattering (VBS) process with W bosons can occur through non-resonance process $pp \rightarrow W^{\pm}W^{\mp}$, through resonance processes $pp \rightarrow Z/\gamma \rightarrow W^{\pm}W^{\mp}$, and through the production of Higgs boson resonance $pp \rightarrow H \rightarrow W^{\pm}W^{\mp}$. Each W boson can either decay

into a lepton and a neutrino ν, or to quarks. In the ssWW analysis, only leptonic decay was considered. Since neutrinos escape the detector without any interaction, this leads to the experimental signature of two leptons (namely electrons (e) or muons (μ)), two jets and missing transverse energy which is carried away by the neutrinos.

There are other non-VBS diagrams that can produce the same final state. These diagrams can either contain electroweak interactions only or both electroweak and strong interactions. In this document, these processes are referred to as the background processes. When looking at the two vector W bosons with the opposite electric charge, electroweak production is not easy to measure, since it has the total cross-section of 91.3 fb that is much smaller than the strong production total cross-section of 3030 fb [15] (although these cross section measurements were done using 8 TeV data, the conclusion still remain valid with 13 TeV data). However, for two W bosons with the same electric charge, the cross-sections for the two kinds of processes are comparable. Therefore, the experimental signature of two same-signed leptons (electrons or muons), missing-transverse energy (which will be explained in Chapter 3) [16], and two jets $l^{\pm}l^{\pm} + E_T^{miss} + jj$ is used because of its relatively low background from diboson production, $t\bar{t}$ and $Z + jets$, as opposed to opposite sign.

The $W^{\pm}W^{\pm} \rightarrow \ell^{\pm}\ell^{\pm} + E_T^{miss} + jj$ is a rare experimental signature with a small cross-section that has not yet been observed by ATLAS experiment, but previous ATLAS searches have found evidence for its existence to a significance of 4.5 σ [17]. These measurements were performed in Run 1 using proton-proton collision data with the center-of-mass energy of 8 TeV. Since the middle of 2015, the LHC began its Run 2 phase running in proton-proton collision mode at a center-of-mass energy of 13 TeV and luminosity of about 1x10^{34} cm^{-2}s^{-1} [18], exceeding the total Run 1 dataset. Due to the increased center-of-mass energy from 8 TeV to 13 TeV, ATLAS and CMS collected a high-statistics dataset providing an opportunity to search for rare SM processes such as the same sign $W^{\pm}W^{\pm}jj$ (ssWW) production. Recently, the CMS experiment has observed ssWW production at a significance of 5.5 σ in 13 TeV data [19]. These measurements exceeded their Run 1 results, which showed the evidence of ssWW production at 2.0 σ [20].

Even though increasing the energy of the collision give a rise to the sensitivity of W boson couplings, the number of background events that can mimic or interfere with the ssWW experimental signature will also increase. This includes W+jet, $t\bar{t}$ and single top where one or two jets fake leptons or are mis-reconstructed as leptons. It is very important to determine whether these types of fake backgrounds can be suppressed by imposing suitable acceptance cuts on signal events. The first step in looking for observables that show a discriminant between the signal and the backgrounds from which one can extract suitable background rejection cuts is to understand how these backgrounds look in the real pp collisions and how they decay.

This thesis focuses on probing jets that fake leptons (non-prompt leptons[1]) in the ssWW analysis by identifying sources of jet-faked leptons in $t\bar{t}$ Monte Carlo samples[2]. The $t\bar{t}$ sample was chosen since it contains a significant fraction of jets that are expected to fake the leptons. So it is assumed that this kind of background is mostly dominated by non-prompt leptons, and thus understanding of its behaviour would help in looking for optimal cuts for fake background rejection.

The remaining chapters are organized as follows: In Chapter 2 is the review of the Standard Model of particle physics and the cross-section calculation of ssWW production at the LHC. Chapter 3 describe the LHC, the layout of the ATLAS detector and its components, the object reconstruction algorithms and the selection of objects through detector readouts. The MC simulation methods that are used to produce samples that match ATLAS real dataset are given in Chapter 4. The topology of VBS and signal events selection are illustrated in Chapter 5. The procedures followed to characterise $t\bar{t}$ events, which contribute to the same sign $W^{\pm}W^{\pm}jj$ production cross-section, are detailed in Chapter 6. Results from characterisation are shown and discussed in Chapter 7, and conclusions are presented in Chapter 8.

[1] A non-prompt lepton originates from the hadronic jet decays.

[2] A simulation of proton-proton collisions at the LHC is important for high-energy physics research. In particle physics, Monte Carlo simulations are used to understand the expected background and signal processes, whether the signal measurements show new physics or evidence of the SM.

Chapter 2

Theoretical overview

What is the matter?

In the Standard Model (SM) of particle physics, properties of the fundamental constituents of matter are described along with their interactions governed by three fundamental forces of nature. Since 1970's, the SM has been repeatedly validated by the discovery of new particles as a result of an increase in experimental energies. The experimental discoveries involve the W and Z bosons (carriers of the weak force), the third generation of fermions and the Higgs boson (which explain how the mass of the W and Z bosons arises). The first section of this chapter is devoted to giving a brief review of the SM, a more general description can be found in reference [21].

This theory does an excellent job of describing the experimental observations, but it also leaves several pieces unsolved, such as a description of the matter and anti-matter asymmetry of the universe. According to the Big Bang theory [22], both the matter and antimatter should be produced in equal amount. Particle physicists have proposed some extensions of the SM that could explain some of these unsolved puzzles. For example, supersymmetry, string theory, and extra-dimensions [23].

2.1 The Standard Model of particle physics

According to the SM, the matter is made up of spin-half fermions, which come in three generations. The generations are arranged in the order of increasing mass. The first generation consists of the lightest and most stable particles whereas the second and third generations consist of heavier and less stable particles. Each generation is composed of two quarks, which experience both electroweak and strong interactions, and two leptons which experience only the electroweak interaction. Making up the proton are two up and one down quarks with an electric charge of $q = +\frac{2}{3}$ and $q = -\frac{1}{3}$, respectively, and an electron (together with its neutrino) with $q = -1(0)$. The particles of the SM are depicted in Figure 2.1.

In the SM, everyday forces are explained by gauge symmetries which predict the existence of massless mediator bosons with integer spin. Fermions

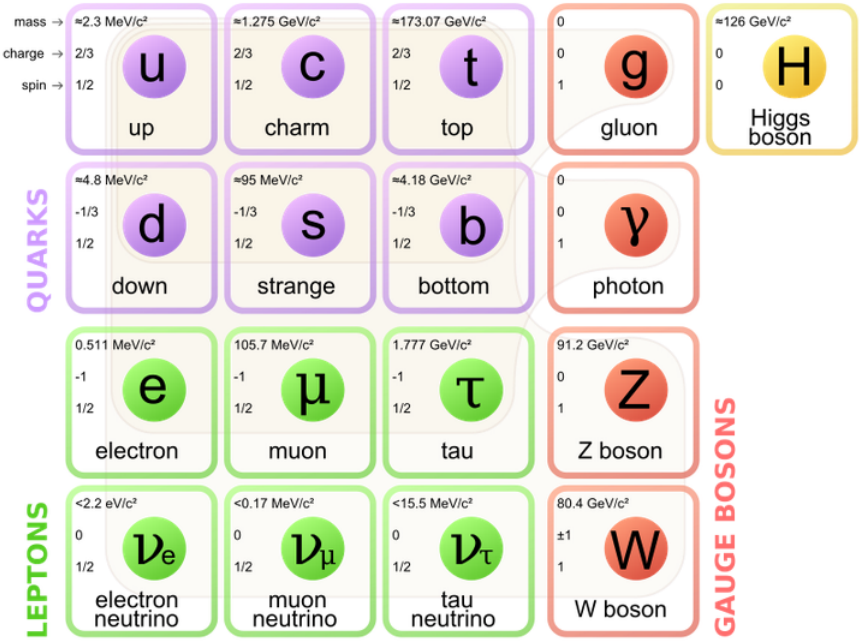

FIGURE 2.1: The standard model of particle physics [24].

communicate or interact through the exchange of bosons. The strong nuclear force is mediated by the gluon (g), which glues quarks together to form hadrons (such as protons and neutrons). This explains why the nucleus does not fall apart as protons remain positively charged and neutrons are neutral. The electromagnetic force is mediated by the photon (γ) and it explains how particles with the same electric charge repel each other. The third interaction, the weak nuclear force, is mediated by the neutral charged Z boson and the charged $W^{\pm}$ boson. The fourth force, gravity, is excluded in the SM because it is too weak to have an observable influence in elementary particles unless there is a black hole nearby.

Each of these forces has their own physics theory that is described by interactions:

Force	Mediator	Theory
Strong	Gluon (g)	Chromodynamics QCD
Electromagnatism	Photon (γ)	Electrodynamics QED
Weak	W and Z	Flavordynamics
Gravitational	Graviton	Geometrodynamics

QED is the theory that describes how the fermions interact through the exchange of a photon without changing any flavour[1] QCD explains how quarks bind together to form hadrons. The particle that changes the flavour in any interaction is the W boson, this is explained by the flavour dynamics theory. The fundamental processes are $e \longrightarrow e + \gamma$, $u \longrightarrow u + g$ and $d \longrightarrow u + W^{-}$ respectively.

[1] In particle physics, the term flavour is used to distinguish versions of fermions that belong to the same group. For instance, quarks come in six flavours: up, down, top, bottom, strange and charm.

In addition, there are other direct couplings of bosons to one another but for the purpose of this thesis, the focus remains the electroweak coupling of two W bosons that decay leptonically. The scattering amplitude of this coupling will be discussed later in this chapter.

In the plain gauge theory[2] the Z and the W bosons should be massless, but in fact, they have quite large masses which are approximately 100 times more than the mass of the proton. The effective mass of these particles is explained by a spontaneous breaking of electroweak gauge symmetry due to the presence of the Higgs field. This field was proposed as an explanation for how the W and the Z boson came to have mass [4, 5] and it was extended to all fields. All massive particles interact with the field directly. The extent to which particles interact with the field gives the indication of their masses. For instance, the top quark is the heaviest particle of the SM because it interacts with the field more strongly than any other particles. The particles interact with the Higgs field through the excitation of the Higgs boson. This is called Higgs mechanism, which will be detailed in Section 2.2.1.

2.2 Gauge structure and electroweak theory

The material in this section is extracted from Griffiths [25], Bettini [26] and Mann [27] books.

In the SM there is a symmetry group that represents each of the theories that were mentioned above: $SU(3) \otimes SU(2) \otimes U(1)$. The strong interaction is described by $SU(3)$. Quarks come in three different colours that transform as triplets under $SU(3)$. Electroweak interaction is described by $SU(2) \otimes U(1)$. The $W^{\pm}$ boson carries weakly charged currents (CC) and are represented by $SU(2)$ while $U(1)$ represents both the neutral currents (NC) mediated by the Z^0 boson for the weak sector and the photon for the electromagnetic sector.

The electroweak theory is asymmetric in the sense that the chiral left-handed and right-handed fermions behave differently in weak interactions. For an example, weakly charged interactions only act on left-handed particles[3] and the left-handed fermions transform as doublets under $SU(2)$, and all fermions carry hypercharge under $U(1)$. The relation between hypercharge(Y) and electric charge Q is given by

$$Y = Q - T^3, \tag{2.1}$$

where T^3 is the $SU(2)$ weak isospin of the particle, thus the left-handed fermions yields $\pm\frac{1}{2}$ and the right-handed fermions is 0.

[2]The plain gauge theory has no spontaneously broken symmetries, it is just the theory of quarks and colour octet gluons.

[3]A particle is left-handed if its spins in the opposite direction as its motion.

In 1960's, Glashow, Weinberg, Salam (GWS) developed a unified theory of weak and electromagnetic interaction - electroweak theory. In the SM Lagrangian the electroweak term, without the Higgs, is expressed as follows:

$$\mathcal{L} = \frac{g}{\sqrt{2}}\left(j_\mu W_\mu^+ + j_\mu W_\mu^-\right) + \frac{g}{\cos\theta_w}\left(j_\mu^3 - \sin^2\theta_w j_\mu^{EM}\right) Z_\mu + g\sin\theta_w j_\mu^{EM} A_\mu \quad (2.2)$$

The terms in the Equation Equation 2.2 represent weak CC, NC, and the electromagnetic interactions, respectively. However, equation requires the $W^\pm$ bosons, the Z boson and photon (γ) to be massless in order to allow for local gauge invariance. This results in a model with massless gauge bosons, which is inconsistent with the observations. Nonetheless, masses can be introduced using this Lagrangian method with the inclusion of the Higgs boson. This mechanism of introducing the Higgs must inviolate $U(1)$ symmetry describing the electromagnetic sector since the mass of the photon is zero in the SM. For a pedagogical introduction to electroweak unification see Bettini [26].

2.2.1 Electroweak symmetry breaking and the Higgs mechanism

The $SU(2) \otimes U(1)$ symmetry is spontaneously broken by the Higgs mechanism. In this mechanism, a complex scalar Higgs field with its associated Higgs particle is introduced. It has a hypercharge of $+\frac{1}{2}$ and transforms as a doublet under $SU(2)$. The Higgs field, (ϕ), interacts with the electroweak field through the exchange of the Higgs giving rise to the masses of the W and the Z bosons and leaving γ massless.

To illustrate the breaking of symmetry, a new Lagrangian is introduced:

$$\mathcal{L} = \Delta\mathcal{L}_{kinametic} - \Delta\mathcal{L}_{potential} \quad (2.3)$$

where

$$\Delta\mathcal{L}_{kinametic} = \frac{1}{2}(\partial_\mu\phi)^*(\partial^\mu\phi) \quad (2.4)$$

and

$$\Delta\mathcal{L}_{potential} = -\frac{1}{2}\mu^2(\phi^*\phi) + \frac{1}{4}\lambda^2(\phi^*\phi)^2 \quad (2.5)$$

Since ϕ is the scalar field, the system can be made gauge invariance under the transformation ($\phi \rightarrow e^{i\theta(x)}\phi$) by introducing a massless weak field A^μ and changing the partial derivatives to covariant derivative $\mathbf{D}_\mu = \partial_\mu + i\frac{q}{\hbar c}A_\mu$.

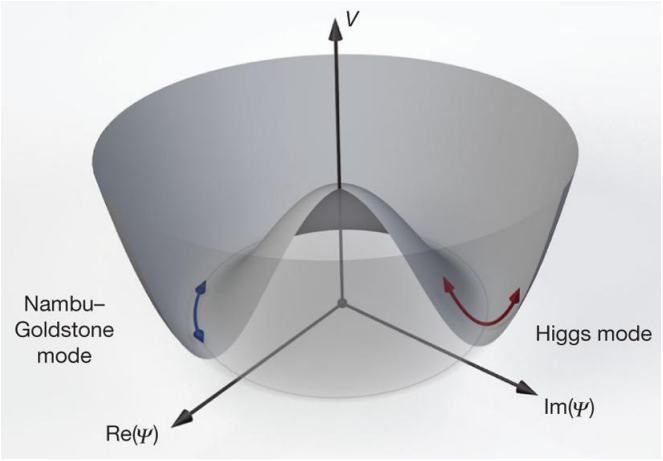

FIGURE 2.2: Higgs potential V as a function of two components, $Im(\phi_1)$ and $Re(\phi_2)$ [28].

Therefore Equation 2.3 becomes

$$\mathcal{L} = \frac{1}{2}\left[\left(\partial_\mu - \frac{iq}{\hbar c}A_\mu\right)\phi^*\right]\left[\left(\partial^\mu + \frac{iq}{\hbar c}A^\mu\right)\phi\right] - \left[-\frac{1}{2}\mu^2(\phi^*\phi) + \frac{1}{4}\lambda^2(\phi^*\phi)^2\right] - \frac{1}{16\pi}F^{\mu\nu}F_{\mu\nu}, \tag{2.6}$$

where $F^{\mu\nu}$ is the field strength tensor.

To demonstrate how the gauge bosons acquire mass, the Feynman calculus is deployed in which the field ϕ is treated as a fluctuation around two minimum energy points in the ground state (see Figure 2.2). Projecting from a higher energy state to a lower energy state, the field A^μ acquires mass. This is attained by taking the derivatives in the potential term, then solve for ϕ:

$$\phi_{1_{min}} = \pm\frac{\mu}{\lambda} \tag{2.7}$$

and

$$\phi_{2_{min}} = 0. \tag{2.8}$$

At these points the field is stable. This movement causes small perturbations around $\phi_{1_{min}}$ by a constant value of η - formation of a new field.

$$\eta_\pm = \phi_1 \pm \frac{\mu}{\lambda} \tag{2.9}$$

Substituting Equation 2.9 into Equation 2.6 results into:

$$\mathcal{L} = \left[\frac{1}{2}(\partial_\mu\eta)(\partial^\mu\eta) - \mu^2\eta^2\right] + \left[-\frac{1}{16\pi}F^{\mu\nu}F_{\mu\nu} + \frac{1}{2}\left(\frac{q}{\hbar c}\frac{\mu}{\lambda}\right)^2 A_\mu A^\mu\right] + \left[\frac{\mu}{\lambda}\left(\frac{q}{\hbar c}\right)^2\eta(A_\mu A^\mu) + \frac{1}{2}\left(\frac{q}{\hbar c}\right)^2(\eta^2)(A_\mu A^\mu) - \lambda\mu\eta^3 - \frac{1}{4}\lambda^2\eta^4\right] + \left(\frac{\mu^2}{2\lambda}\right)^2. \tag{2.10}$$

The massive scalar field, η, associated with a Higgs particle of mass of

$$m_h = \sqrt{2v^2\lambda}, \tag{2.11}$$

where $v = \sqrt{\frac{\mu^2}{\lambda}}$ and physical constant $\hbar = c = 1$, interact with the gauge field A^μ. Hence the mass of the weak mediator becomes:

$$m_A = 2\sqrt{\pi}\left(qv^2\right). \tag{2.12}$$

This is how the Higgs boson was predicted in 1964 [5]. In a search for the SM Higgs boson in 2012 at the LHC, a new particle with a mass of 125 GeV and properties consistent with the Higgs boson was observed by ATLAS and CMS collaborations [10, 11]. Equation 2.10 shows that the particle's mass is proportional to the coupling of the Higgs boson to SM particles. For a review of the Higgs mechanism see [29, 30]

2.2.2 Vector boson scattering amplitude

The Higgs boson plays a crucial role in vector boson scattering (VBS). The non-abelian structure of the $SU(2)$ gauge symmetry leads to self-interactions among the electroweak gauge bosons and allows them to scatter off each other. The scattering of massive gauge bosons is closely related to the electroweak symmetry breaking mechanism as the longitudinal polarization modes correspond to the Goldstone modes of the broken symmetry. In order to demonstrate this relation, the scattering amplitude for the process $W^\pm W^\pm \longrightarrow W^\pm W^\pm$ is discussed in the following.

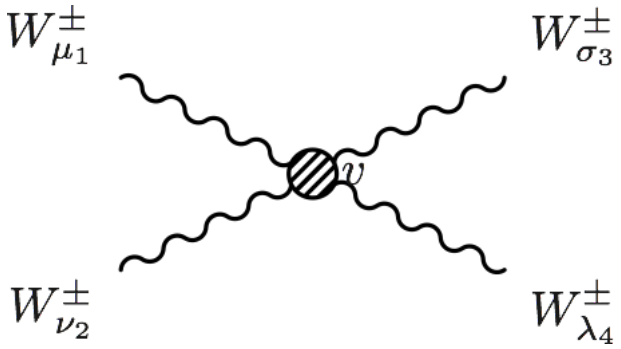

FIGURE 2.3: The diagram for $W^\pm W^\pm$ scattering [31]. The incoming fields are labelled as $W^\pm_{\mu_1}$ and $W^\pm_{\nu_2}$ with four-momenta μ_1 and ν_2 while the outgoing fileds are labelled as $W^\pm_{\sigma_3}$ and $W^\pm_{\lambda_4}$ with four-momenta σ_3 and λ_4.

The general diagram of the process is given in Figure 2.3 where vertex v is a joining point of four fields - incoming gauge bosons W_1 and W_2 and outgoing W_3 and W_4. It should be noted that inside v there will be various particles interacting with one another, such as quartic gauge boson, triple gauge boson

couplings and Higgs boson exchange. In Feynman calculus this is denoted by internal lines. The scattering amplitude can be generally parametrised as

$$i\mathcal{M} = i\epsilon_{\rho}^{\nu}(p_1)\epsilon_{\rho}^{\sigma}(p_3)\mathcal{M}_{\nu\mu\sigma\lambda}\epsilon_{\rho}^{\mu}(p_2)\epsilon_{\rho}^{\lambda}(p_4) \tag{2.13}$$

where ϵ_ρ is the polarization vector for the external gauge boson, with $\rho = \pm$ or 0 for transverse or longitudinal polarization mode. Each ϵ_ρ has a corresponding momentum p [32].

In the center-of-mass frame, the four-momenta of the incoming and outgoing fields are given as:

$$p_1^{\mu} = (E, 0, 0, p) \tag{2.14}$$

$$p_2^{\nu} = (E, 0, 0, -p) \tag{2.15}$$

$$p_3^{\sigma} = (E, 0, p\sin\theta, p\cos\theta) \tag{2.16}$$

$$p_4^{\lambda} = (E, 0, -p\sin\theta, -p\cos\theta) \tag{2.17}$$

and longitudinally polarized vectors becomes:

$$\epsilon_0^{\nu} = \begin{pmatrix} \frac{p}{m_w} \\ 0 \\ 0 \\ \frac{E}{m_w} \end{pmatrix}, \epsilon_0^{\mu} = \begin{pmatrix} \frac{p}{m_w} \\ 0 \\ 0 \\ -\frac{E}{m_w} \end{pmatrix}, \epsilon_0^{\sigma} = \begin{pmatrix} \frac{p}{m_w} \\ 0 \\ \frac{E}{m_w}\sin\theta \\ \frac{E}{m_w}\cos\theta \end{pmatrix}, \epsilon_0^{\lambda} = \begin{pmatrix} \frac{p}{m_w} \\ 0 \\ -\frac{E}{m_w}\sin\theta \\ -\frac{E}{m_w}\cos\theta \end{pmatrix} \tag{2.18}$$

where θ is the scattering angle and m_w is the mass of the scattered particle.

Given these parametrisation matrices together with matrix elements from Feynman rules (in table 2.1) for GWS, one can calculate the scattering amplitude for W bosons coupling.

There are several ways of drawing Feynman diagrams that contribute to the process $W^{\pm}W^{\pm} \to W^{\pm}W^{\pm}$. In this thesis, the Higgs exchange diagrams of the $W^{\pm}W^{\pm} \to W^{\pm}W^{\pm}$ process do not include the $s-$channel since the charge is not conserved. Hence, the total scattering amplitude in Equation 2.13 will be the sum of all individual contributions shown in Figure 2.4.

$$i\mathcal{M} = i\left(\sum \mathcal{M}\right) \tag{2.19}$$

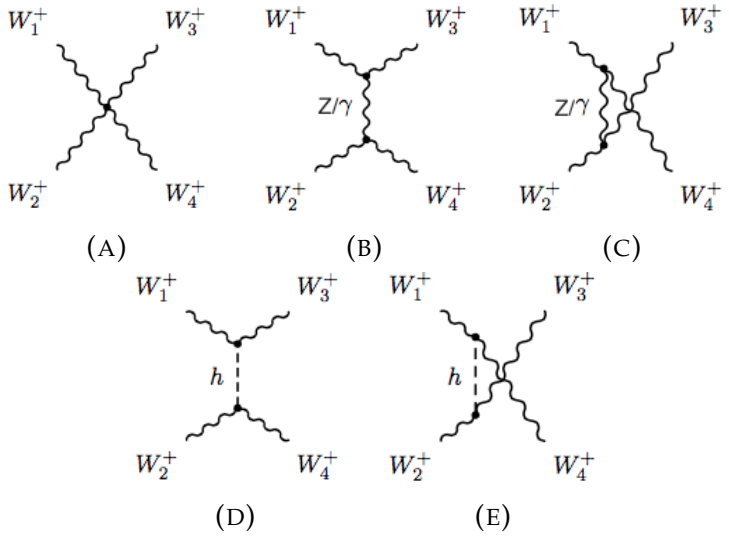

FIGURE 2.4: Leading order diagrams for $W^{\pm}W^{\pm}$ scattering: (a) quartic gauge bosons couplings QGC, (b and c) triple gauge boson couplings TGC in the $t-$ channel and $u-$ channel, and Higgs boson exchange in the $t-$ channel (d) and $u-$ channel (e)

The amplitude for each of these diagrams can be expressed as follows [32]:

$$\begin{aligned} i\mathcal{M}_{TGC}^{\text{t-channel}} = i\epsilon^{\mu}(p_1)\epsilon^{\sigma}(p_3)\,&[g_{\mu\sigma}(p_1-p_3)_{\tau} - g_{\mu\tau}(q+p_1)_{\sigma} + g_{\tau\sigma}(q+p_3)_{\mu}] \\ &\times [g_{\nu\lambda}(p_2-p_4)_{\tau} - g_{\nu\tau}(q+p_2)_{\lambda} + g_{\tau\lambda}(q+p_4)_{\nu}] \\ &\times \left[\frac{g_w^2\cos^2\theta_w g_{\tau}}{t-m_z^2} + \frac{g_w^2\sin^2\theta_w g_{\tau}}{t}\right]\epsilon^{\nu}(p_2)\epsilon^{\lambda}(p_4) \end{aligned} \tag{2.20}$$

$$\begin{aligned} i\mathcal{M}_{TGC}^{\text{u-channel}} = i\epsilon^{\mu}(p_1)\epsilon^{\sigma}(p_4)\,&[g_{\mu\sigma}(p_1-p_4)_{\tau} - g_{\mu\tau}(q+p_1)_{\sigma} + g_{\tau\sigma}(q+p_4)_{\mu}] \\ &\times [g_{\nu\lambda}(p_2-p_3)_{\tau} - g_{\nu\tau}(q+p_2)_{\lambda} + g_{\tau\lambda}(q+p_3)_{\nu}] \\ &\times \left[\frac{g_w^2\cos^2\theta_w g_{\tau}}{u-m_z^2} + \frac{g_w^2\sin^2\theta_w g_{\tau}}{u}\right]\epsilon^{\nu}(p_2)\epsilon^{\lambda}(p_3) \end{aligned} \tag{2.21}$$

$$i\mathcal{M}_{QGC} = ig_w^2\epsilon^{\mu}(p_1)\epsilon^{\sigma}(p_3)(2g_{\mu\lambda}g_{\nu\sigma} - g_{\mu\nu}g_{\lambda\sigma} - g_{\mu\sigma}g_{\nu\lambda})\epsilon^{\nu}(p_2)\epsilon^{\lambda}(p_4) \tag{2.22}$$

$$i\mathcal{M}_{Higgs}^{\text{t-channel}} = -ig_w^2 m_w^2\epsilon^{\mu}(p_1)\epsilon^{\sigma}(p_3)\frac{g_{\mu\sigma}g_{\nu\lambda}}{t-m_H^2}\epsilon^{\nu}(p_2)\epsilon^{\lambda}(p_4) \tag{2.23}$$

$$i\mathcal{M}_{Higgs}^{\text{u-channel}} = -ig_w^2 m_w^2\epsilon^{\mu}(p_1)\epsilon^{\sigma}(p_4)\frac{g_{\mu\sigma}g_{\nu\lambda}}{u-m_H^2}\epsilon^{\nu}(p_2)\epsilon^{\lambda}(p_3) \tag{2.24}$$

Substituting the form of the longitudinal polarization vector into each of the above equations and using the Mandelstam variables[4] for a $2 \to 2$ process with particles of equal masses, the amplitudes becomes

[4]the center-of-mass energy squared $s = (p_1+p_2)^2 = (p_3+p_4)^2$, $t = (p_1-p_3)^2 = (p_2-p_4)^2$ and $u = (p_1-p_4)^2 = (p_2-p_3)^2$

$$
\begin{aligned}
i\mathcal{M}_{TGC} &= i\mathcal{M}_{TGC}^{\text{t-channel}} + i\mathcal{M}_{TGC}^{\text{u-channel}} \\
&= -\frac{g^2}{4}\left[-\frac{s^2}{m_w^4} + \frac{2t^2}{m_w^4} + \frac{2st}{m_w^4} + \frac{3s}{m_w^2} + \frac{16t^2}{m_w^2 s} + \frac{8t}{m_w^2} + \frac{32t}{s} + \frac{96t^2}{s^2}\right] \\
&- \frac{g^2}{4}\left[+4\sin^2\theta_w\left(\frac{s-u}{t} + \frac{s-t}{u}\right) + \frac{(1-2\sin\theta_w)^2}{1-\sin\theta_w}\left(\frac{s-u}{t-m_z^2} + \frac{s-t}{u-m_z^2}\right)\right] \\
&- g^2
\end{aligned}
\tag{2.25}
$$

and

$$
i\mathcal{M}_{QGC} = -\frac{g^2}{4}\left[\frac{s^2}{m_w^4} - \frac{2t^2}{m_w^4} - \frac{2st}{m_w^4} - \frac{4s}{m_w^2} - \frac{16t^2}{m_w^2 s} - \frac{8t}{m_w^2} - \frac{32t}{s} - \frac{96t^2}{s^2}\right]. \tag{2.26}
$$

Summing over the gauge amplitudes ensures the cancellation of the order $\frac{s^2}{m_w^4}$ terms of the quartic gauge bosons couplings and the triple gauge boson couplings:

$$
\begin{aligned}
i\mathcal{M}_{Guage} &= i\mathcal{M}_{QGC} + i\mathcal{M}_{TGC} \\
&= -\frac{g^2}{4}\left[-\frac{s}{m_w^2}\right] \\
&- \frac{g^2}{4}\left[+4\sin^2\theta_w\left(\frac{s-u}{t} + \frac{s-t}{u}\right) + \frac{(1-2\sin\theta_w)^2}{1-\sin\theta_w}\left(\frac{s-u}{t-m_z^2} + \frac{s-t}{u-m_z^2}\right)\right] \\
&- g^2.
\end{aligned}
\tag{2.27}
$$

For a fixed non-zero scattering angle θ_w, the second term in the gauge amplitude inside the square brackets is negligible. Setting aside the Z/γ exchange contribution, which is not important for checking the high-energy behavior in the limit of $s >> m_w^2$. Then the amplitude reduces to the Goldstone boson scattering:

$$
i\mathcal{M}_{Guage} \simeq \frac{g^2}{4}\left[\frac{s}{m_w^2} - constant\right]. \tag{2.28}
$$

In the absence of the Higgs Feynman diagrams, the scattering amplitude $\mathcal{M}$ will increase as a function of s. Therefore the predicted probability for VBS in proton-proton collisions will exceed unity at about 1 TeV. This is one of the reasons why the Higgs boson is important in the SM and moreover, the reason why scientist knew that they would discover new physics at the LHC with energy higher than 1 TeV.

The scattering amplitude for a Higgs exchange after adding the longitudinal polarization vector is

$$\begin{aligned} i\mathcal{M}_{Higgs} &= i\mathcal{M}_{Higgs}^{\text{t-channel}} + i\mathcal{M}_{Higgs}^{\text{u-channel}} \\ &= \frac{g^2}{4}\left[-\frac{s}{m_w^2} + 4 + \left(\frac{m_H^2}{m_w^2} + 4 + \frac{4m_w^2}{m_H^2} + \frac{8m_H^2}{s}\right)\left(\frac{m_H^2}{t-m_H^2} + \frac{m_H^2}{u-m_H^2}\right)\right] \\ &+ \frac{g^2}{4}\left[\frac{2m_H^2}{m_W^2} + \frac{16m_H^2}{s}\right]. \end{aligned} \tag{2.29}$$

Adding the Higgs terms to the scattering amplitude of the gauge bosons; the $s-$ dependent term from Higgs diagram is cancelled by other electroweak s contributions in Equation 2.27. Therefore, the total scattering amplitude for $W^{\pm}W^{\pm} \to W^{\pm}W^{\pm}$ becomes

$$\begin{aligned} i\mathcal{M} &= i\mathcal{M}_{Gauge} + i\mathcal{M}_{Higgs} \\ &= \frac{g^2}{4}\left[\frac{m_H^2}{m_w^2}\left(\frac{t}{t-m_H^2} + \frac{u}{u-m_H^2}\right)\right] \\ &+ \frac{g^2}{4}\left[4\left(1 + \frac{m_w^2}{m_H^2} + \frac{2m_H^2}{s}\right)\left(\frac{m_H^2}{t-m_H^2} + \frac{m_H^2}{u-m_H^2}\right) + \frac{16m_H^2}{s}\right]. \end{aligned} \tag{2.30}$$

This equation shows that $\mathcal{M}$, for each diagram, increases with the opposite sign as s increases leading to a combined scattering amplitude, which asymptotes to a constant. In other words, unity is preserved [12, 13, 14].

TABLE 2.1: The matrix elements for the gauge and Higgs interactions in W bosons scattering

Diagram	Vertex	Matrix element
b	$2(WZ_\tau/\gamma_\tau(q)W)$(t-channel)	$i\left[g_{\mu\sigma}(p_1-p_3)_\tau - g_{\mu\tau}(q+p_1)_\sigma + g_{\tau\sigma}(q+p_3)_\mu\right]$ $\times\left[g_{\nu\lambda}(p_2-p_4)_\tau - g_{\nu\tau}(q+p_2)_\lambda + g_{\tau\lambda}(q+p_4)_\nu\right]$ $\times\left[\frac{g_w^2\cos^2\theta_w g_\tau}{q^2-m_z^2} + \frac{g_w^2\sin^2\theta_w g_\tau}{q^2}\right]$
c	$2(WZ_\tau/\gamma_\tau(q)W)$(u-channel)	$i\left[g_{\mu\sigma}(p_1-p_4)_\tau - g_{\mu\tau}(q+p_1)_\sigma + g_{\tau\sigma}(q+p_4)_\mu\right]$ $\times\left[g_{\nu\lambda}(p_2-p_3)_\tau - g_{\nu\tau}(q+p_2)_\lambda + g_{\tau\lambda}(q+p_3)_\nu\right]$ $\times\left[\frac{g_w^2\cos^2\theta_w g_\tau}{q^2-m_z^2} + \frac{g_w^2\sin^2\theta_w g_\tau}{q^2}\right]$
a	$WWWW$	$ig_w^2(2g_{\mu\lambda}g_{\nu\sigma} - g_{\mu\nu}g_{\lambda\sigma} - g_{\mu\sigma}g_{\nu\lambda})$
d and e	$2(WhW)$(t,u-channel)	$-ig_w^2 m_w^2 \frac{g_{\mu\sigma}g_{\nu\lambda}}{q^2-m_H^2}$

2.3 $W^{\pm}W^{\pm}$ production at the LHC

In the ssWW analysis, the production of the $W^{\pm}W^{\pm}$ process at the LHC has been chosen to study electroweak symmetry breaking. The SM description of this process is validated by comparing theoretical predictions from Monte Carlo calculations to the observed number of events passing some specific selection criteria. The expected/predicted number of events is parametrised as:

$$N = \int \mathcal{L}dt \cdot \sigma \cdot A \cdot \epsilon, \tag{2.31}$$

where $\mathcal{L}$ denotes the instantaneous luminosity, defined as the number of particles that could interact per second. σ denotes the cross-section, which is the probability for the $W^{\pm}W^{\pm}$ process to occur in a pp collision. ϵ is the efficiency of a detector to reconstruct $W^{\pm}W^{\pm}$ events that pass within the detector acceptance A, which is the fraction of phase space that is visible to the detector. The product of $\sigma \cdot A$ gives a fiducial cross section, which is a rate to produce events in the fiducial region. In the ssWW analysis, the word fiducial region is used to refer to the phase space of all the final state particles that pass the selection criteria. In $W^{\pm}W^{\pm}$ events, the fiducial region includes the final state particles that come from both the QCD and electroweak mediated diagrams. Efficiency is deduced from the simulation of the interaction of final state particles with the detector. The fiducial cross section of $W^{\pm}W^{\pm}$ production is evaluated theoretically.

Given two initial partons[5], the cross section for $W^{\pm}W^{\pm}$ production in the center of mass frame can be written as:

$$\sigma = \frac{1}{2\sqrt{s}^2} \int \left(\prod_f \frac{d^3p_f}{(2\pi)^3} \frac{1}{2E_f} \right) |\mathcal{M}|^2 (2\pi)^4 \delta^4 \left(\sum p_f \right), \tag{2.32}$$

where $\sqrt{s}$ is the center-of-mass energy of the collision, E_f and p_f are the energy and momenta of the initial state partons and $|\mathcal{M}|^2$ is the scattering amplitude for $W^{\pm}W^{\pm}$. The information about the interaction is contained in the matrix-element $\mathcal{M}$.

The above cross section represent the interaction of two initial state partons. However, at the LHC particles being collided are protons composed of the mixture of quarks and gluons. Transforming Equation 2.32 into a cross section for pp initial state is done using parton distribution functions (PDF) [33, 34, 35]. PDFs are theoretical methods used to calculate the probability of finding a parton of a particular flavour with a certain fraction of the proton's momentum. They depend on the energy of each incoming proton beam, E_{beam}. The total collision energy is then given by $Q = (x_1 + x_2)E_{beam}$, where x_1 and x_2 are the fraction of the proton's momentum carried by each incoming parton

[5] Partons refer to constituents of a hadron

i_1, i_2 respectively. Thus the cross section in Equation 2.32 becomes

$$\sigma = \sigma_{x_1 x_2}(Q). \tag{2.33}$$

In order to translate this expression into a cross section for pp collision at $\sqrt{s}$, the cross section must be weighted by proton PDFs.

$$P_{x_1 x_2} = f_{x_1}(x_1, Q^2) f_{x_2}(x_2, Q^2). \tag{2.34}$$

This is the probability to find partons i_1 and i_2 in a given pp collision carrying proton's momentum fraction of i_1 and i_2. From PDFs the final cross section for pp collisions is:

$$\sigma_{pp} = \sum_{i_1 i_2} \int \int dx_1 dx_2 P_{x_1 x_2} \sigma_{x_1 x_2}(Q). \tag{2.35}$$

The production of two same charge W bosons requires two initial state quarks with the same electric charge. In case the initial state particle is a gluon(s), the LO production of two same sign W bosons does not occur.

2.4 Top quark production

The heaviest particle within the SM is the top quark, which has a mass of 173.21 ± 0.51 GeV [36] and it is produced mainly via the strong interactions. The $t\bar{t}$ (top-antitop) events are produced via gluon fusion (gg) and $q\bar{q}$ annihilation, illustrated in Figure 2.5 and Figure 2.6, respectively. The cross section for gg and $q\bar{q}$ interactions is the same. Hence, as shown in Figure 2.7, at 13 TeV the parton luminosity at the LHC is mostly gluons. Thus, increasing the center of mass energy and assuming that the sum of the proton's momentum carried by each gluon ($x_1 + x_2$) is greater than $\frac{2m^{top}}{6.5\text{ TeV}}$, that is

$$x_1 + x_2 > \frac{2m^{top}}{6.5\text{GeV}} = \frac{2(173.21\text{ GeV})}{6.5\text{ TeV}} = 0.0533, \tag{2.36}$$

where m^{top} is the pole mass production for a top quark, the contribution of gluon fusion in pp collision increases. This implies that at very high center of mass energies of the LHC, the most dominant process for $t\bar{t}$ production is the gluon fusion [37].

2.6.

The top quark has a very short life time ($\approx 10^{-24} s$ [36]) which leads it to hadronising before it decay [39]. From the CKM quark-mixing matrix [40, 41, 42] the top quark decay predominantly into a W boson and a b quark. The branching fraction of this dominant decay is $BF = \Gamma(t \to Wb)/(t \to Wq(q = b, s, d)) = 0.91 \pm 0.04$ [36]. The other top quark decay modes predicted by the SM are $\Gamma(t \to \gamma q(q = u, c))/\Gamma(t \to Wb) < 0.0059$ and $\Gamma(t \to Zq(q = u, c))/\Gamma(t \to Wb) < 0.0021$ (also from Ref. [36]). Hence the final state of $t\bar{t}$

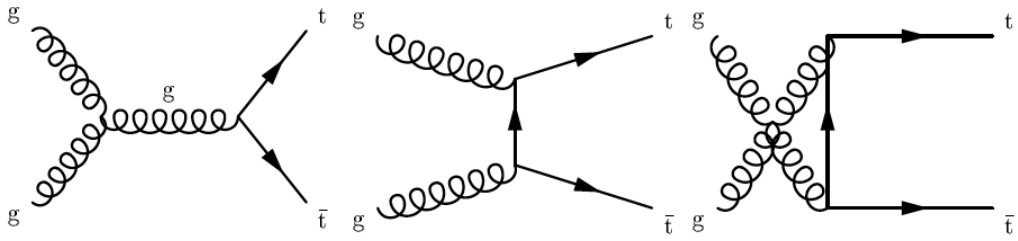

FIGURE 2.5: Feynman diagrams showing gluon fusion in $t\bar{t}$ production.

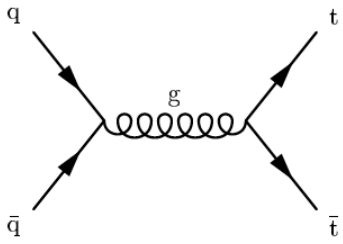

FIGURE 2.6: Feynman diagram showing $q\bar{q}$ annihilation in $t\bar{t}$ production.

events depends on the decay of the W boson. A $t\bar{t}$ event has three different decay modes:

- **Leptonic decay**: $t\bar{t} \rightarrow W^+bW^-\bar{b} \rightarrow \ell^+\nu\ell^-\bar{\nu}b\bar{b}$
  Each W boson decay into a charged lepton with its corresponding neutrino. As a results the final state signature comprises of two charged leptons, two jets originating from the hadronisation of two b quarks and a missing transverse energy arising from two neutrinos which can not be detected or seen within the detector: $\ell^+\ell^- + E_T^{miss} + jj$.
- **Semileptonic decay**: $t\bar{t} \rightarrow W^+bW^-\bar{b} \rightarrow \ell^\pm\nu q\bar{q}'b\bar{b}$
  One W boson decay into a charged (positive/negative) lepton with its corresponding neutrino while the other decays into a quark-antiquark ($q\bar{q}'$) pair. Thus, the final state signature contain one charged lepton, four jets (two from b quarks hadronisation and two from $q\bar{q}'$ pair) and a missing transverse energy: $\ell^\pm + E_T^{miss} + 4j$.
- **Fully hadronic decay**: $t\bar{t} \rightarrow W^+W^-b\bar{b} \rightarrow q\bar{q}'q\bar{q}'b\bar{b}$
  Both W bosons decay into a quark-antiquark pair. The final state of these events contain atleast six jets with a high transverse jet-momentum $p_{T,jet}$ [43].

Only the first two decay modes are considered in this dissertation. These are the most frequent $t\bar{t}$ event topologies in the same sign $W^\pm W^\pm \rightarrow \ell^\pm\ell^\pm + E_T^{miss} + jj$ events. In the topology of leptonic $t\bar{t}$ events, $\ell^+\ell^- + E_T^{miss} + jj$, one lepton can undergo charge misidentification during reconstruction resulting in an event with two same charge leptons in the final state. In the topology of semileptonic $t\bar{t}$ events, $\ell^\pm + E_T^{miss} + 4j$, one of the jets can fake a lepton or

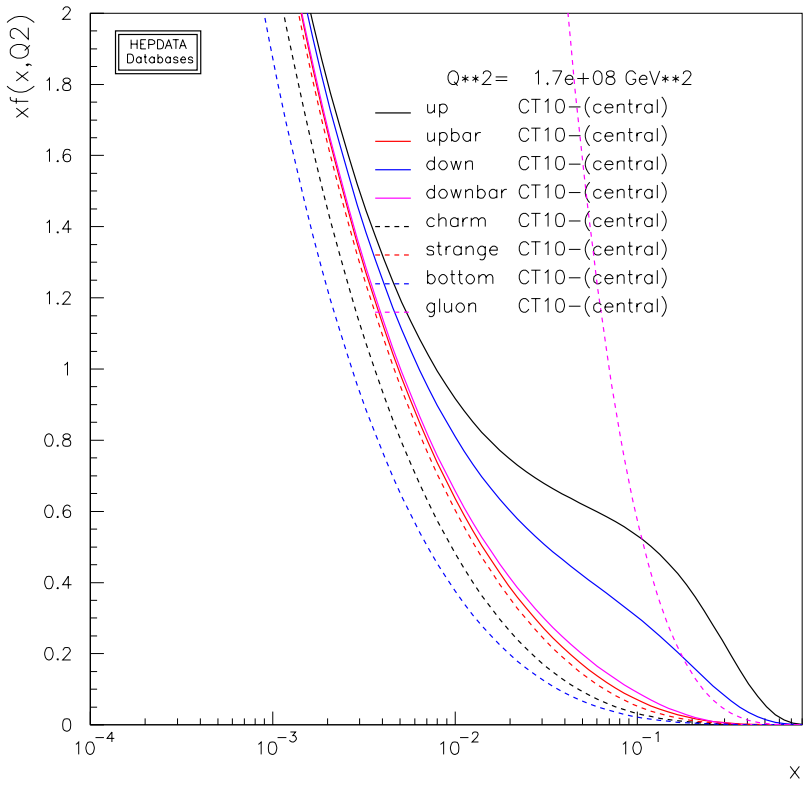

FIGURE 2.7: CT10 parton distribution functions for $Q^2 = 169 \times 10^8$ GeV^2 [38].

decay into a lepton with the same charge as the prompt lepton from W boson decay.

Chapter 3

The ATLAS Detector at the LHC

The Large Hadron Collider (LHC) [9] is the hadron accelerator machine located at the European Center for Nuclear Research (CERN) in Geneva, Switzerland. ATLAS [44] is one of the four detectors installed around the LHC ring. The ATLAS collaboration is comprised of about 3000 members conducting research in the field of high-energy particle physics. This chapter gives a description of the accelerator, detector and experimental techniques that are being used at the LHC to study high luminosity proton-proton collisions.

3.1 The Large Hadron Collider

The LHC is the world's largest particle accelerator with a circumference of 26.7 km, located on the border of France and Switzerland near Geneva. It was built to examine the smallest building blocks of the matter by colliding protons. The two all-purpose detectors are the ATLAS [44] and CMS [45] experiments, which are used to study a wide range of physics processes. In 2012, both discovered the Higgs boson. The other two experiments are the LHCb [46], which is designed to detect B-hadrons, and ALICE [47], which is designed to study strongly interacting matter in heavy ion collisions.

The final energy of a single beam in the LHC ring is attained by first accelerating ionized protons into four different stages [9], all performing different processes and feeding each other before reaching the LHC. They are the LINAC2, the Proton Synchrotron (PS) Booster, the Proton Synchrotron (PS) and the Super Proton Synchrotron (SPS). This arrangement is depicted in Figure 3.1.

At the very beginning of the accelerating process, there is a source chamber of hydrogen atoms. From the hydrogen atoms, electrons are stripped off, leaving behind positively ionized protons, which are hadrons. These protons are accelerated by LINAC 2 to an energy of 50 MeV traveling at approximately one-third of the speed of light (c). From the LINAC 2, they are then injected into a PS Booster, which is 127 m in circumference. In order to increase the intensity, the beam of protons is divided into four vertically stacked rings with the circumference of 157 m, which further accelerates the protons to 1.4 GeV.

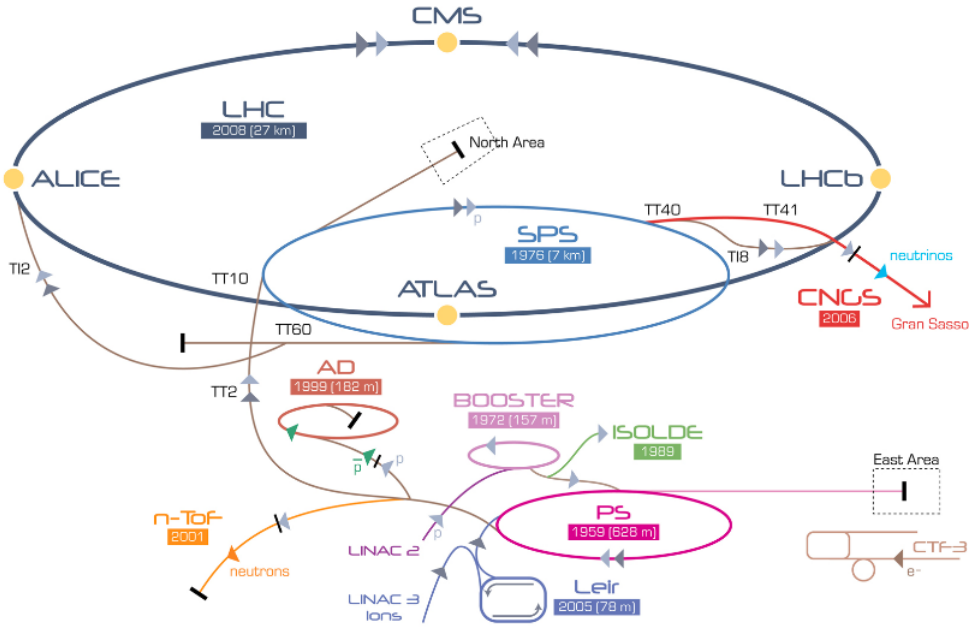

FIGURE 3.1: Schematic overview of the particle accelerator complex at CERN [9].

Thereafter, the protons recombine and enter into the PS, which is 628 m in circumference, where they accelerate up to 25 GeV for 1.2 seconds reaching a velocity of 0.999 times the speed of light. To further the process, they are then injected into the SPS which increases the 25 GeV beam up to an energy of 450 GeV. Finally, the protons are injected into the LHC where they are accelerated to a final energy of about 6.5 TeV, corresponding to a center-of-mass energy of $\sqrt{s} = 13$ TeV, before the collision. The beam entering the LHC is partitioned into bunches, each of which contains approximately 115 billion protons. These bunches are separated by 25 ns.

Beams of protons are brought into collision at the interaction/collision points within the experiments, providing a luminosity of about 10^{34} cm^{-2} s^{-1}. Once most of the beam has been lost due to the collisions, the remaining beam is dumped and a new beam is injected. This process happens after every $10-20$ hours.

Since the ATLAS experiment dataset is used to do the study on ssWW production cross-section, only the layout of the ATLAS detector hardware is described and illustrated in the following section. For more detailed explanation on the detector hardware, see ATLAS collaboration paper [44].

3.2 The ATLAS Detector

The ATLAS detector, shown in Figure 3.2, is a general-purpose particle detector, having a diameter of 25 m and length of 44 m. It was particularly

designed to investigate a wide range of particle physics phenomena originating from proton-proton collisions. It is made up of a cylindrical barrel region with end-cap disks on both sides. Both the barrel and the end-cap are comprised of many sub-detectors that are classified into three categories:

1. An inner tracking detector (ID), closest to the point of collision, measures the momentum of charged particles by measuring the curvature of their tracks.
2. The calorimeters, responsible for measuring the energy of particles such as electrons, photons, and hadrons. Muons do also deposit little energy in the calorimeters. Calorimeters stop the particles and absorb their energies. The energy of electrons and photons are measured in the electromagnetic calorimeter (EM) while the hadronic calorimeter measures the energy of hadrons.
3. The muon spectrometer (MS) is the outermost sub-detector that measures the momenta of muon objects. It has toroidal coils that produce a strong magnetic field, which bends charged objects for momentum measurements.

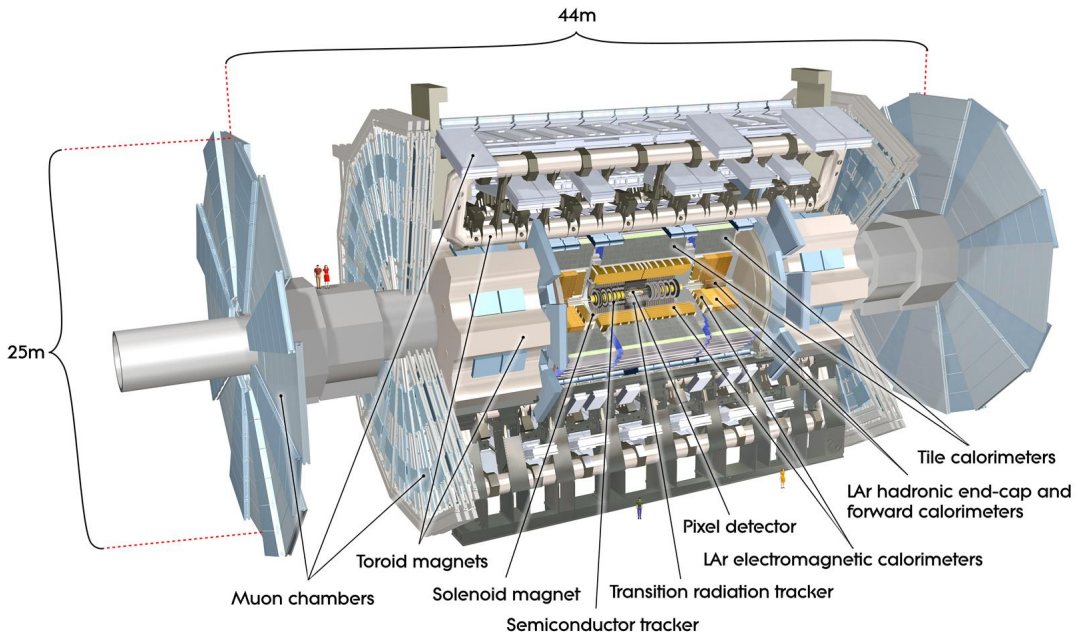

FIGURE 3.2: Layout of the ATLAS detector [44].

3.2.1 The coordinate system of ATLAS

The protons collide at the center of the detector which is the origin of the ATLAS coordinate system, see Figure 3.3. The $y-$axis points upward perpendicular to the beam axis, while the $x-$axis points toward the center of the

LHC ring and the $z-$axis is parallel to the beam axis. The azimuthal angle,

$$\phi = \arctan \frac{y}{x}, \tag{3.1}$$

is measured in the xy-plane which is transverse to the beam axis and the polar angle (θ) is measured from the beam axis in yz-plane. It is also possible for interactions to happen inside the detector (along the beam pipe) but not at the interaction point. The rapidity (y) is often used as opposed to polar angle. The rapidity is given as:

$$y = \frac{1}{2} \ln \frac{E + p_z}{E - p_z}, \tag{3.2}$$

where E and p_z define the energy and momentum of the particle along the $z-$axis, respectively.

At the hadron colliders, scientist deal with very energetic products of the collisions, in the highly relativistic regime. Highly relativistic particles are boost invariant but y is not. Hence, the rapidity reduces to the pseudo-rapidity (η) given by

$$\eta = -\ln \left(\tan \frac{\theta}{2} \right). \tag{3.3}$$

, which is Lorenz invariant. The distance between two particles is then defined as:

$$\Delta R = \sqrt{(\Delta\eta)^2 + (\Delta\phi)^2}. \tag{3.4}$$

These variables help in determining the exact location of particles within the

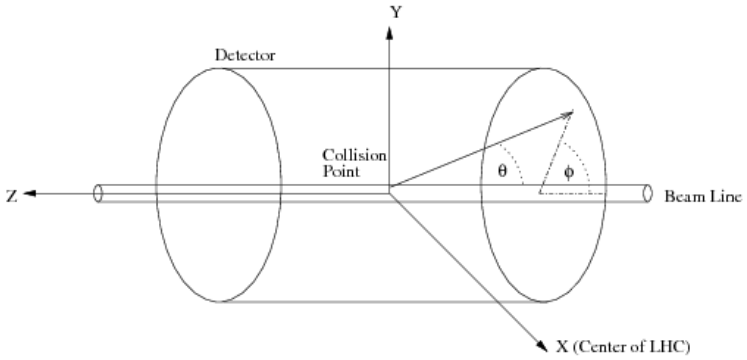

FIGURE 3.3: ATLAS detector coordinates system in 3-D view [48].

detector at a particular point in $\eta - \phi$ space.

3.2.2 Inner Detector

The ID has a radius of 1.05 m and a length 6.2 m. It is made up of three independent sub-detector systems: the pixel detector, the semiconductor tracker (SCT) and the transition radiation tracker (TRT). When a charged particle

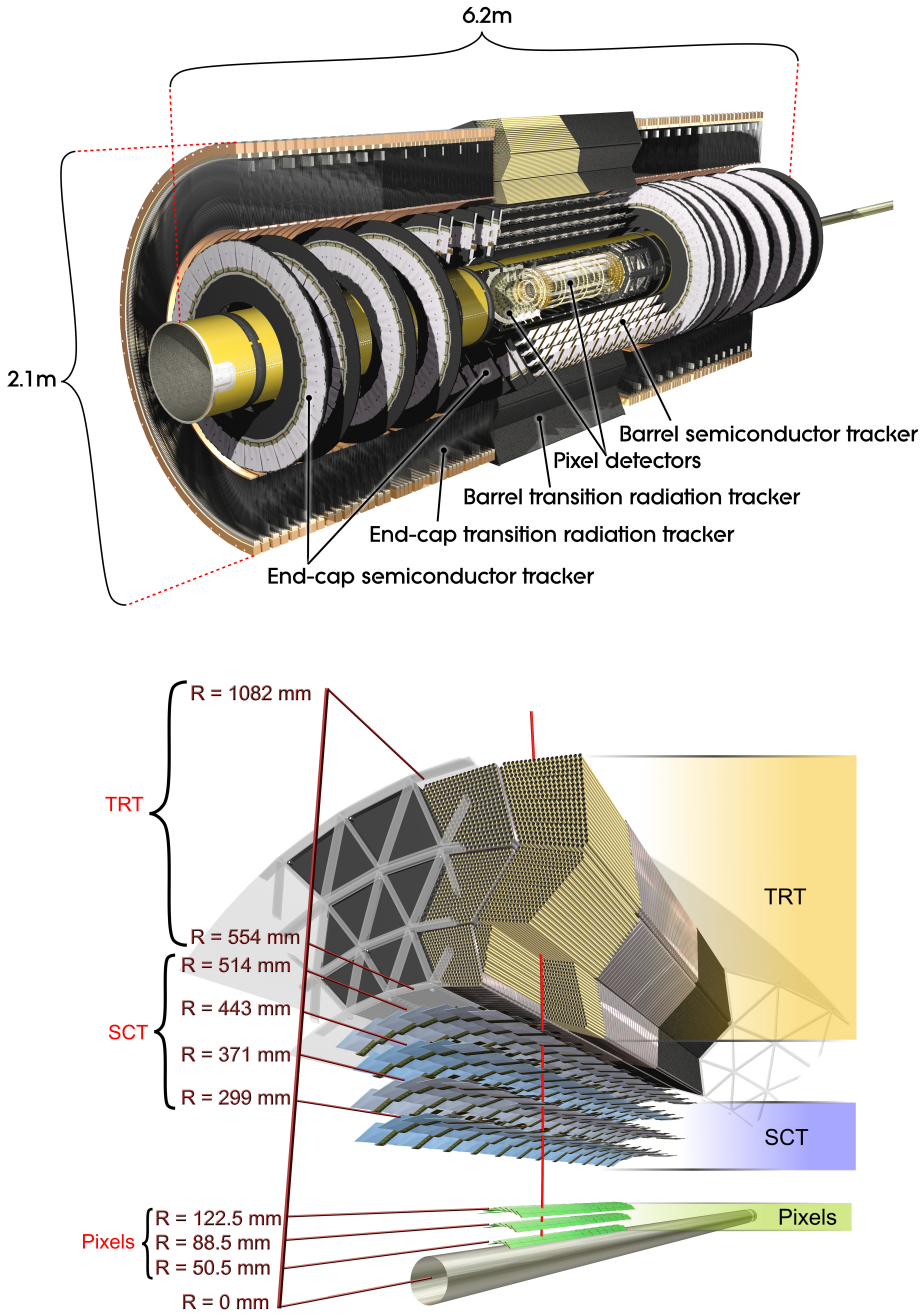

FIGURE 3.4: A cut-away of sub-systems of the inner detector in barrel and end-caps regions (top) [44] and the radial layout of sub-systems in the barrel region of the inner detector (below) [49].

originating from the interaction point passes through the ID, it leaves multiple hits in each of these systems. Due to the high magnetic field created by a solenoid coil surrounding the ID, the trajectory of the particle is reconstructed by fitting a helical path to these hits. Using this track, the transverse momentum of the corresponding particle can be determined. The full layout of the ID with its sub-detector systems is illustrated in Figure 3.4.

The **pixel detector** is the innermost sub-detector and is composed of silicon modules divided into small pixels, with a size of 50 μm $\times$ 400 μm. These modules are installed in three regions, in the barrel region, and in both end-cap (forward) regions, providing a coverage of $|\eta| < 2.5$. Each module is connected to the lower layer of silicon sensor. As the charged particle goes through each pixel, it ionizes the silicon, leaving holes and free electrons behind. These charge carries move to the edges of the pixel by an applied electric field creating an electric current which is then collected and read out as a hit in (η, ϕ) plane. The pixel detector has about 80.4×10^6 readout channels.

The **SCT** is situated outside the pixel detector and it performs the same function as the pixel detector. The only difference is that it consists of silicon modules which are instrumented with many sets of microstrips to provide orthogonal measurement, thereby improving the resolution to track measurement. Rather than reading out a set of pixels separately, a silicon module with microstrips, the hit is read out from a single coordinate. The SCT has the total number of about 6.3×10^6 readout channels. As in the pixel detector, three regions are instrumented with sets of strips providing a coverage out to $|\eta| < 2.5$.

The **TRT** is the outermost part of the ID and consists of many straw tubes, each having a diameter of 4 mm. Each tube is filled with a mixture of xenon and CO_2 gasses and a high voltage gold-plated tungsten wire in the center. When a charged particle passes through the gas, it creates free electrons, thereby ionizing the gas. Due to a high electric field produced by the high voltage, the free electrons move toward the wires and create electrical signals which are registered as a hit. The three regions of the detector, two end-caps and one barrel (as with the pixel and SCT detector) and has a maximal coverage out to $|\eta| < 2.0$. The TRT detector is used to identify particles at very high energies. It improves the detection efficiency and is used to discriminate between the electron and the pion tracks. It is sensitive to the function $\gamma = \frac{E}{mc^2}$. The amount of radiation measured, γ, in the TRT, is higher for an electron than a pion.

3.2.3 Calorimeters

Outside the ID is the **EM calorimeter**, which is used to measure the energy of particles that interact through the electromagnetic force, such as electrons and photons. It consists of two regions, a barrel in the region of $|\eta| < 1.475$ and two calorimeters in each end-cap region that extend over a coverage out of $1.475 < |\eta| < 3.2$. Both regions contain a liquid argon (LAr) bath (active

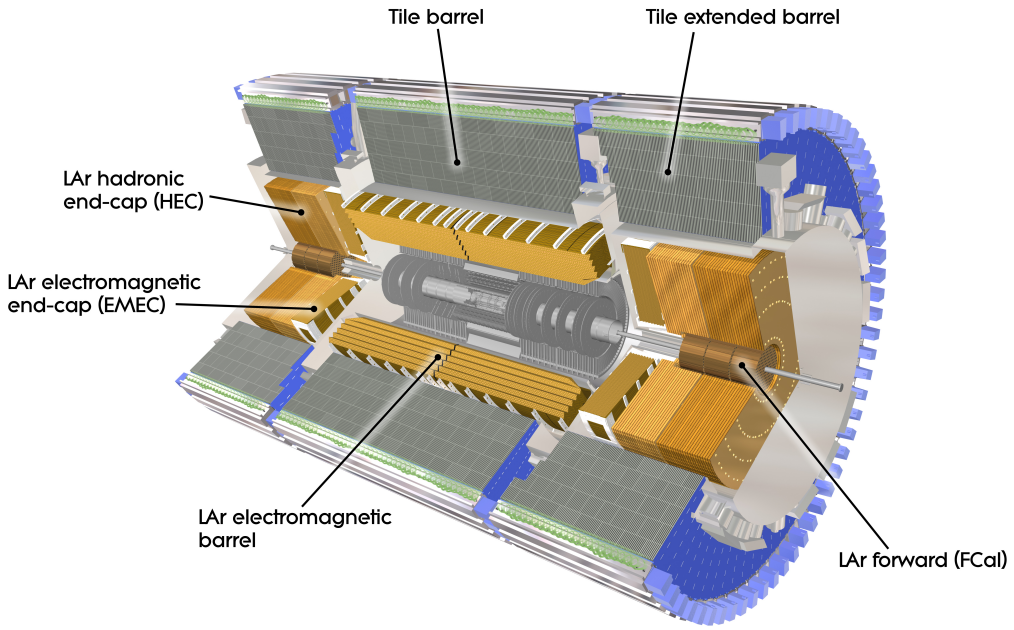

FIGURE 3.5: A schematic view of the calorimeters, EM and hadronic [44].

medium) and lead material (passive medium). When charged particles enter the calorimeter, they either ionize the liquid argon or first produce a shower of electrons and photons in the lead which ionizes the liquid argon. During ionization, free electrons are produced and collected by electrodes (copper plates), and their charges are measured to represent the amount of energy deposited by particles in the calorimeter. A pre-sampler, which is made up of a thin layer of liquid argon, is installed before the EM calorimeter in order to sample the shower from ID before it goes to the EM calorimeter. This betters the energy reconstruction measurements.

The **hadronic calorimeter** compliments the EM calorimeter. It detects heavy nuclei (hadrons such as a proton and a neutron) and showers that extend through the EM calorimeter. It functions the same way as the EM calorimeter but differs in the fact that it uses plastic tiles as the active material and steel or iron tiles as the absorber material. These materials are situated in the barrel region providing a coverage of $|\eta| < 1.7$. In the end-cap regions, the coverage is extended to $|\eta| < 3.2$ and uses the same principles as the LAr EM calorimeter with additional copper plates to support the showering of hadrons. The barrel region of the hadronic calorimeter consists of alternating tiles of iron and plastic. The plastic tiles are used to convert the shower initiated by particles in the iron tiles into the light. The light signal created by the deposition of energy in the calorimeter cells is transmitted to a system that converts it to an electrical signal, which is then read out and calibrated to represent the amount of energy deposited for each cell. A cut-away view of the calorimeter layout is depicted in Figure 3.5.

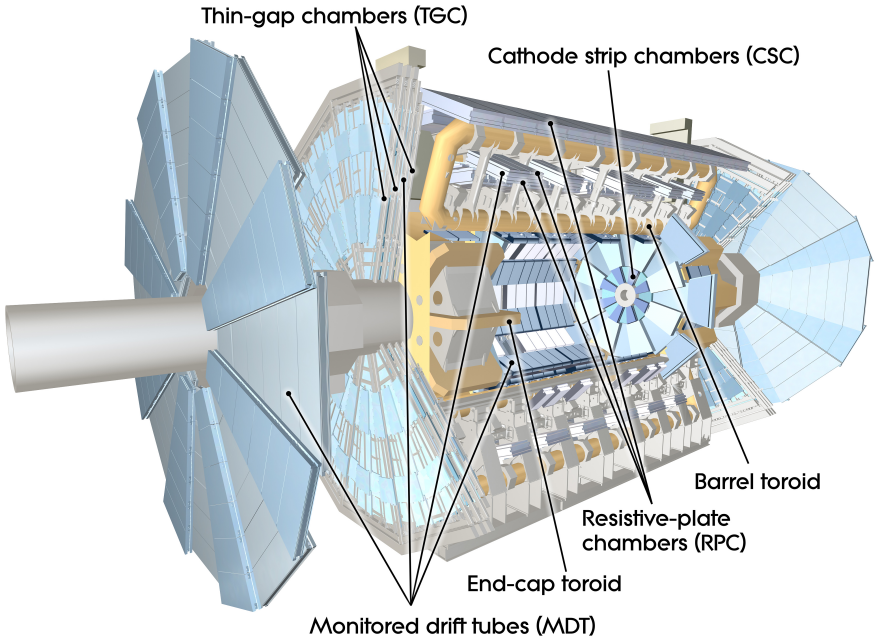

FIGURE 3.6: A schematic layout of the ATLAS muon spectrometer systems [44].

3.2.4 Muon spectrometer

The muon spectrometer (MS) surrounds the calorimeters. It uses four subsystems and a toroid magnet, to register the hits left by passing muons. The magnetic field of 0.5 T produced by the toroid magnets bend the particles as they traverse through the MS. From this curvature, the momenta of muons can be calculated. The four subsystems are cathode strip chambers (CSC), monitored drift tube chambers (MDT), thin gap chambers (TGC), and resistive plate chambers (RPC). Each of these systems is responsible for collecting charge from the gas ionized by the passage of a charged particle. The way in which charge is collected varies for each subsystem. The RPC in the barrel region $|\eta| < 1.0$, collects charge using two resistive plates while the TGC in the end-cap regions $1.0 < |\eta| < 2.4$, uses two conducting materials with parallel wire to collect the charge. Both the MDT and the CSC placed throughout the entire muon system in the region of $2.0 < |\eta| < 2.7$ are used for precise track measurements. The MDT functions in a similar way as the TRT straw tubes while the CSC function as the TGC but with a smaller spacing between wires. These subsystems provide better time resolution by delivering track information within a spread of 15-25 ns for the initial trigger that looks for an event with muons. The layout of the MS system with its chambers is shown in Figure 3.6.

Now that the configuration and the geometry of the ATLAS detector hardware have been explained, the following section focus on the techniques used in ATLAS experiment to reconstruct events from pp collisions.

3.3 Vertex and object reconstruction and identification

Electronic signals from each of the above-mentioned detector components are then passed through reconstruction algorithms that are used to identify objects based on the track information and the energy. During proton-proton interaction, different kinds of new particles can be formed which then decay to stable particles. Some have a short life span and decay immediately into other particles, such as the W/Z bosons, Higgs boson and top quark. Due to color confinement, quarks hadronise before interacting with the detector. The detector can only reconstruct a specific range of final state objects which include electrons, muons, photons and hadronic jets. Each final state particle leaves a unique signature in the detector, as shown in Figure 3.7. This section gives details on the performance of the ATLAS detector components in terms of tracking and vertexing, as well as reconstruction and identification of final state particles used in this project.

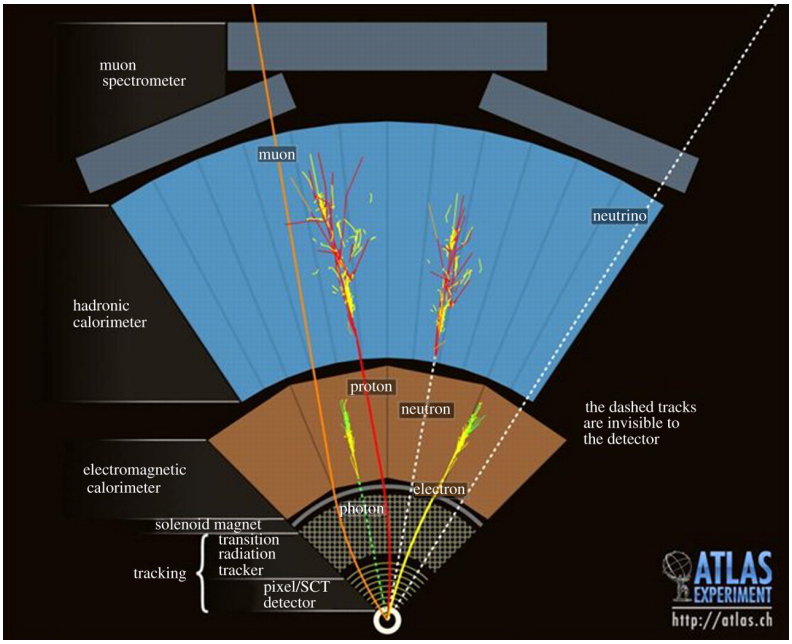

FIGURE 3.7: A schematic of a transverse slice through ATLAS detector showing the interaction of particles with the sub-detectors [44].

3.3.1 Track and vertex reconstruction

In ATLAS, track reconstruction starts with an inside-out algorithm [50] that reconstructs the tracks from hits in the pixel detector and the SCT detector. The word "tracks" refers to the trajectories of charged particles that are created by fitting a helical path to the collection of hits. Each track is identified by five parameters: two angles defining the direction (η and ϕ), the radius of

curvature, and the transverse and longitudinal impact parameters defining the distance between the track and its origin. It is also possible for a single hit to be associated with more that one track; for this case quality criteria are applied to reject fake tracks. The remaining tracks are extended from the silicon track to the TRT by refitting. To increase track reconstruction efficiency, the outside-in algorithm is used, which takes unused TRT hits and tries to trace them back through the silicon layers. This efficiency differs depending on the particle, for instance, electrons have less reconstruction efficiency than muons. This is due to the fact that electrons undergo bremsstrahlung[1] in the detector while muons go straight to the MS.

The vertex is the point at which two particles from opposite direction proton beams collide. Vertices are reconstructed using tracks that are consistent with originating from the same interaction region [50]. A vertex position is determined by applying fitting procedures to selected tracks and removing the contribution from outliers. After multiple iterations of the fitting, the remaining tracks that are incompatible with the fitted vertex are then used to reconstruct new vertices. This procedure is repeated until all the tracks have their associated vertex. Only the vertex with at least three associated tracks and highest $\sum p_T^2$ is considered to be a primary vertex.

During each proton-bunch crossing, multiple collisions occur which results in the reconstruction of more than one vertex in a single recorded event. The events associated with vertices other than the primary vertex are called *in-time pileup* events. The detector imperfection can also be caused by collision events from previous bunch crossings which then becomes background events in the current bunch crossing. This is known as *out-of-time pileup* events.

3.3.2 Electron and photon reconstruction and identification

An electron candidate is reconstructed from a track in the ID that points to a localized cluster of energy, a group of energy deposited into various cells in the EM calorimeter. A neutral particle like a photon, which has no track in the ID, is reconstructed from the energy it deposits in the EM calorimeter.

A sliding-window algorithm [51] is used to reconstruct energy clusters contained in a window size of 0.075 in η and 0.125 in ϕ with a transverse energy (E_T) greater than 2.5 GeV. These clusters serve as seeds for electron object reconstruction. To form electrons, clusters are matched to tracks reconstructed in the inner detector, only the ones within a cone of $\Delta R = 0.4$ are considered. After track matching, the reconstructed electron candidate energy is deduced from the cluster while its charge and transverse momentum are derived from the tracks associated to the clusters.

[1] Electromagnetic radiation caused by the interaction of a charged object with the detector material.

At this point, a reconstructed electron candidate is either real or jet-faked[2]. To improve efficiency for isolated high-p_T electron selection, a cut-based standard ATLAS identification algorithm is applied. This algorithm has three sets of selection that are based on shower shape, track quality, and track-to-calorimeter cluster matching:

- **Loose** criteria is a simple selection that has a loose track-to-calorimeter cluster matching and simple shower-shape requirements.
- **Medium** criteria tighten the shower-shape cuts using information from the first layer of EM calorimeter. It also requires the reconstructed track to have a minimum of seven precision hits in the silicon sub-detectors, and the transverse and the longitudinal impact parameters to fulfill $|d_0| < 2$ mm and $|z_0 - Z_v| \times \sin\theta < 10$ mm, respectively. The position of the primary vertex along the beam axis is denoted by Z_v, while the polar angle of the track is denoted by θ.
- **Tight** criteria, in addition to medium cut requirements, enhance track-to-calorimeter cluster matching. To reject more photon conversions and background from charged hadrons, a track must have a hit in a vertexing-layer and in a TRT sub-detector.

These reconstructed electron candidates are further required to have transverse momentum $p_T > 25$ GeV, and fall within the detector acceptance of $|\eta| < 2.47$ and outside the calorimeter crack region $1.37 \leq |\eta| \leq 1.52$. They are also required to pass isolation criteria, which is the sum of the transverse momentum of the tracks or transverse energy deposited in the calorimeter cells in a cone size of $\Delta R = 0.3$ excluding the electron cells in the calorimeter and tracks in the inner detector.

So far, the reconstruction of objects that deposits energy in the EM calorimeter has been discussed. An object that extends throughout the calorimeter has a slightly different reconstruction algorithm and this is what follows in the next sub-section.

3.3.3 Muon reconstruction and identification

A muon object is mainly reconstructed from the track segment it leaves in the muon spectrometer (MS), in the inner detector (ID) and/or both. It is also possible to reconstruct a muon in the calorimeters due to ionisation. Thus, a muon is identified by tracks in the ID and MS, combined with the small amount of energy deposited in the calorimeters along its trajectories.

There are four types of muons reconstructed by the ATLAS sub-detectors:

- **Standalone** muons are only reconstructed in the MS. Their flight distance and the track impact parameters are determined by tracing the

[2] A lepton that is faked by a jet is usually non-isolated, with more hadronic activity around its track

track in the MS to the beam line, taking into account the amount of energy loss.

- **Combined** muons have their trajectories reconstructed independently in the ID and MS, which are then combined. This improves the estimation of the muon candidate kinematics.
- **Segment-tagged** muons are identified by matching the ID tracks with the MS segments. In the matching process, the ID tracks are extrapolated through the calorimeters to the MS segments. This process improves the muon reconstruction efficiency in the regions with limited MS coverage.
- **Calorimeter-tagged** muons have tracks in the ID that point to the energy deposited in the calorimeters.

All reconstructed muons used in ATLAS analyses are combined muons. These muons are required to fulfill the selection criteria recommended by the Muon Combined performance group [52]. There are additional kinematic cuts that are applied to further exclude muons coming from additional pileup collisions or originating from background jets. The inner detector track associated with the muon is required to originate from the primary reconstructed vertex. This requirement is implemented by selecting only the muon with the flight path intersecting the beam axis within the distance of 0.5 mm of the primary vertex. This muon is then required to have $p_T > 25$ GeV, and fall within a detector acceptance of $|\eta| < 2.5$. In order to reduce the number of muons coming from multi-jet processes or from the decays of heavy flavours, muons are required to be isolated in the inner detector (ID) and also in the calorimeters within a cone of $\Delta R = 0.3$.

A muon object failing this cone requirement is non-isolated and this type of muon usually originate from a jet. Below are the jet reconstruction and identification algorithm.

3.3.4 Jet reconstruction and identification

Quarks and gluons hadronise or decay into stable particles before interacting with a detector. Their decay products appear as collimated clusters of particles in the detector, known as jets. ATLAS uses a variety of jet-clustering algorithms to reconstruct each jet. One of the commonly used jet-clustering algorithms is the anti k_T algorithm [53], which works by taking all the pairs, ij, of reconstructed detector objects and analyses them by comparing the distance between i and j, d_{ij}, to the distance of object i relative to the beam line, d_{iB}. These two distances are computed as follows:

$$d_{ij} = min(p_{T,i}^2, p_{T,j}^2)\frac{\Delta R_{ij}^2}{R^2}, \tag{3.5}$$

then

$$d_{iB} = p_{T,i}^2. \tag{3.6}$$

In the above equations, $p_{T,i}$ and $p_{T,j}$ represent the transverse energy of object i and j, respectively. The ΔR_{ij}^2 is the distance between i and j in $\eta - \phi$ space while R is an adjustable distance parameter used to control the size of the jet. If the minimum distance found is d_{ij}, then objects i and j are added together to form a new object by combining their 4-momenta and i and j are removed from the algorithm. Otherwise, if d_{iB} is the minimum, then i is considered to be a complete jet on its own and is removed from the algorithm. This process is repeated, resulting in new distances of d_{ij} and d_{iB} until all the object clusters are combined to be part of a jet. In ATLAS, the distance parameters used as standards are $R = 0.4$ for narrow jets and $R = 0.6$ for wider jets.

3.3.5 $b-$jet tagging

The material in this section is taken from ATLAS collaboration [54] and Claudia [55].

Hadronic $b-$jets have unique features. Due to the fact that they contain a heavy $b-$quark, they also have a longer lifetime than any other quarks and can travel a measurable distance before decaying. The B hadrons tend to live longer than other hadrons because they decay via the electroweak interaction. A typical lifetime or decay length of $B-$hadrons is approximately 1.5 ps or 450 μm. These properties lead to the formation of a secondary vertex (SV - it's a decay vertex of a $B-$hadrons) displaced from the primary vertex (interaction vertex) In the case of a semi-leptonic decaying $B-$hadron, the $b-$jet can be seen by the presence of a muon with the jet. The branching fraction is about 20% including the three following decays: $b \to \mu + X$, $b \to c + X$ and $c \to \mu + X$, where X denotes the sum of all additional particles within the jet.

ATLAS has several algorithms that exploit these facts to search for evidence of a $B-$hadron decay using reconstructed tracks associated with the jet. The IP3D algorithm uses a likelihood ratio based on two-dimensional distributions of transverse and longitudinal impact parameter significances to classify the jet in question. Two other algorithms, SV1 and JetFitter, work by reconstructing the SV within the jet and exploit the properties of the vertex (e.g invariant mass of all tracks making up the vertex, the ratio between the sum of the momenta of vertex tracks and the jet energy) to classify jets. SV1 only makes one vertex for b decays while JetFitter attempts to analyse b and c decays within the jet. In Run 2, these three algorithms are combined using a Boosted Decision Tree method called MV2 tagging algorithm which is trained with different jet proportions. For an example, MV2c20 used in this analysis was trained with 20% of c jets and 80% of light jets to provide the best compromise between c jet and light jet rejection.

The reconstruction and identification algorithms discussed above, are only applicable to objects that ATLAS detector is able to capture. How about undetectable particles such as a neutrino?

3.3.6 E_T^{miss} reconstruction

Neutrinos can not be directly detected by the ATLAS detector, they appear as missing transverse energy, E_T^{miss}. If the momentum in the transverse plane is conserved, the vector sum of all the particles detected in a given event should be zero. However this is not the case for ATLAS analyses that search for final experimental signatures with neutrinos, instead, there is an imbalance in the observed transverse momenta which is caused by missing transverse energy of undetectable particles.

The E_T^{miss} is calculated from the energy deposited in the calorimeters and reconstructed muon tracks in the MS. All the energy clusters formed in the calorimeter are associated with reconstructed and identified high p_T objects and calibrated according to the following order: electrons, photons, hadronically decaying $\tau-$leptons, jets and muons. Jets with low $p_T < 20$ GeV are considered to be soft particles. In addition, other clusters that are not associated with any of these objects are also included in the calculation of E_T^{miss} [48, 56],

$$E_{x,y}^{miss} = E_{x,y}^{miss,calo} + E_{x,y}^{miss,reco-mu}, \tag{3.7}$$

where

$$\begin{aligned} E_{x,y}^{miss,calo} = E_{x,y}^{miss,e} + E_{x,y}^{miss,\gamma} + E_{x,y}^{miss,\tau} + E_{x,y}^{miss,jets} + E_{x,y}^{miss,soft-jets} + \\ E_{x,y}^{miss,other-clusters} + E_{x,y}^{miss,calo-\mu}. \end{aligned} \tag{3.8}$$

Each term in Equation 3.8 is computed as the negative sum of the reconstructed and calibrated physics objects, projected onto x and y directions:

$$E_x^{miss} = -\sum_{i=1}^{N_{cell}} E_i \sin\theta_i \cos\phi_i, \tag{3.9}$$

$$E_y^{miss} = -\sum_{i=1}^{N_{cell}} E_i \sin\theta_i \sin\phi_i, \tag{3.10}$$

where E_i, θ_i and ϕ_i denotes each cell energy, polar angle and azimuthal angle, respectively. Therefore,

$$E_T^{miss} = \sqrt{\left(E_x^{miss}\right)^2 + \left(E_y^{miss}\right)^2}. \tag{3.11}$$

In ATLAS experiment not all events with reconstructed objects go to the storage. The ATLAS trigger system [44] is designed to further process the data and select events that show interesting features.

3.4 Trigger, readout and data acquisition systems

The LHC has reached its designed luminosity with a collision rate of 40 MHz. This is the huge amount of data that can not all fit in the storage system. For this reason it very important to pre-select only events with interesting physics processes. The ATLAS trigger system demonstrated in Figure 3.8 was developed to do just that. It is organised into three levels, with each level refining the previous decision by using advanced algorithms to further reduce data before sending it to a storage system. The data acquisition (DAQ) system stores, processes, and transfers detector read-out data according to the trigger decisions.

3.4.1 Trigger system

The L1 trigger select objects with high transverse-momentum p_T, as well large transverse energy using information from different sub-detector regions. Muons with high p_T are identified using trigger chambers in the barrel and end-cap regions of the MS while the calorimeter objects are selected using the information from calorimeters. The results are processed in the central trigger processor. Events selected L1 trigger are then passed to the next stage in the trigger chain, which is the DAQ. In addition, the L1 trigger defines Regions-of-Interest (RoI's), which are the regions of the detector where the trigger found interesting features. The L2 trigger selection uses this RoI's information to further reduce the trigger rate to about 1 kHz. The last stage of the trigger system is the event selection done by event filter (EF) that reduces the event rate to about 0.1 kHz. The event filter selection is based on offline analysis procedures.

3.4.2 Readout and data acquisition systems

Information of the event selected by the L1 trigger is transferred off the detector to the Readout Driver's (ROD's), which are sub-detector specific elements of the front-end electronic systems [57]. The ROD's, are located after L1 trigger between the front-end electronics and readout systems, are used to enhance data concentration. They include analog-to-digital processing. Digitised signal front-end data streams are formatted as raw data objects and then transmitted to the DAQ system. The first step in processing data in DAQ, the readout systems stores the data temporarily in local buffers. At the following step, the information about the RoI's associated with L1 selected

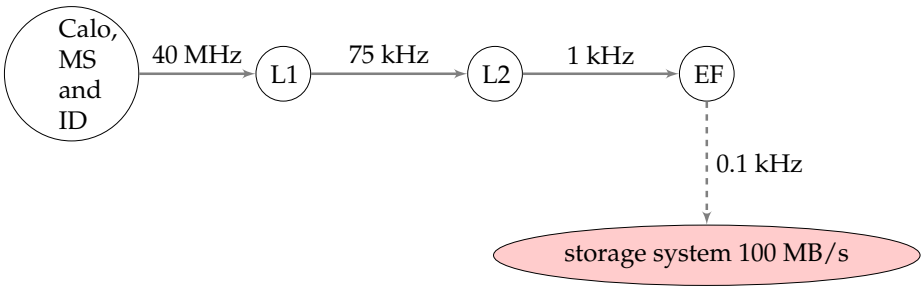

FIGURE 3.8: The layout of the ATLAS trigger system.

events is added. Events selected by the L2 trigger are passed to the event-building system and event filter (EF) for final selection. All events accepted by the full trigger chain are sent to the CERN central storage systems to be made available for physics analysis. The DAQ also does hardware control and monitoring of the performance of the detector during the data taking period.

In this chapter, the geometry and various components of the ATLAS detector have been describing together with the reconstruction and selection of physics objects produced in actual pp collisions at the LHC. Depending on the analysis, the selected objects can be used to look for evidence of the SM processes. However the data may contain statistical fluctuations, thus experimental measurements rely on theory to correct for mis-modeling in data. The following chapter details the MC techniques use in HEP to simulate pp collisions.

Chapter 4

Event simulations

This chapter gives details on the simulation of events occurring in proton-proton collisions at the LHC and the evolution of final state particles. In addition, it gives details on the simulation of physical objects interactions within the ATLAS detector.

4.1 Monte Carlo simulations

A simulation of the processes occurring during proton-proton collisions at the LHC is important for HEP research. Computer simulation tools are used to understand the expected background and signal processes, and to test whether the signal measurements from the data shows new physics or contribution of the SM. On that note, Monte Carlo (MC) methods play a role in the generation of events and simulation of detector response to particles. Further information about MC methods used in a simulation of high-energy physics data is in these references [58, 59, 60].

Proton-proton collisions at the LHC are complex to describe. A full simulation of data from the ATLAS detector takes into account the following [60]:

1. event generation:
   - matrix element of a hard scatter,
   - parton shower algorithm with NLO effects,
   - QCD processes leading to the formation of final state objects,
   - modeling of secondary interactions
2. the response of various ATLAS sub-detectors to produced particles, and
3. the energy deposited in the sensitive regions of the simulated ATLAS detector is converted into electronic signals for comparison with the readouts of the real detector.

ATLAS experiment has dedicated computer software that combines all the above-mentioned steps to produce a sample of simulated events that look

similar to the real data produced by the LHC and recorded by the ATLAS detector. The study in this project is only done on simulated Monte Carlo samples referred as MC samples, no real data was used. Throughout the entire analysis, the MC simulated samples are used to characterise leptons from top quark decays.

4.1.1 Factorisation theorem and matrix element integration

Due to the large number of dimensions of the phase space (space-time, spin, and flavour of n final state particles) that needs to be evaluated, MC techniques are particularly suitable for the application to processes in high-energy physics. In MC integration, the full process is factorised into sub-processes occurring at different energy scales of hadronic collisions. This is performed using the factorisation theorem [61], demonstrated in Figure 4.1, where partons are treated as free particles of the initial state despite their confinement at lower energies [62] .

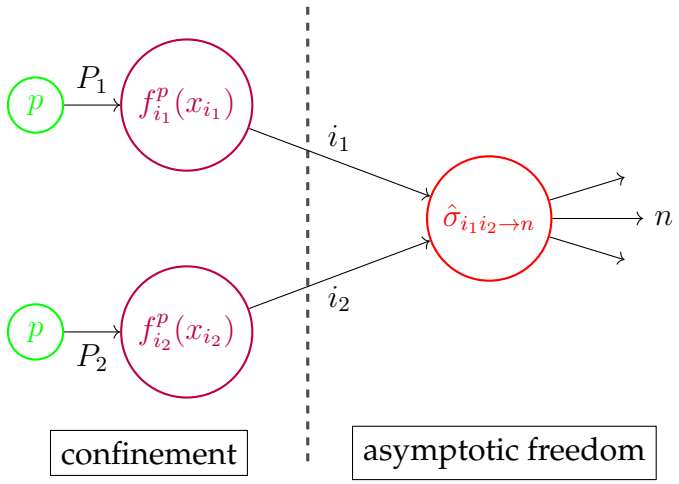

FIGURE 4.1: Illustration of the factorisation of the cross section [63]. This diagram shows the scattering process of $i_1 i_2 \to n$ with initial partons of flavour i_1, i_2 and final state particles represented by n. The function $f_i^p(x_i)$ is the PDF of the initial parton i carrying a momentum fraction x of the original hadron P and $\hat{\sigma}_{i_1 i_2 \to n}$ is the partonic cross-section.

The total cross section of a scattering process, $i_1 i_2 \to n$, at a hadron collider can be written as the integral over all the final-state phase space Φ_n as follows:

$$\sigma_{i_1 i_2 \to n} = \sum_{i_1, i_2} \int_0^1 dx_{i_1} dx_{i_2} \int d\Phi_n f_{i_1}^{h_1}(x_{i_1}, \beta_F) f_{i_2}^{h_2}(x_{i_2}, \beta_F) \frac{1}{2\hat{s}} |M_{i_1 i_2 \to n}|^2(\Phi_n; \beta_F, \beta_R), \tag{4.1}$$

where i_1, i_2 are the initial particles, n are the final state particles, β_F is the factorisation energy scale and β_R is the re-normalisation scale.

The matrix element $|M_{i_1 i_2 \to n}|^2$ is the sum over all possible Feynman diagrams for the process $i_1 i_2 \to n$, weighted by PDFs $f_i^h(x_i, \beta_F)$. The matrix element integration is done by sampling the phase space Φ_n and calculating the differential cross section $d\sigma$ at different sampling points. Summing over all $d\sigma$ results in the total σ of the partonic processes. Formation of hadrons/jets are not included in the integration.

For the generation of events, the above sampling points are treated as events with weight $d\sigma$. The events are un-weighted with an acceptance-rejection method [64] to produce a physical sample of events with unity weights. It generates a uniform random number, say h, between the values of 0 and 1 according to a given probability density. For the event to be rejected, the ratio of the event weight over the maximum event weight, $\frac{d\sigma}{d\sigma_{max}}$ must be higher than h. Otherwise, the event is rejected.

4.1.2 Event sequential formation stages

The final state of a hard scatter, calculated from the matrix element, contains stable/unstable particles. Leptons and photons in the final state are stable, and partons are non-observable. The evolution of final state particles in a simulated event is illustrated in Figure 4.2. The hard interaction is indicated by the red region in the center, while the secondary hard scattering is indicated by the purple region. The parton shower emissions are represented by blue. Hadron decays are represented by the dark green regions. QED radiations from parton showers are indicated by thin yellow lines.

Matrix element and parton showering. The matrix element of an event is calculated up to a fixed order in perturbation theory thereby ignoring the higher-order corrections. This is because higher-order corrections are computationally difficult and they have fairly large effects on particle kinematics. Therefore, it is important to build up the matrix element events by adding higher order contributions which include decays of unstable particles, a formation of hadrons, and underlying events.

To put into consideration the effects of higher order QCD corrections and hadronisation, events are passed into a parton shower and hadronisation algorithm. Parton showers explore different kinematic regions in QCD radiation. In Markov Chain processes[58], the hard sub-processes are built up by the addition of consecutive branching of one parton into two other partons. This algorithm is limited to soft partons and collinear gluon splitting.

The evolution parameter T is chosen to be either a time-like or space-like variable together with the starting value t. For a splitting of parton of flavour i, the following value or new scale T is determined by solving equation

$$\Delta_i(t, T_0) = \mathcal{R}\Delta_i(T, T_0), \tag{4.2}$$

where $\mathcal{R}$ is a random value sampled from a uniform distribution in $[0, 1]$ and T_0 is a infrared cutoff scale, which is about 1 GeV. The probability of parton of

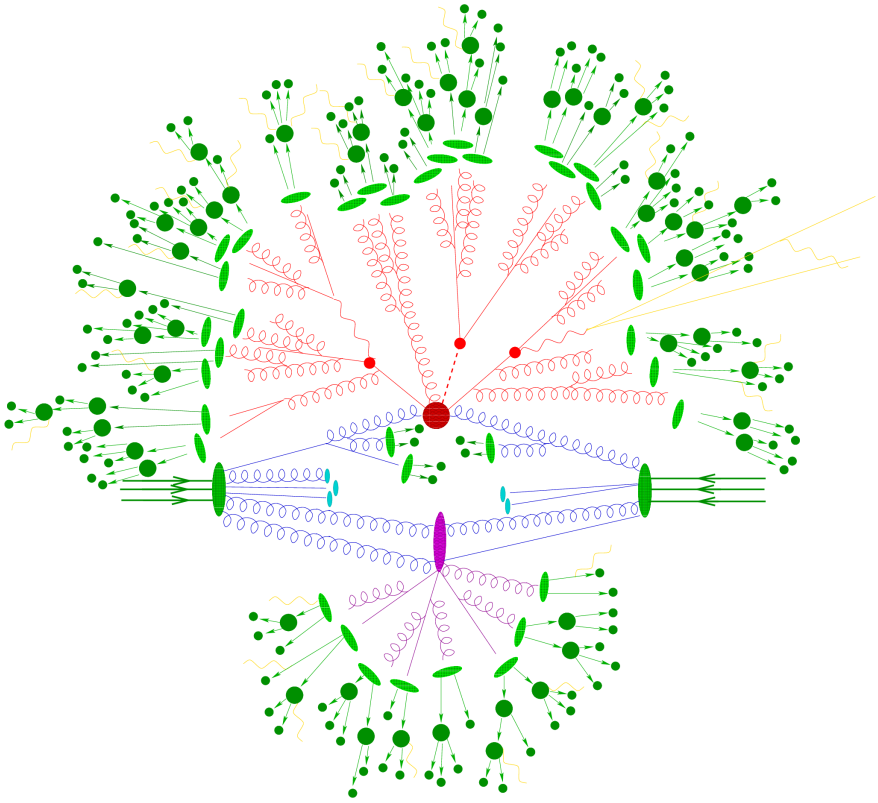

FIGURE 4.2: Evolution of final states in MC event [65]. Shown is the hard interaction (red), parton shower emissions (blue), hadronised partons (green), hadron decays (dark green) and QED radiation (yellow lines). Additional interactions are depicted in purple.

flavour i not to split during evolution from scale q_1 to scale q_2 is described by the *Sudakov form factor* [66], $\Delta_i(q_1, q_2)$. In cases where the new scale T is less than cutoff scale T_0, the splitting of parton i is discontinued. Otherwise, the splitting of parton i to partons $j+k$ is continued by solving equation 4.2 with a new value of $\mathcal{R}$ for the parton j and k at the new initial scale [67]. Lastly, the initial parton i is replaced by a shower of partons travelling in similar direction.

Hadronisation. Following parton showering is the formation of colour neutral composite states, hadrons, from the combination of partons. Hadronisation is modeled with several methods that are based on generic properties of QCD. The commonly used models in current event generators are the string and cluster models [68, 69]. These models describe all possible combinations of partons into hadrons using the pre-confinement of parton showers (clusters) and the linear confinement of partons (strings).

QED radiation. The radiation of photons from electrically charged particles, electromagnetic radiation, can occur at different stages of the event. Modeling of QED radiation is based on YSF [70] formalism, which accurately simulates higher-order QED corrections [71, 72, 73].

Additional partonic interactions. In addition to hard scattering, which contribute to the main collision, a multitude of interactions take place between other partons in the colliding protons and need to be simulated.

4.1.3 Monte Carlo event generators

Monte Carlo generators used to model proton-proton collisions in this thesis are listed below.

Sherpa

Sherpa [74] is a general purpose MC event generator for the Simulation of High-Energy Reactions of Particles in proton-proton collisions. It is designed to simulate all possible interactions of the SM by following an approach which automatically includes all contributing Feynman diagrams up to given orders of magnitude in the electroweak and strong couplings. In addition, SHERPA is used as a cross-section integrator with high accuracy for leading-order (LO) diagrams. The effects from next-to-leading-order (NLO) diagrams, which are emissions of additional partons, are taken into account by Sherpa's built-in generators. The built-in generators are tree-level matrix element calculators for the hard scattering processes with several outgoing jet multiplicities[1]. These results are then matched with detector simulated parton showers to optimize descriptions of the kinematics. The reader is directed to the paper by Hoeche [75] for more details on the calculation of matrix elements for several jet multiplicities together with the parton shower simulation.

Powheg

Since general purpose MC event generators include dominant QCD processes at the LO level but do not enforce NLO accurately, one could not directly compare experimental measurements with NLO calculations precisely. Hence shower MC programs were improved by deploying another method called Powheg. A positive weight hardest emission generator (Powheg), like its name, is designed to produce positive-weighted events. It is capable of calculating cross-sections with higher accuracy at parton level using the NLO QCD matrix elements. At the next stage, the calculations of these hard processes are then matched with parton shower simulations from Pythia8 [76] to account for any overlap between calculations arising from real radiations. More details on the implementation of the electroweak and strong $W^{\pm}W^{\pm}jj$ production processes in Powheg is available in reference [77, 78].

[1]The jet multiplicity is the number of jets in a given event.

Pythia

In the scope of this analysis, the event generator Pythia8 [76] is used for its parton shower algorithm applied to parton-level events produced by PowHeg. Nevertheless, it is also possible to generate matrix element for VBS processes with Pythia. With that, processes such as $pp \to \ell\ell\nu\nu$ are factorised in the emission of two W bosons using the effective W boson approximation (EWA) approach for high energy collisions [79]. Currently, EWA does not provide results of the full integration [80].

4.1.4 Detector response

After event generation, the simulation chain has a task to mimic the passage of final state particles through different materials of the detector. In ATLAS, the detector response is simulated with a GEANT4 [81] based toolkit. This framework has a complete geometry description of the detector which is used to simulate physics interactions within it.

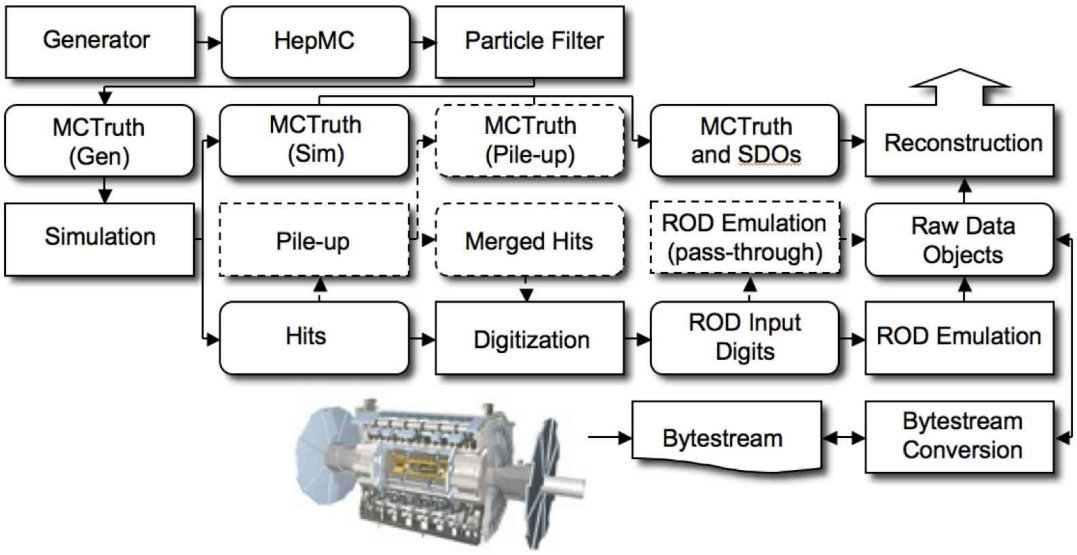

FIGURE 4.3: ATLAS simulation and data taking chain [82]. The flow of data is shown from MC generators through different algorithms to the output, which is identical to the data read out from the detector. The output from the event generators is in HepMC format. This output is taken through some event filtering, which is followed by simulation and digitisation to simulate the detector read-out drivers (RODs). At each stage of the simulation chain, MC truth information is stored including interactions in the Geant4. The link of the truth information to hits is stored in simulated data objects (SDOs).

Shown in Figure 4.3 is the full ATLAS simulation and data taking chain. Algorithms and applications to be run are indicated with sharp-cornered boxes while data objects are indicated with round-cornered boxes.

MC generated events in the HepMC [83] format are passed through the particle filter selecting events according to kinematic requirements. The generator level, MC truth, of these events is then passed into the detector simulation. The resulting kinematic variables, such as energy deposition signal, and their position in the detector are stored as analog signals known as hits. Once more, at the simulation level, information about tracks and particle decays within the detector (e.g. photon pair production) is kept in the MC truth record. Matches from simulated hits of the detector to truth-level particles in the MC truth record are in Simulated Data Objects (SDOs). The energies deposited in Hits are converted into digital signals similar to the signals from the detector read-out drivers (RODs).

Lastly, the resulting events are passed through reconstruction. They are in the same structure and have the same content as events from the ATLAS data acquisition system 'Bystestream', which convert real hits into the Raw Data objects. As in real data, the simulated data from the detector configurations run through ATLAS trigger systems and reconstruction packages. When doing particle reconstruction, there is often some additional contributions due to event pile-up, this is also added to the simulation. [82]

The simulation chain is partitioned in this way to simplify software validation. Event generation jobs are run for several events and stored in memory before being passed to the next step. This makes it possible to run the same events with different detector configurations. Simulation jobs can take several minutes with large output files of the event generation algorithm. Therefore, each file is split into sub-files with at most 50 events so that fewer events may be complete quicker. Digitisation jobs are configured to run approximately 100 events at a time far easy file handling. Digitisation algorithm also takes care of the consistency between the detector geometry used for a simulation job and succeeding digitisation job.

The production of large-scale MC samples is done on the LHC computing Grid. A single task is divided into several jobs to minimize running time. Each job is allowed to run on the Grid for the maximum of 2-3 days. To do some validation of a particular sample, one can either download the sample from the Grid to the local machine or submit a job to the Grid.

4.2 Levels in Monte Carlo samples

Each MC event sample contains process-specific pp collision events that were passed through the full simulation chain described above. Figure 4.4 shows different levels of simulation available in MC samples for analyses in HEP experiments like ATLAS [63].

Truth contain particles described by matrix element calculation without parton shower, QED radiation and hadronisation. These particles include undecayed leptons and partons which are produced at the final stage of a collision event.

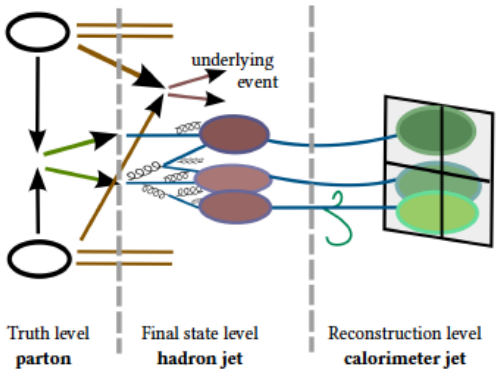

FIGURE 4.4: Levels in MC samples [63].

Final state contain information on stable particles and underlying events or objects. Particles can be either from hard processes or hadronisation.

Reconstruction contains particles reconstructed by algorithms run on full detector simulation. Decayed particles, detector effects, and response are simulated. In addition, events from $pile - up$ interactions are included.

The truth and final state levels form part of the MC truth information which is kept in the reconstructed MC simulation. Thus MC samples contain two sets of information: the truth information and reconstructed information. All the samples used to do this analysis may be found in Appendix A.1 together with their production tags. Each sample in ATLAS is assigned a tag at the end of its name to help the user to quickly find information about the sample in question. The production tag encodes information such as simulation, calibration and reconstruction versions used to simulate events in a sample.

4.2.1 Vertices and pile-up corrections

The MC samples are produced before all data collection is finalised using an estimate of the anticipated number of interactions per bunch crossing. Thus, the MC distribution does not agree with the bunch crossing distribution observed in data. Therefore, the average number of bunch crossing in MC samples is re-weighted at the event level to correct for the actual bunch crossing distribution after the data has been taken. In addition to this pileup correction, the MC does not simulate the position of the primary vertex accurately along the beam line. This is also taken into account by applying event weights in MC simulations.

Chapter 5

Event selections in ssWW analysis

The generation phase space for $VVjj$ production samples is defined using the topology of VBS events. Pure electroweak $W^{\pm}W^{\pm}jj$ events are expected to have little hadronic activity in the region between tagging jets due to the lack of QCD radiation in the central region. The characteristic signature of a $W^{\pm}W^{\pm}jj$ production process is the presence of two high energy back-to-back jets with large invariant mass[1], missing transverse energy and two same-sign leptons ($\ell^{\pm}\ell^{\pm} + E_T^{miss} + jj$). Selecting these signatures in an event can significantly reduce most of SM background processes. For these characteristics, the same sign $W^{\pm}W^{\pm}$ has been chosen to be a promising channel to study VBS processes. Objects from VBS processes have distinct kinematic properties to be used when selecting signal events: each initial quark from the colliding protons emits a vector boson, and the remaining quarks form two back-to-back jets with large momentum and pseudorapidity. The event topology for vector-W bosons scattering is shown in Figure 5.1. When

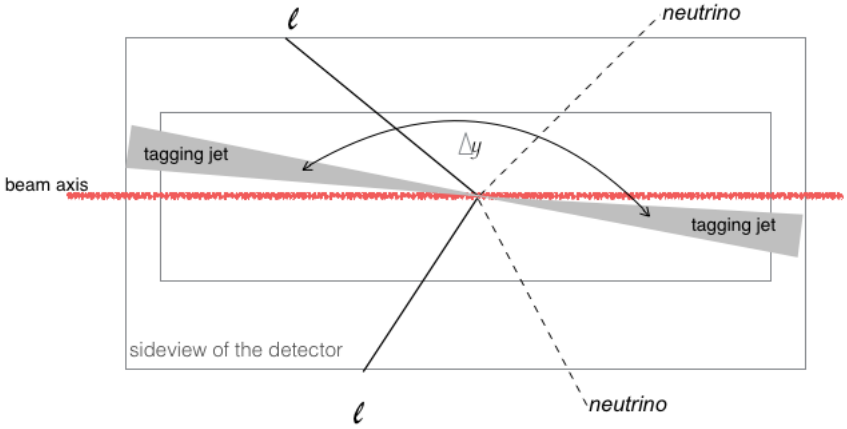

FIGURE 5.1: Event topology for VBS. This particular event contains two tagging jets in forward directions separated by rapidity Δy, two leptons ℓ and two neutrinos that carry away E_T^{miss}.

defining the phase space region for same sign $W^{\pm}W^{\pm}jj$ events, this topology

[1]The large invariance mass is selected since the vector bosons resulting from the decays of massive resonances are highly boosted, so decay products of each hadronic decaying boson are reconstructed as a single jet. Thus, the signature of the heavy resonance decay is a resonance structure in the invariant mass spectrum of dijets.

needs to be considered. In addition, the phase space region is required to sufficiently contain all signal contributions as well as additional SM processes, which might have entered into the signal region during the full simulation stage.

5.1 Signal events

The signal region is defined as the phase space which maximizes the contribution of events coming from $W^{\pm}W^{\pm}$ compared to other processes (background processes) that can produce the same signature. Each signal event should contain two final state prompt leptons (which are products of W bosons decay) of the same electric charge. In the analysis, the signal region includes events from both the electroweak and QCD mediated diagrams. Events from the electroweak and strong production of $W^{\pm}W^{\pm}jj$ are simulated separately using Sherpa and normalised to NLO cross section, calculated with CT10 [84] PDFs, to match the signal region.

5.1.1 Signal event selection

Details on the selection criteria applied to the analysis are given below. Moreover, reconstructed objects may overlap with each other in $\eta - \phi$ space, the description and order of overlap removal are also described below.

Trigger selection

During data collection, ATLAS selects events using fast algorithms called Triggers, which use the full readout of the detector. The ssWW analysis uses $e\mu$, ee and $\mu\mu$ events selected with single lepton triggers with $p_T > 24$ GeV, $p_T > 24$ GeV and $p_T > 24$ GeV for electrons, and with $p_T > 24$ GeV and $p_T > 24$ GeV for muons. Triggers with low p_T are pre-scaled[2].

After data taking is complete, trigger efficiency in MC is corrected to match with data using the scale factors. These trigger scale factors are computed by the Combined Performance groups [85].

Pre-selection

More event cleaning cuts are applied to the events to select samples with high-quality pp collision events:

[2]Pre-scaling is to reduce the number of events that pass the trigger requirement by integer division.

- Good Runs List (GRL), removes luminosity blocks[3] with poor detector quality. For the detector quality to be good, all sub-systems of the detector must be switched on during data-taking, no faulty regions of the detector and/or no noise bursts in the calorimeter cells.
- Electrons in the event should pass loose quality cuts defined in Chapter 3.
- Calorimeter quality flags are required to be good to reject corrupt events due to problems in the calorimeters.
- Events with a jet identified as bad with the JetSelectorTool[4] are vetoed.
- Events with missing information are vetoed.
- At least one reconstructed vertex, primary vertex, is required to be associated with at least three tracks of $p_T > 0.5$ GeV.

Below are the event based cuts that were applied to further reduce background from other SM processes while increasing the signal to background ratio.

Overlap removal

The overlap removal [86] procedure follows object reconstruction. It removes possible duplicates due to the one physical object being reconstructed as two separate objects or two different objects overlapping in the same detector region. In this analysis, there are three different types of overlap removal:

1. $electron/jet$: Since both electron and jet are reconstructed from the cluster of energy deposited in calorimeters, if a reconstructed jet falls within $\Delta R = 0.3$ around a selected electron, both objects are discarded.
2. $muon/electron$: A photon radiated from a muon will make an EM cluster. Since a muon leaves a track in the ID, this energy cluster of a photon in the EM calorimeter will be associated with the ID muon track. Therefore an electron will be reconstructed overlapping with the muon. When an electron and a muon happens to fall within the cone size of $\Delta R = 0.1$, the electron is vetoed.
3. $muon/jet$: Muons that originate from the decay of hadrons are called non-prompt muons. When a jet is reconstructed within $\Delta R < 0.3$ around the selected muon, it is highly likely that the muon comes from hadron. Hence the event is a non-prompt background and is thus vetoed.

[3] Luminosity blocks are the smallest time intervals for data-taking. Each block usually last for two minutes.

[4] The JetSelectorTool removes jets that deposit most of their energy in the scintillator gap between the barrel and end-cap tile calorimeters

Jets

Jets are constructed from calorimeter energy clusters using an anti-k_T algorithm with a cone size of $R = 0.4$. These jets are then calibrated using an E_T and η dependence correction factor based on MC simulations. These calibrated jets are required to have $p_T > 30$ GeV at the hadronic energy scale, which is the calibration energy scale, and $|\eta| < 4.5$. Since $t\bar{t}$ events contain b jets, a $b-$tagging algorithm is used during event selection to identify these $b-$jets with 85% tagging efficiency working point of the MV2 tagger. All the events that have been $b-$tagged are removed, to reduce fake leptons from $t\bar{t}$ decays.

Each event is required to have at least two jets with the transverse momentum of $p_T > 30$ GeV and they should both pass the detector acceptance of $|\eta| \leq 4.5$. The two tagged jets with the highest p_T are selected. The dijet invariant mass is required to be $m_{jj} \geq 500$ GeV. The VBS signal region is extracted by imposing another additional cut on the two tagged jets: the separation distance between the two jets $\Delta y_{jj} = |y_{j1} - y_{j2}| > 2.4$.

Dilepton

Since this analysis is only focusing on same sign $W^{\pm}W^{\pm}$ production, two charged leptons, highest p_T and second-highest p_T, are required to have the same electric charge. In addition, each lepton should have the transverse momentum of $p_T > 25$ GeV, fall within the detector region of $|\eta| < 2.5$ to minimize jets and not overlap with any object. If one of the objects is the muon, is further required to pass ID and tight quality cuts. Otherwise, all electrons used are Tight. The same-sign signal region can also contain charge flip events for electrons coming from $Z/\gamma^* \rightarrow ee$ processes. In order to reduce this type of background, a $Z-$veto cut of $|m_{ee} - m_Z| > 10$ GeV has been applied in the case where both leptons are electrons, the $ee-$channel. Only lepton pairs with the invariant mass $m_{\ell\ell} > 20$ GeV are considered. This requirement reduces the uncertainty that arises when modeling Z/γ^* processes.

Summary of event selection cuts

These selection cuts are summarized below:

1. Event cleaning
2. Overlap removal: $\Delta R(\ell, j) > 0.3$ and $\Delta R(\mu, e) > 0.1$
3. Exactly two leptons (ℓ and ℓ') with same sign, $q_\ell \times q_{\ell'} > 0$. Both leptons have $p_T > 25$ GeV and $|\eta| < 2.5$
4. $m_{\ell\ell'} > 20$ GeV
5. $|m_{\ell\ell'} - m_z| > 10$ GeV in $ee-$channel

6. Two jets with $p_T > 30$ GeV and $|\eta| < 4.5$
7. m_{jj} ≥500 GeV
8. $b-$tagged jet veto at 85% using the MV2 tagger.
8. $\Delta y_{jj} > 2.4$

There are background events that can enter the signal region, and the following section will focus on different background processes.

5.2 Background events

Background events come from three dominant classes of processes; prompt, photon conversion and non-prompt.

5.2.1 Prompt

In the prompt process, both leptons come from the decay of vector bosons: $W^{\pm}Z$. Events from $W^{\pm}Z$ Drell-Yan background processes are simulated exactly as in $W^{\pm}W^{\pm}jj$ production with the cross-section calculation done using VBFNLO [87]. VBFNLO (Vector Boson Fusion at NLO) is a parton level MC program for the simulation of vector boson fusion in hadronic collisions at NLO. The normalization is done at the parton level since the parton showering should not interfere with VBFNLO. The decay products of hard scattering processes are identified using the truth record in Sherpa.

5.2.2 Non-prompt

Non-prompt is defined as a process in which one or both leptons in an event come from hadronic jet decays or when hadrons are misidentified as leptons. This type of process can contribute to the selected same-sign $W^{\pm}W^{\pm}$ VBS events when both leptons pass the analysis selection criteria. Leptons from hadron decays, that is $b-$ and $c-$hadron decays, or jets that are misidentified as leptons are categorised as fake background. The evaluation of the non-prompt background is the primary focus of this thesis.

5.2.3 Photon conversion

The first type of events that enter the signal region contains two prompt leptons with opposite-sign but the charge of one/both leptons is misidentified. This happens when the prompt lepton, say e^{-}, radiates a highly energetic photon that converts into an $e^{-}e^{+}$ pair. The final state electron with the highest momentum will be selected. If that selected lepton is e^{+} then the charge is

misidentified. The general term for the background arising from the misidentification of the electric charge of reconstructed lepton candidates is called *charge flip*. The charge flip rate is significant for electrons and negligible for combined muons [88], since the charge flip effect only happens in final states where at least one electron is present as the charge flip rate is inversely proportional to the square of the mass of the particle. Hence, for muons, the rate of energy loss by electromagnetic radiation is suppressed by $(m_e/m_\mu)^2$ relative to that for electrons. Events that are due to charge flip consist of $t\bar{t}$ decays and Drell-Yan dilepton production. The second type of events that can also enter signal region contains two same-sign leptons that are produced from $W^{\pm}\gamma$ processes. This happens when the photon converts to a pair of e^-e^+ in the detector. The photon conversion background is not evaluated in this thesis.

In the $t\bar{t}$ background sample under study, all the jets cuts are dropped except $b-$jet veto.

Chapter 6

Characterisation of the non-prompt background

MC datasets generated from top processes ($t\bar{t}$) provide the best basis to probe non-prompt backgrounds since they contain a significant amount of jets. Information about particles from event generators, prior to taking detector effects into account, is referred to as MC truth information. To account for detector effects, the truth information is passed to a detector simulation algorithm which models their interaction with detector material [1]. The output of the detector simulation is further passed to digitisation[2] and reconstruction algorithms to produce physics signatures. The truth information is not discarded but stored along with reconstruction information.

Truth objects can be matched to reconstructed objects using MC truth based classification algorithms, which is the main focus of this thesis. To compare the *reco* to *truth*, each reconstructed object is required to have a corresponding truth object within a specified distance ΔR in $\eta - \phi$ space:

$$\Delta R(reco, truth) = \sqrt{\Delta\eta^2 + \Delta\phi^2}. \tag{6.1}$$

By comparing the two objects, MC data can be used to explain mis-modelling of particle signatures in real data. This chapter explains how information from the MC truth record can be useful in classifying $t\bar{t}$ events that fake the signal in the ssWW analysis.

6.1 MC truth event record

A given event usually contains many particles and vertices[3] along the decay chain. Every interaction has a list of incoming and outgoing particles. Outgoing particles of one vertex may become incoming particles of another. Each particle in the event record is assigned a unique identity in the form of

[1] The reader may refer to Chapter 4 for details about event simulation in ATLAS.

[2] Digitisation is the conversion of the analog signal from the detector read out drivers to digital signals that are readable by a computer.

[3] A vertex is the point of interaction.

a barcode[4], status[5], kinematics and a Particle Data Group Identity (pdgId). The pdgId [36] is an identification number of each truth particle and is used instead of the full particle name (e.g electrons are identified as Id 11 and -11 is used for positrons). Understanding the format of the event generator record is an important step in classifying the reconstructed signatures as the truth information may differ from one generator to another. The following section explains the data format used in ATLAS analyses.

6.2 Data format in ATLAS

In the MC data, most reconstructed objects have links to the truth particles from which they were built. The most important one is the link from the inner detector tracks since most reconstructed charged particles leave signatures here. Links to truth objects are stored inside the dataset object containers. In this thesis there are two types of datasets used, *full* and *reduced*. The *full* dataset format contains full information of each event record and object based containers:

- Main truth record: hadrons; Non$-$SM particles and their decay products; W, Z, H, γ and their decay products; $t-$quarks and their decay products; and the ancestors of all of the above
- Dedicated containers: muons, electrons, photons, neutrinos, truth jets and MET

The *full* $t\bar{t}$ dataset used in this thesis has 49386600 simulated pp collision events, which is too large to be analysed conveniently. Hence a *reduced* $t\bar{t}$ dataset was used. The files in the *reduced* dataset are produced directly from the *full* dataset using the derivation framework [89]. This framework has preselection criteria that are looser than the analysis selection criteria in order to allow easy handling of the data and to select events with objects that are interesting[6] for the analysis. Below are the pre-requirements imposed to filter uninteresting events:

- muons requirements: $p_T \geq 15$ GeV, $|\eta| < 2.6$ and muon must leave hits in the ID.
- loose muons requirements : $p_T \geq 20$ GeV and muon passes ID hits cuts.
- electrons requirements : $p_T \geq 15$ GeV, $|\eta| < 2.6$ and electron passes loose, medium or tight quality.

[4]Each particle along the decay chain of the event has a unique number. This number is lower for particles closer to pp collision, as the chain grow the numbers also increase

[5]The status code is used to denote whether the truth particle is stable (code 1) or not (code 3 or 2)

[6]Interesting physics objects to have high transverse momentum, p_T, and must be in a particular region of the detector depending on the process under study.

- loose electrons requirements : $p_T \geq 20$ GeV and electron passes very loose, loose, medium or tight quality.
- each event is required to have at least two charged leptons with any possible combination of the above-selected objects.

All the muons selected in the dataset undergo energy corrections. During the derivation, these corrections are added as part of the pre-requirements, thus the *reduced* dataset will contain muons that have already been corrected while the *full* dataset contain uncorrected muons. Hence, if one has to run over the *full* dataset, the muon energy corrections must be added as part of the analysis selection criteria. The ATLAS experiment has a default tool called MuonCorrectionTool for energy and momentum corrections. The tool takes in information from two tracking systems of the ATLAS detector: the inner detector (ID) and the muon spectrometer (MS). The MS track is then extrapolated back to the ID track, the momentum is corrected for the amount of energy loss due to the material crossed before reaching the MS. Otherwise, if the ID track is not available, the MS track is extrapolated to the interaction point. For this scenario, not only is the momentum corrected but also η and ϕ coordinates. To calculate new corrected values, the tool deploys the smearing method, which smears random variables according to the resolution function that is Gaussian.

After the derivations were complete, the resulting *reduced* $t\bar{t}$ dataset had 11219240 events. This kind of dataset format has:

- Thinned, skimmed or slimmed truth event record.

  Thinning involves removing all unwanted objects from the event following some criteria.

  Slimming involves removing useless information from within the object but keeping the whole object.

  Skimming is where the whole event is removed from the event record.

  All these operations are done to limit the size of data needed to do the analysis.

- Extra dedicated particle containers, such as truth electrons, truth muons, truth jets and MET (for missing transverse energy calculated from the truth level information).
- Some classification; origin and type of truth objects. These variables are linked to dedicated particle containers. More information about how classification variables are extracted from truth information using ATLAS standard algorithms is given in Section 6.3. However, not all objects in the dataset have classification variable, these cases will also be discussed in the same section.

6.3 MC Truth classification methods

Classification of truth particles relies on a pair of numbers, class of particle (type), and where it has come from (origin). The MCTruthClassifier [90] is the ATLAS official classifier tool used to classify reconstructed signatures of the final state candidates according to their truth origin and type. In the truth record of the *reduced* dataset, classification variables are added automatically as extra variables to the particles at the derivation stage (production of *reduced* dataset from *full* dataset). One would expect each reconstructed object passed into MCTruthClassifier to have a pair of these variables, but this is not true, not all the reconstructed objects have a truth origin. The MCTruthClassifier may fail to do truth classifications in some cases. This happens mostly in the cases where the truth type is a hadron but the reconstructed type is a lepton. Classification of these fake leptons is important for understanding the non-prompt background coming from a decay of hadrons and not directly from W boson. For these cases where the ATLAS tool fails, MyMCTruthClassifier tool has been developed to do a better job in classification. This section reports the performance of these tools, which will then later be tested on the datasets. The flow chart depicted in Figure 6.1 shows the flow of information between the tools. The functionality of the tools and their default requirements are detailed in the following sub-sections.

6.3.1 MCTruthClassifier tool

MCTruthClassifier [90] tool was developed by the ATLAS analysis software group in order to classify reconstructed objects such as electrons, muons, taus and photons according to their truth origin or ancestry.

In this tool, the leptons are divided into four categories:

- Isolated (or prompt) - this is a signal particle. For example, a particle with $truthType = 2$ and $truthOrigin = 12$ would be an isolated electron ($isoe$) from a W boson decay.
- Non-isolated (or non-prompt) - particle originates from the decay of a $c-$ or $b-$flavoured hadron (meson or baryon)
- Background (abbreviated as Bkg) - particles not mentioned above are categorised as background including $b\bar{b}$ and $c\bar{c}$ mesons decays.
- Unknown - if the classification algorithm failed to find a production (or original) vertex, it classifies the truth particle as unknown (electron, muons, taus or photons)

In addition to the classification of leptons, the tool can also classify hadrons. In cases where the truth particle is a hadron, the tool will just inform the user that the truth particle is of type hadron (either B,C,S or Light hadron) with non-defined origin. Nuclei with pdgId $\geq 10^8$ and neutrinos are not classified

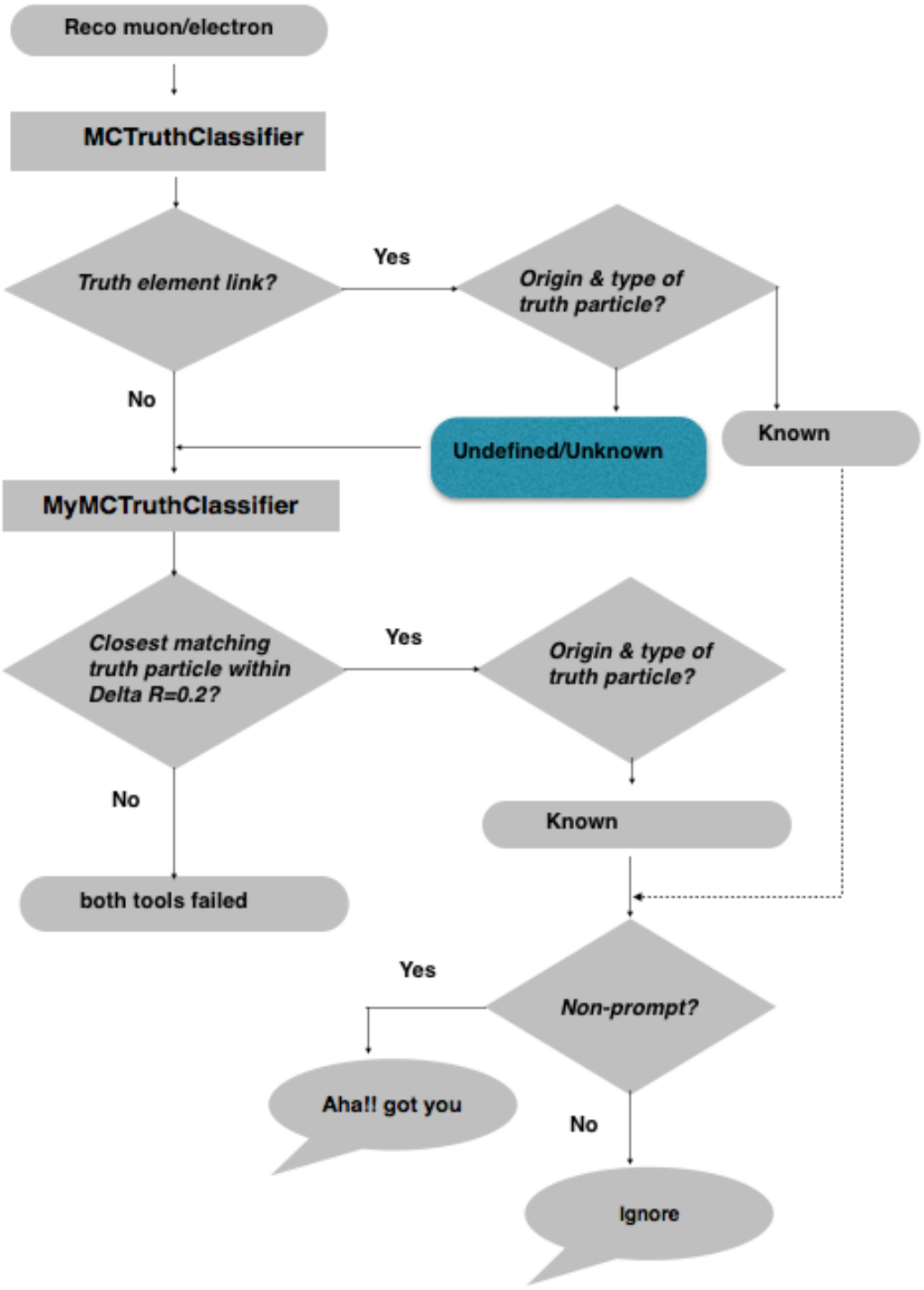

FIGURE 6.1: Flow of information between two classification tools.

by the tool. For these objects, the tool will return unknown type with non-defined origin.

MCTruthClassifier has three classification methods: ID track, forward (beam direction) electron/gamma and jet classifications. ID track classification is based on the link between the reconstructed object track and the truth track. This link is provided by the method called getGenPart(track), which checks for the minimum $\Delta R(recoTrack, truthTrack)$. The default values for cone matching size are $\Delta R < 0.2$ (or $\Delta\phi < 0.2$ for TRT only tracks where the number of hits in the silicon layers is less than 3). For forward electrons and photons there is no track matched by the ID track algorithm, thus the truth particles are extrapolated to the EM calorimeter. In the case of forward electrons the extrapolated truth particles are matched with the cluster in the EM layer requiring the cone size of $\Delta R < 0.15$. In the case of photons, the extrapolated truth particles are required to be stable (with status of 1) and have a barcode less than 200000. These truth particles are then matched to the cluster within an elliptical cone of $\Delta\eta \times \Delta\phi = 0.025 \times 0.050$. As mentioned above, the MCTruthClassifier method is also used to classify jet with the same default cone matching of $\Delta R < 0.2$. It provides the origin of the jets by looking for the ancestry of all particles involve in the hadronisation until the parton level particle is found. Thus, the process giving rise to a particular jet is defined from this parton level particle. For an example, a parton level particle of a $b-$jet is a $b-$quark which then undergoes the hadronisation process and becomes a $B-$hadron. Table 6.1 gives a summarised classification scheme of the MCTruthClassifier extracted from Ref. [90].

6.3.2 MyMCTruthClassifier tool

For the cases where a lepton passed the selection criteria but was not decorated with classification variables during the derivation, MyMCTruthClassifier tool takes the same lepton and returns the list of all the closest *truth* particles within the cone of $\Delta R(reco, truth) \leq 0.2$ and energy of $E_{truth} > 0.8 \times E_{reco}$. At the next stage, it picks the particle with minimum ΔR_{min} from the list as the truth type. If the truth type is a lepton and its truth parent is the W boson, then the truth type will be an isolated lepton with truth origin as a W boson. Otherwise, if the truth lepton originates from the decay of $b-/c-$flavoured hadron, the truth type will be a non-isolated lepton. The origin of the non-isolated lepton may differ depending on the flavour of a quark; giving rise to hadronisation. For cases where the truth particle is not a lepton, MyMCTruthClassifier returns pdgId of this truth particle as the closest truth type. The truth origin is extracted from the ancestry tree of the truth particle (this is done manually by the user from looking at the truth decay chain for each event with a lepton of non-defined truth origin).

MyMCTruthClassifier follows the same classification scheme as MCTruthClassifier with additional particles such as K, π, proton (p), nucleus and parton. It was developed by the author when the MCTruthClassifier was unable

TABLE 6.1: Standard classification scheme used in ATLAS MC data analysis.

truthType	truthOrigin	Comments
Unknown	Non-defined	Nuclear fragments (particles with pdgid $\geq 10^8$) and neutrinos
Hadron	Non-defined	Includes Bottom hadron, Charm hadron, Strange hadron or light hadron
Unknown e, μ, τ and γ	Non-defined	Algorithm failed to defined origin or particle has no production vertex
Isolated e, μ, τ and γ	W	Single lepton originating directly from W
	top quark	$t \to W \to \ell\nu$
Non-Isolated e, μ, τ and γ	Bottom meson	Non-prompt (fake) leptons/photons from B hadrons
	Bottom baryon	
	Charmed meson	Non-prompt (fake) leptons/photons from C hadrons
	Charmed baryon	
	τ decay	$\tau \to e\nu/\mu\nu$, originating from gauge bosons are excluded
Non-Isolated γ	FSRphoton	Photon originating from final state radiation
Bkg e	γ conversion	Electron from QED radiation (Isolated lepton radiated a photon)
	Dalitz decay	Electron from QED radiation (light meson from a jet goes to 2 photons)
Bkg μ	$c\bar{c}$ meson	Muon from QCD radiation

to classify all events. The Input to this new truth matching algorithm are the particles that were defined as row 1-3 in Table 6.1. The classification scheme of this tool is shown in Table 6.2.

All the methods that are used to classify reconstructed object according to their truth origin and type have been described. Section 6.4 presents the implementation of these methods and procedure followed to classify all $t\bar{t}$ events that pass the ssWW selection cuts.

TABLE 6.2: New classification scheme for truth particles with none defined origin as an output of MCTruthClassifier tool.

truthType	truthOrigin	Comments
Isolated e, μ, τ and γ	W	single lepton originating directly from W
	top quark	$t \to W \to \ell\nu$
Non-Isolated e, μ, τ and γ	Bottom meson	Non-prompt (fake) leptons/photons from B hadrons
	Bottom baryon	
	Charmed meson	Non-prompt (fake) leptons/photons from C hadrons due to the W decaying hadronically
	Charmed baryon	
	τ decay	$\tau \to e\nu/\mu\nu$, originating from gauge bosons are excluded
K, π and p	Non-defined	algorithm failed to defined origin
K	Charmed hadron	Kaon from a hadronically decaying W boson or B hadron
	s quark decay	A quark originating from W boson
	u quark decay	A quark from pp collision
π	Strange hadron	Hadronic jet from W boson
	Charmed hadron	
	Light hadron	
	$W \to \tau \to \pi$	Hadronic τ leptons
Nucleus	Non-defined	algorithm failed to defined origin where the closest truth particles has pdgid $\geq 10^8$)
Parton	Non-defined	algorithm failed to defined origin of a jet
Unknown	Non-defined	algorithm failed

6.4 Classification of $t\bar{t}$ events

At the beginning of the classification algorithm, 11219240 events from the *reduced* $t\bar{t}$ dataset listed in Appendix A.1 were required to pass all the ssWW analysis cuts (in Chapter 4) excluding jet cuts in order to allow more $t\bar{t}$ events . The resulting events were then classified using output variables of MCTruthClassifier, $truthOrigin$ and $truthType$. After running over the whole dataset, 1444 events were classified out of 1456. From these numbers, 12 events were not classified because they each contained a $reco$ lepton with unknown truth type from undefined truth origin. All these 12 cases where the $reco$ leptons had an unknown $truthOrigin$, got passed into MyMCTruthClassifier. However, there were still 10 unclassified events which will be discussed in Section 6.4.2. Table 6.3 shows different classified cases where this type of background can end up with two same charge leptons in the final

state. It is important to note that each class can appear more than once in the dataset. The arrangement of columns is of no particular order, this means that particles in the first column may not necessarily have the highest momentum (leading lepton) in the events. Electric charge with red colour and a question mark next to it indicates that the charge of the truth origin has not been verified yet. This part of the analysis will follow in the next section.

TABLE 6.3: Classified $t\bar{t}$ events from the *reduced* $t\bar{t}$ dataset listed in Appendix A.1.

$\ell^{\pm}_{reco1}$	$\ell^{\pm}_{reco2}$
$truthOrigin_1 \rightarrow truthType_1$	$truthOrigin_2 \rightarrow truthType_2$
$W^{\pm} \rightarrow isolated\_\mu^{\pm}$	$PhotonConv.^{0?} \rightarrow Bkg\_e^{\pm}$
$W^{\pm} \rightarrow isolated\_e^{\pm}$	$PhotonConv.^{0?} \rightarrow Bkg\_e^{\pm}$
$W^{\pm} \rightarrow isolated\_\mu^{\pm}$	$W^{\mp ?} \rightarrow isolated\_e^{\mp}$
$W^{\pm} \rightarrow isolated\_e^{\pm}$	$W^{\mp ?} \rightarrow isolated\_e^{\mp}$
$PhotonConv.^{0?} \rightarrow Bkg\_e^{\pm}$	$PhotonConv.^{0?} \rightarrow Bkg\_e^{\pm}$
$W^{\pm} \rightarrow isolated\_\mu^{\pm}$	$FSRPhoton \rightarrow nonIsolated\_\gamma$
$W^{\pm} \rightarrow isolated\_\mu^{\pm}$	$BottomMeson^{\mp ?} \rightarrow nonIsolated\_\mu^{\pm}$
$W^{\pm} \rightarrow isolated\_e^{\pm}$	$BottomMeson^{\mp ?} \rightarrow nonIsolated\_\mu^{\pm}$
$W^{\pm} \rightarrow isolated\_\mu^{\pm}$	$BottomMeson^{\mp ?} \rightarrow nonIsolated\_e^{\pm}$
$W^{\pm} \rightarrow isolated\_e^{\pm}$	$BottomMeson^{\mp ?} \rightarrow nonIsolated\_e^{\pm}$
$W^{\pm} \rightarrow isolated\_e^{\pm}$	$BottomBaryon^{\mp ?} \rightarrow nonIsolated\_\mu^{\pm}$
$W^{\pm} \rightarrow isolated\_\mu^{\pm}$	$BottomBaryon^{\mp ?} \rightarrow nonIsolated\_\mu^{\pm}$
$W^{\pm} \rightarrow isolated\_\mu^{\pm}$	$CharmedMeson^{\mp ?} \rightarrow nonIsolated\_\mu^{\pm}$
$W^{\pm} \rightarrow isolated\_e^{\pm}$	$CharmedMeson^{\mp ?} \rightarrow nonIsolated\_\mu^{\pm}$
$W^{\pm} \rightarrow isolated\_\mu^{\pm}$	$CharmedMeson^{\mp ?} \rightarrow nonIsolated\_e^{\pm}$
$W^{\pm} \rightarrow isolated\_\mu^{\pm}$	$CharmedBaryon^{\mp ?} \rightarrow nonIsolated\_\mu^{\pm}$
$W^{\pm} \rightarrow isolated\_\mu^{\pm}$	$TauLep^{\mp ?} \rightarrow nonIsolated\_\mu^{\pm}$
$W^{\pm} \rightarrow isolated\_e^{\pm}$	$TauLep^{\mp ?} \rightarrow nonIsolated\_\mu^{\pm}$
$W^{\pm} \rightarrow isolated\_\mu^{\pm}$	$W^{\mp ?} \rightarrow Isolated\_\mu^{\pm}$
$W^{\pm} \rightarrow isolated\_\mu^{\pm}$	$c\bar{c}Meson^{\mp ?} \rightarrow Bkg\_\mu^{\pm}$
$W^{\pm} \rightarrow isolated\_\mu^{\pm}$	$c\bar{c}Meson^{\mp ?} \rightarrow Bkg\_e^{\pm}$
$W^{\pm} \rightarrow isolated\_e^{\pm}$	$c\bar{c}Meson^{\mp ?} \rightarrow Bkg\_\mu^{\pm}$
$W^{\pm} \rightarrow isolated\_\mu^{\pm}$	$DalitzDecay^{\mp ?} \rightarrow Bkg\_e^{\pm}$
$W^{\pm} \rightarrow isolated\_e^{\pm}$	$DalitzDecay^{\mp ?} \rightarrow Bkg\_e^{\pm}$

6.4.1 Electric charge investigation

Investigating the charge of MC truth helps in identifying whether the final state leptons of the same sign during object reconstruction are due to charge misidentification or a physical process like $B-$ hadron.

Charge mis-identification

Even though most of the events from top production were removed by the $b-$veto and the same sign charge cuts, some events could still pass the final selection cut due to charge misidentification of one electron. The ATLAS official classifier tool classifies them as background electrons from photon

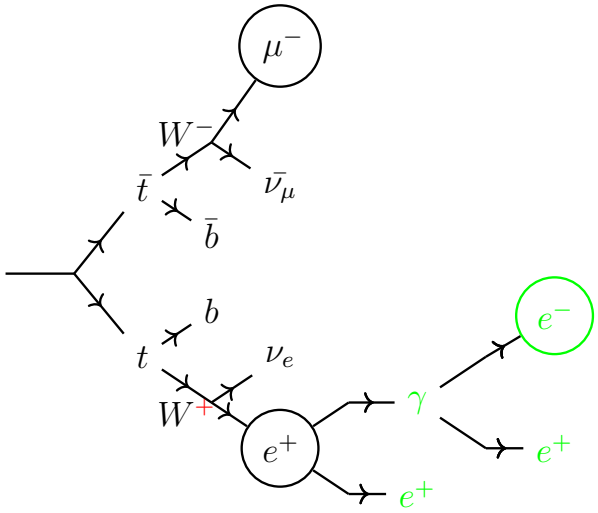

FIGURE 6.2: Illustration of photon conversion process in the final state.

conversions. These events, shown in rows 2,3 and 4 of Table 6.4, they became the most dominant class in the classification list of $t\bar{t}$ dataset. However, there are classes of events that the ATLAS official tool classifies as two isolated leptons with opposite sign but when looking at the details of the truth record, the reason they pass the selection is that there is a photon conversion that is not property recorded by the tool. According to the study, all the event classes in Table 6.4 are due to photon conversion but the tool separates them and it is not understood why.

TABLE 6.4: List of events due to charge flip as a result of photon conversion.

$truthOrigin_1 \rightarrow truthType_1$	$truthOrigin_2 \rightarrow truthType_2$
$W^{\pm} \rightarrow isolated\_\mu^{\pm}$	$PhotonConv.^{0?} \rightarrow Bkg\_e^{\pm}$
$W^{\pm} \rightarrow isolated\_e^{\pm}$	$PhotonConv.^{0?} \rightarrow Bkg\_e^{\pm}$
$PhotonConv.^{0?} \rightarrow Bkg\_e^{\pm}$	$PhotonConv.^{0?} \rightarrow Bkg\_e^{\pm}$
$W^{\pm} \rightarrow isolated\_\mu^{\pm}$	$W^{\mp?} \rightarrow isolated\_e^{\mp}$
$W^{\pm} \rightarrow isolated\_e^{\pm}$	$W^{\mp?} \rightarrow isolated\_e^{\mp}$

The truth chain of these events does not show any photon conversion process since this happens within GEANT4 toolkit that simulates the detector response (indicated with green in Figure 6.2).

Non-prompt leptons

The sources of non-prompt/fake leptons are hadronic jets. Table 6.5 shows different origins of fake leptons as defined by classification tools. Figure 6.3 demonstrates how each of these event classes were followed in the event chain until the final state fake lepton was recovered. In event number 10679726

of the $t\bar{t}$ dataset, the $b-$quark hadronised to a $B-$hadron. When there is b hadronisation involved along the decay channel, a lepton from hadron decay may be reconstructed as isolated electron. This particular event has two reconstructed leptons, the first lepton is associated with *truth* e^- and the second lepton is associated with *truth* μ^-. Thus, the event passed the same sign selection cut of the analysis.

TABLE 6.5: List of events with non-prompt (fake) lepton in the final state. In the truth MC data, pdgId 92 indicates fragmentation.

$truthOrigin_1 \rightarrow truthType_1$	$truthOrigin_2 \rightarrow truthType_2$
$W^{\pm} \rightarrow isolated\_\mu^{\pm}$	$BottomMeson^{\mp?} \rightarrow nonIsolated\_\mu^{\pm}$
$W^{\pm} \rightarrow isolated\_e^{\pm}$	$BottomMeson^{\mp?} \rightarrow nonIsolated\_\mu^{\pm}$
$W^{\pm} \rightarrow isolated\_\mu^{\pm}$	$BottomMeson^{\mp?} \rightarrow nonIsolated\_e^{\pm}$
$W^{\pm} \rightarrow isolated\_e^{\pm}$	$BottomMeson^{\mp?} \rightarrow nonIsolated\_e^{\pm}$
$W^{\pm} \rightarrow isolated\_e^{\pm}$	$BottomBaryon^{\mp?} \rightarrow nonIsolated\_\mu^{\pm}$
$W^{\pm} \rightarrow isolated\_\mu^{\pm}$	$BottomBaryon^{\mp?} \rightarrow nonIsolated\_\mu^{\pm}$
$W^{\pm} \rightarrow isolated\_\mu^{\pm}$	$TauLep^{\mp?} \rightarrow nonIsolated\_\mu^{\pm}$
$W^{\pm} \rightarrow isolated\_e^{\pm}$	$TauLep^{\mp?} \rightarrow nonIsolated\_\mu^{\pm}$

As mentioned earlier, single τ leptons from W bosons were not considered in the analysis as final state objects. However, it was found that a τ from B hadrons or $W \rightarrow \tau \rightarrow lightmeson(a_1(1260))$ is part of the non-prompt background. This was confirmed by looking at the details of the truth record in event number 3818238 and 2032282. The corresponding event chains of these events are in Figure 6.3.

Non-prompt leptons can also come from a hadronically decaying W boson. The W boson decays to a pair of c and s quarks. Just like the b quark, the c quark hadronises to become a c hadron. Different categories of this process are shown in Table 6.6.

TABLE 6.6: List of events with non-prompt (fake) lepton from hadronisation of c quarks.

$truthOrigin_1 \rightarrow truthType_1$	$truthOrigin_2 \rightarrow truthType_2$
$W^{\pm} \rightarrow isolated\_\mu^{\pm}$	$CharmedMeson^{\mp?} \rightarrow nonIsolated\_\mu^{\pm}$
$W^{\pm} \rightarrow isolated\_e^{\pm}$	$CharmedMeson^{\mp?} \rightarrow nonIsolated\_\mu^{\pm}$
$W^{\pm} \rightarrow isolated\_\mu^{\pm}$	$CharmedMeson^{\mp?} \rightarrow nonIsolated\_e^{\pm}$
$W^{\pm} \rightarrow isolated\_\mu^{\pm}$	$CharmedBaryon^{\mp?} \rightarrow nonIsolated\_\mu^{\pm}$

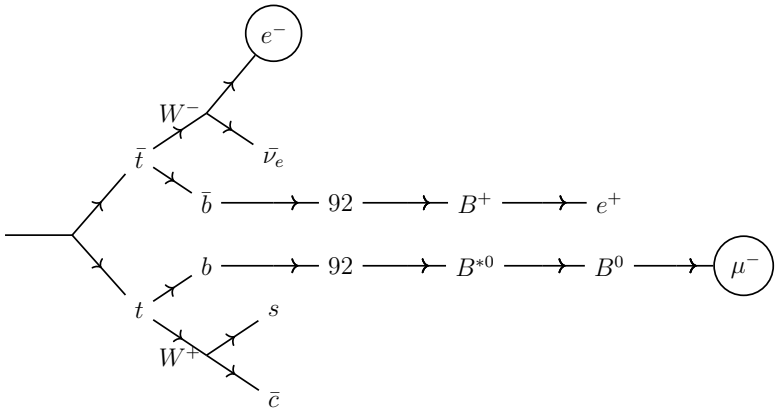

(A) Event number 10679726

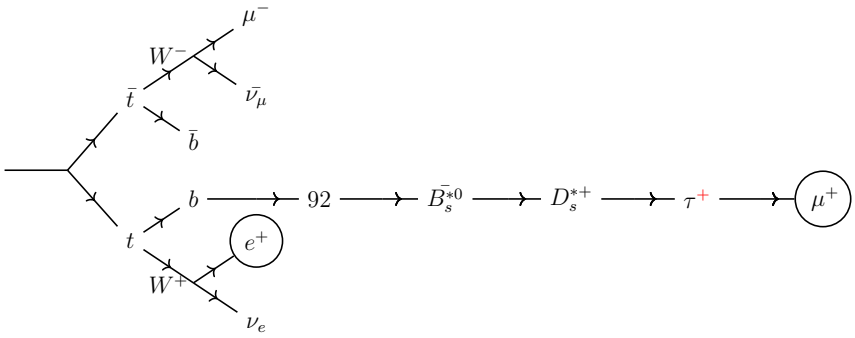

(B) Event number 3818238

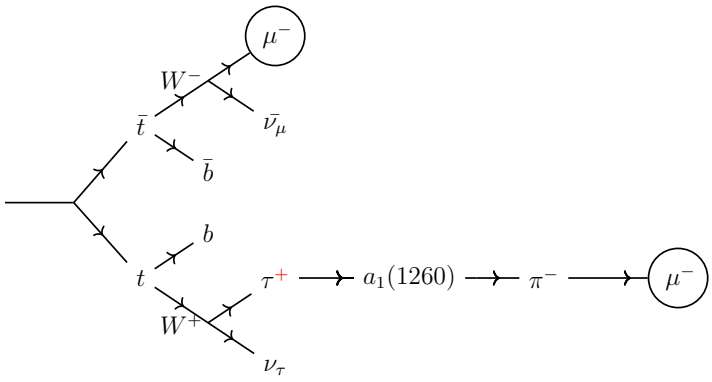

(C) Event number 2032282

FIGURE 6.3: Illustration of $t\bar{t}$ events with at least one non-prompt lepton.

Investigation of mis-modeling

Mis-modeling of $t\bar{t}$ events can happen in the case where an event has two leptons initially produced with opposite charge but one get assigned an incorrect charge and/or incorrect type due to detector effects. Therefore, events with such types of leptons can contribute to the two same sign leptons signal region. An example of such events is illustrated in Figure 6.4. This event, classified in Table 6.7 as $W^- \rightarrow isolated\_\mu^-$ and $W^+ \rightarrow isolated\_\mu^-$, was supposed to be classified as $W^- \rightarrow isolated\_\mu^-$ and $W^+ \rightarrow isolated\_e^+$, respectively. This was confirmed by computing the distance in $\eta - \phi$ space and the energy (E) between a $reco$ lepton and a truth level lepton.

As seen in the table and in the truth record shown in the diagram, the first reconstructed lepton ($\ell^{\pm}_{reco1}$) with values of $\eta = 0.26$, $\phi = -0.72$ and $E = 27.40$ was correctly matched to an isolated truth muon (μ^-) with $\eta = 0.26$, $\phi = -0.72$ and $E = 27.50$ GeV.

The second reconstructed lepton ($\ell^{\pm}_{reco2}$) with values of $\eta = -2.38$, $\phi = 1.90$ and $E = 6583.81$ GeV was matched to an isolated truth muon (μ^-), which originates from an opposite charge W boson. Thus, the charge has been incorrectly assigned. In addition, the truth record shows that the second muon with a negative charge in the event is from the decay of a $B-$hadron (non-isolated μ^-) with values of $\eta = -2.70$, $\phi = 2.64$ and $E = 43.25$ GeV. The distance between $\ell^{\pm}_{reco2}$ and this non-isolated μ^- is $\Delta R(\ell^{\pm}_{reco2}, truth\_\mu^-) = 0.81$ and the energy of μ^- is 0.66 of $\ell^{\pm}_{reco2}$. Hence the second reconstructed lepton was also assigned an incorrect truth origin and truth type.

Nonetheless, in the truth record there was one prompt electron (e^+) with values of $\eta = -2.38$, $\phi = 1.90$ and $E = 941.31$ GeV produced along with a photon (γ) of $\eta = -2.39$, $\phi = 1.97$ and $E = 0.07$ GeV. This truth level e^+ is in the same coordinate as $\ell^{\pm}_{reco2}$. The only possible explanation to this ambiguity is that at the reconstruction level, γ might have converted to a pair of opposite charge muons. So if a negative charge muon from photon conversion overlaps with e^+ then μ^- was selected. However the sum of energies of e^+ and γ (941.31+0.07=941.38 GeV) is still smaller than the energy of $\ell^{\pm}_{reco2}$ (6583.81 GeV), this was not well understood. For the reason that ($\ell^{\pm}_{reco2}$) has an energy approximately equal to the energy of each colliding proton in the beam pipe, there must be something else going on in the event or rather the truth record is broken.

TABLE 6.7: Truth level information of a mis-modeled lepton in event number 457711.

$\ell^{\pm}_{reco1}(\eta = 0.26, \phi = -0.72, E = 27.40$ GeV)	$\ell^{\pm}_{reco2}(\eta = -2.38, \phi = 1.90, E = 6583.81$ GeV)
$truthOrigin_1 \rightarrow truthType_1$	$truthOrigin_2 \rightarrow truthType_2$
$W^- \rightarrow isolated\_\mu^-$	$W^+ \rightarrow isolated\_\mu^{-?}$

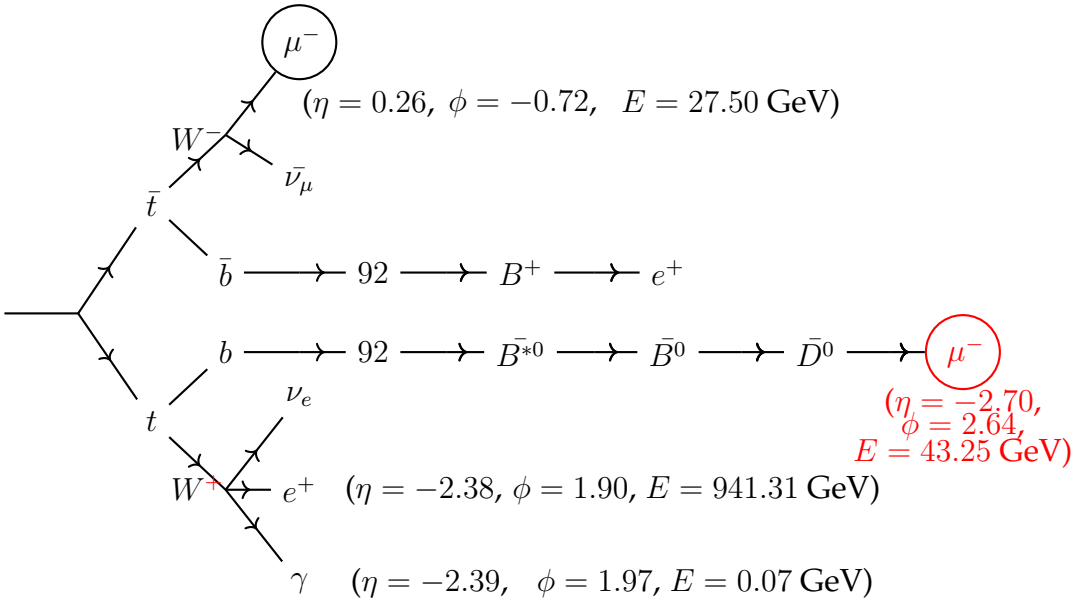

FIGURE 6.4: Truth level decay chain of event number 457711 with a mis-modeled lepton.

6.4.2 Non-defined truth origins

A total of ten events in the *reduced* dataset is not classified. Each of the unclassified event cases shown in Table 6.8 may occur more than once in the dataset. As mentioned above, the *full* dataset format has the full truth record. It was thought that it will be better to look for these 10 unclassified events in the *full* $t\bar{t}$ dataset. To make sure that the same objects were being used in the *full* dataset as in *reduced* dataset, the η and ϕ space between the $reco$ leptons from the *reduced* dataset and the $reco$ leptons from the *full* dataset of the same event was set to zero.

$$\Delta R(recoLepton_{full}, recoLepton_{reduced}) = 0 \tag{6.2}$$

There was only one event which failed this requirement with $\Delta R = 0.002$. This event displays abnormal behaviour and it will be explained at the end of the section. For now, the discussion is only going to be about the 9 events that were able to pass this criterion.

TABLE 6.8: Unclassified $t\bar{t}$ events from the *reduced* $t\bar{t}$ dataset.

$\ell^{\pm}_{reco1}$	$\ell^{\pm}_{reco2}$
$truthOrigin_1 \rightarrow truthType_1$	$truthOrigin_2 \rightarrow truthType_2$
$W^{\pm} \rightarrow isolated\_\mu^{\pm}$	$Undefined^{\mp}? \rightarrow Unknown^{\pm}$
$W^{\pm} \rightarrow isolated\_e^{\pm}$	$Undefined^{\mp}? \rightarrow Unknown^{\pm}$
$BottomMeson^{\mp} \rightarrow nonIsolated\_\mu^{\pm}$	$Undefined^{\mp}? \rightarrow Unknown^{\pm}$
$Undefined^{\mp}? \rightarrow isolated\_\mu^{\pm}$	$Undefined^{\mp}? \rightarrow Unknown^{\pm}$
$Undefined^{\mp}? \rightarrow isolated\_e^{\pm}$	$Undefined^{\mp}? \rightarrow Unknown^{\pm}$

As in the *reduced* data, similar classification algorithm was followed in the *full* data . However, the maximum cone size of $\Delta R = 0.2$ was increased to a half coverage of the ATLAS detector $\Delta R = 3.5$ in MyMCTruthClassifier, keeping the energy requirement the same. This format of the event record was expected to do better in classification since the links to the truth objects are not broken. Unfortunately, only 2 events were classified. At this point,

TABLE 6.9: Classification of $t\bar{t}$ events from the *full* dataset containing non-skimmed event record.

$\ell^{\pm}_{reco1}$	$\ell^{\pm}_{reco2}$
$truthOrigin_1 \rightarrow truthType_1$	$truthOrigin_2 \rightarrow truthType_2$
$W^{\pm} \rightarrow isolated\_e^{\pm}$	$BottomMeson^{\mp} \rightarrow \gamma$
$W^{\pm} \rightarrow isolated\_\mu^{\pm}$	$BottomMeson^{\mp} \rightarrow \pi^{\pm}$
$W^{\pm} \rightarrow isolated\_e^{\pm}$	$Undefined^{\mp}? \rightarrow Nucleus$ (appeared three times)
$W^{\pm} \rightarrow isolated\_\mu^{\pm}$	$Undefined^{\mp}? \rightarrow \pi^0$
$W^{\pm} \rightarrow isolated\_e^{\pm}$	$Undefined^{\mp}? \rightarrow \bar{u}$
$W^{\pm} \rightarrow isolated\_\mu^{\pm}$	$Undefined^{\mp}? \rightarrow d$
$BottomMeson^{\mp} \rightarrow nonIsolated\_\mu^{\pm}$	$Undefined^{\mp}? \rightarrow \pi^{\pm}$

1448 events are classified. There are 8 more remaining, including one event that was not well understood. The only way to understand these events is to look at their truth record, the outcomes of which can be seen in Figure 6.5. The origins of truth particles are indicated with blue color corresponding to the undefined in Table 6.9.

Abnormal event

Event number 36677173 had two different outputs in the *reduced* and *full* data . When running the *reduced* data, one tight electron passed all the cuts and got classified, while a medium/tight muon passed all the cuts but failed to classified. In the *full* data there were two very loose $reco$ muons not passing the lepton definition cuts and one tight electron passing all the cuts. Following is the description of this strange event from the *full* data.

Since *full* datasets contain reconstructed muon objects that have uncorrected energy, it is the user's task to add muon energy corrections as part of the analysis selection. Taking the advantage of that, it was decided to check the kinematic variables of both of these very loose muons before and after the muon corrections. It was discovered that η and ϕ variables do not get corrected, only the energy. The next step was to check the kinematics and energy difference between the muon from the *reduced* dataset and the closest loose muons in the *full* dataset, and here are the results:

- $reco$ muon from *reduced* data ($reco_{reduced}$ muon):
  $E = 150.20$ GeV, $\eta = -2.427263$ and $\phi = 1.723730$
- $reco$ muon from *full* ($reco_{full}$ muon):
  $E = 11.79$ GeV, $\eta = -2.428368$ and $\phi = 1.715684$

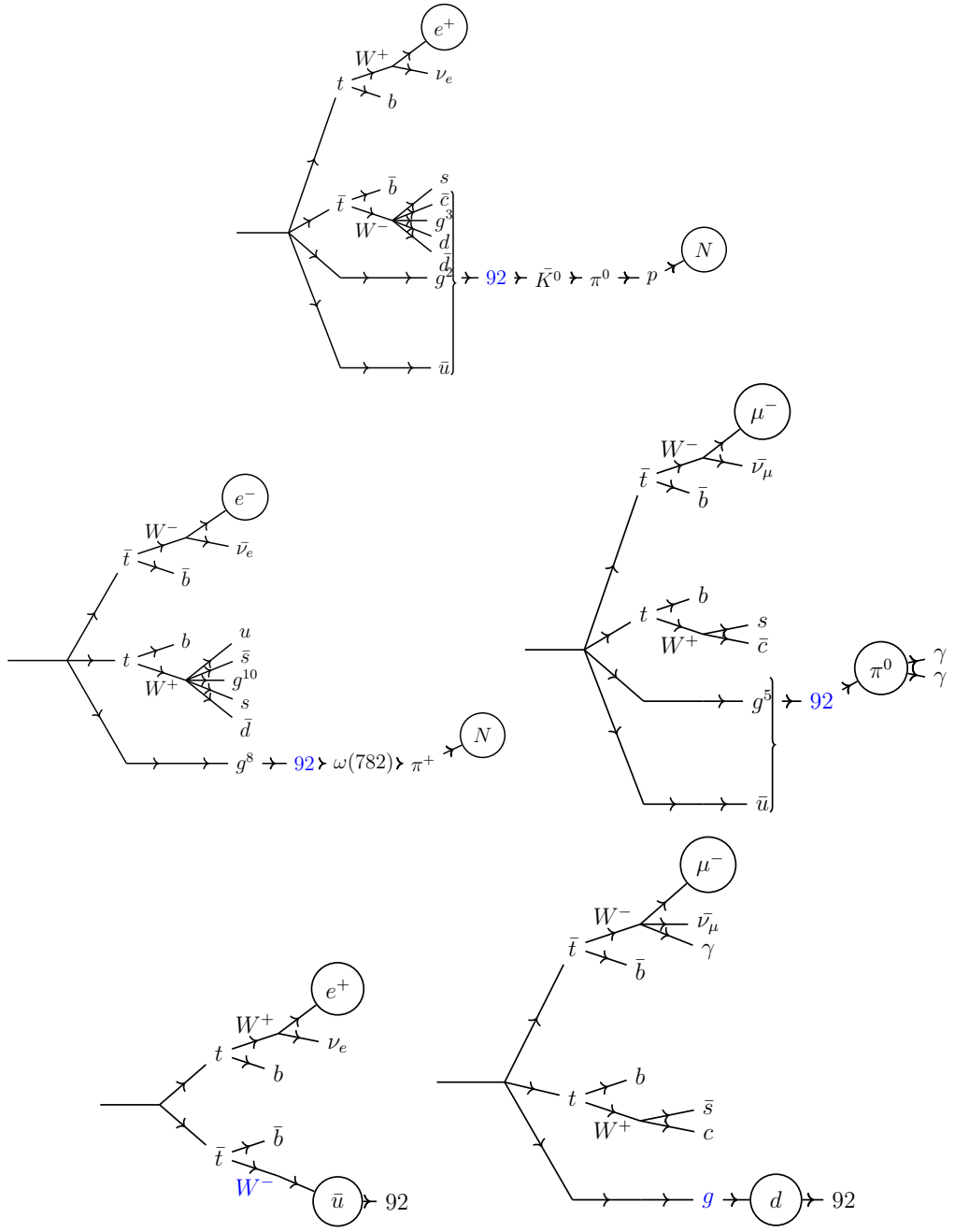

FIGURE 6.5: Decay chain for $t\bar{t}$ events that failed classification tools. The truth types are circled.

The η and ϕ values seemed to be very similar but the reason behind the differences was not well understood. The energy of the $reco_{full}$ muon is far smaller. A possible explanation to this might be that the muon correction tool uses a smearing method that is based on random variables. Thus the output of the correction tool might differ each time smearing is applied. Using this very loose $reco_{full}$ muon (failed ID cuts) in MyMCTruthClassifier with the energy requirement removed, an electron (in the circle) was found to be the closest truth particle originating from the jet (this is indicated with blue in Figure 6.6).

TABLE 6.10: Truth classification of the last event in $t\bar{t}$ background.

$\ell^{\pm}_{reco1}$	$\ell^{\pm}_{reco2}$
$truthOrigin_1 \rightarrow truthType_1$	$truthOrigin_2 \rightarrow truthType_2$
$W^{\pm} \rightarrow isolated\_e^{\pm}$	$Undefined^{\mp}? \rightarrow Unknown$

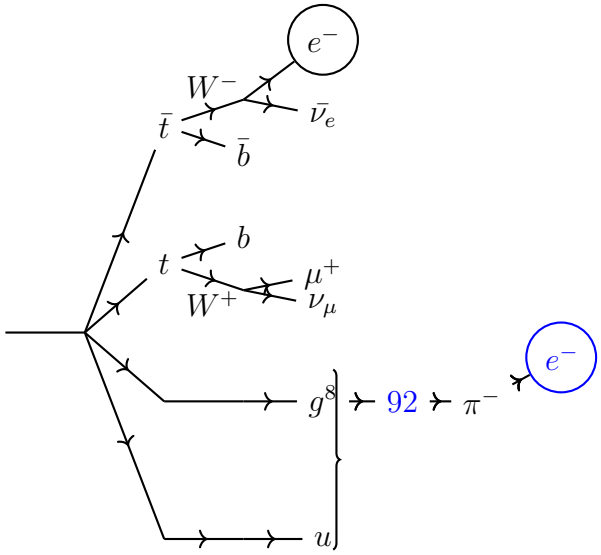

FIGURE 6.6: Truth decay chain in the last event of $t\bar{t}$.

The final results from the classification methods and truth decay chains are combined together in Chapter 7.

Chapter 7

Results and discussion

This chapter presents the results from the 2015 MC dataset simulated at 13 TeV. Section 7.1 presents results obtained from classification methods and MC truth decay chains in Chapter 6. Section 7.2 presents the results from both the same sign $W^{\pm}W^{\pm}jj$ signal and $t\bar{t}$ background. As mentioned in the previous chapter, all results were obtained by dropping selections on the multiplicity and the jet kinematics to allow more $t\bar{t}$ events. The histograms shown in this chapter are referred to as "ATLAS simulation work in progress", to indicate that the ATLAS ssWW analysis is still under study and different MC samples are still being validated.

7.1 Background events observation

Events that survived a $b-$jet veto cut were required to have at least two highest p_T $reco$ leptons (passing object selections) of the same electric charge and must not originate from a $Z-$boson. The event yield after each selection is given in Table 7.1.

TABLE 7.1: Events yield in $t\bar{t}$ sample.

Cut definition	**Yield event**	**Percentage** (%)
preselection	2938267	100.00
b veto	783673	26.67
atleast 2 leading leptons, Z veto	180836	6.15
2 same sign leptons, $m_{\ell\ell} > 20$ GeV, $\Delta R_{\ell\ell} > 0.3$	1456	0.05

When looking at the top quark decays in Chapter 2, a SM process like $t\bar{t}$ should produce two opposite sign leptons. However, the yield events after same sign requirement shows that it is possible to reconstruct same sign lepton events in $t\bar{t}$ background. In Chapter 6, these events were found to be from different sources, either known (Table 6.3) or undefined (Table 6.9). After investigation of undefined sources and electric charge using the MC truth decay chains, all the events in $t\bar{t}$ sample were classified and the final results are shown in Table 7.2. Each row in the table contains each event class; and the number of times the same event class appeared when running over the sample is indicated in the third column. A category with a question mark

in the table belongs to the strange event that was discussed in the previous chapter, its truth record has been given in Appendix A.3.

The results in Table 7.2 show that there are 8 different categories where $t\bar{t}$ background can fake the signature of $l^{\pm}\nu l^{\pm}\nu jj$ events. The combined output of both classification tools shows that the dominant class is due to photon conversion with 75.4%, followed by b jets with 22.0% and c jets with 1.03%. The other 1.57% is the sum of all the remaining categories. Breaking down these event classes by channels; $e\mu-$channel has 56.80% of events, $ee-$channel has 31.80% of events and $\mu\mu-$channel has 10.58% of events. These channels still show that events containing an electron are still dominant due to high charge flip rate. According to these findings, trying to reduce $t\bar{t}$ background using an understanding of non-prompt event classes will not have much effect because events with charge flip from electrons are still dominant. Hence, the aim of the thesis, which is to probe jets in the non-prompt background, has not really been achieved. So the way to suppress these background contributions has to do with $b-$jets identification in ATLAS. There are different ways to look for the region where a particular sample of events can be discriminated, such as missing transverse energy distribution. For the scope of this thesis, this has been idealized on the kinematic variables (η and p_T). The discussion is given in the following section. The ssWW analyses group is investigating more cuts that can possibly evade background events.

TABLE 7.2: Classification of each event in the $t\bar{t}$ sample together with its corresponding number of appearances.

$\ell_1^{\pm}$ (correct)	$\ell_2^{\pm}$(incorrect)	
$truthOrigin_1 \rightarrow truthType_1$	$truthOrigin_2 \rightarrow truthType_2$	number of appearances
$W^{\pm} \rightarrow \mu^{\pm}$	$PhotonConv. \rightarrow Bkg\_e^{\pm}$	660
$W^{\pm} \rightarrow e^{\pm}$	$PhotonConv. \rightarrow Bkg\_e^{\pm}$	437
$W^{\pm} \rightarrow \mu^{\pm}$	$FSRPhoton \rightarrow \gamma$	1
$W^{\pm} \rightarrow \mu^{\pm}$	$BottomMeson^{\mp} \rightarrow \mu^{\pm}$	131
$W^{\pm} \rightarrow e^{\pm}$	$BottomMeson^{\mp} \rightarrow \mu^{\pm}$	124
$W^{\pm} \rightarrow \mu^{\pm}$	$BottomMeson^{\mp} \rightarrow e^{\pm}$	22
$W^{\pm} \rightarrow e^{\pm}$	$BottomMeson^{\mp} \rightarrow e^{\pm}$	22
$W^{\pm} \rightarrow e^{\pm}$	$BottomBaryon^{\mp} \rightarrow \mu^{\pm}$	11
$W^{\pm} \rightarrow \mu^{\pm}$	$BottomBaryon^{\mp} \rightarrow \mu^{\pm}$	7
$W^{\pm} \rightarrow \mu^{\pm}$	$BottomMeson^{\mp} \rightarrow \pi^{\pm}$	1
$W^{\pm} \rightarrow e^{\pm}$	$BottomMeson^{\mp} \rightarrow \gamma$	1
$W^{\pm} \rightarrow \tau^{\pm} \rightarrow \pi^{\pm}$	$BottomMeson^{\mp} \rightarrow \mu^{\pm}$	1
$W^{\pm} \rightarrow \mu^{\pm}$	$CharmedMeson^{\mp} \rightarrow \mu^{\pm}$	9
$W^{\pm} \rightarrow e^{\pm}$	$CharmedMeson^{\mp} \rightarrow \mu^{\pm}$	4
$W^{\pm} \rightarrow \mu^{\pm}$	$CharmedMeson^{\mp} \rightarrow e^{\pm}$	1
$W^{\pm} \rightarrow \mu^{\pm}$	$CharmedBaryon^{\mp} \rightarrow \mu^{\pm}$	1
$W^{\pm} \rightarrow \mu^{\pm}$	$TauLep^{\mp} \rightarrow \mu^{\pm}$	2
$W^{\pm} \rightarrow e^{\pm}$	$TauLep^{\mp} \rightarrow \mu^{\pm}$	1
$W^{\pm} \rightarrow \mu^{\pm}$	$c\bar{c}Meson^{\mp} \rightarrow Bkg\_\mu^{\pm}$	4
$W^{\pm} \rightarrow \mu^{\pm}$	$c\bar{c}Meson^{\mp} \rightarrow Bkg\_e^{\pm}$	1
$W^{\pm} \rightarrow e^{\pm}$	$c\bar{c}Meson^{\mp} \rightarrow Bkg\_\mu^{\pm}$	1
$W^{\pm} \rightarrow \mu^{\pm}$	$DalitzDecay^{\mp} \rightarrow Bkg\_e^{\pm}$	1
$W^{\pm} \rightarrow e^{\pm}$	$DalitzDecay^{\mp} \rightarrow Bkg\_e^{\pm}$	1
$W^{\pm} \rightarrow e^{\pm}$	$Jet \rightarrow nucleus$	3
$W^{\pm} \rightarrow e^{\pm}$	$W^{\mp} \rightarrow \bar{u}$	1
$W^{\pm} \rightarrow \mu^{\pm}$	$Jet \rightarrow \pi^0$	1
$W^{\pm} \rightarrow e^{\pm}$	$Jet \rightarrow e^{\pm}?$	1
$W^{\pm} \rightarrow \mu^{\pm}$	$g \rightarrow d$	1
$W^{\pm} \rightarrow \mu^{\pm}$	$W^{\mp} \rightarrow \mu^{\mp}$	1

$\ell_1^{\pm}$ (incorrect)	$\ell_2^{\pm}$(incorrect)	
$truthOrigin_1 \rightarrow truthType_1$	$truthOrigin_2 \rightarrow truthType_2$	number of events
$PhotonConv. \rightarrow Bkg\_e^{\pm}$	$PhotonConv. \rightarrow Bkg\_e^{\pm}$	4

Total number of events is 1456

7.2 Combined results of background and signal

The search for regions where the $t\bar{t}$ background can be discriminated from the $W^{\pm}W^{\pm}jj$ signal sample was done on the kinematics variables, η and p_T. The kinematic distributions from each of the categories in $t\bar{t}$ and signal samples are plotted together in Figure 7.1. The left plot shows the η distributions and the right plot shows the transverse momentum p_T distributions of a leading[1] (denoted by superscript 0) and sub-leading (denoted by superscript 1) leptons.

In the η distributions, the total $t\bar{t}$ events (in red colour) predicts the peaks at the forward (end cap) regions of the ATLAS detector, $1.5 < |\eta| < 2.5$, while the signal contribution peaks near the central regions. For an example, one might impose an additional cut of $|\eta| < 1.5$ to same sign $W^{\pm}W^{\pm}jj$ to reject more background. Nevertheless, for the purpose of the study, the interest was in the regions where one can highlight the non-prompt event class from the rest of the events. Thus, the discriminant was only observed in p_T distribution where $W^{\pm}B-$ hadron $\rightarrow \ell^{\pm}\ell^{\pm}$ class (light blue colour) shows a sharp peak at low p_T. Looking at both plots, no strong arguments can be drawn, since the non-prompt background (light blue colour and purple) does not have enough statistics.

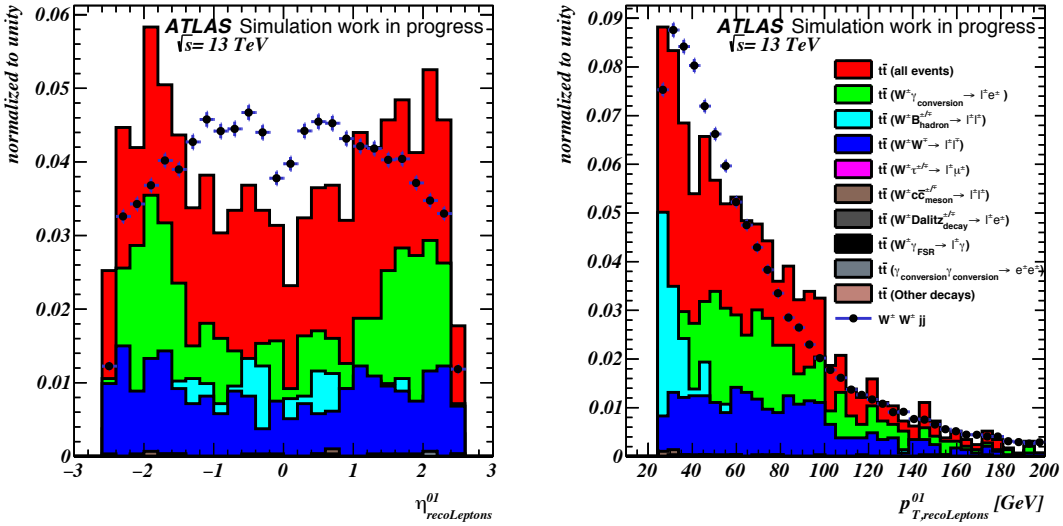

FIGURE 7.1: Kinematic distributions of the leading and second leading lepton (ℓ) in $pp \rightarrow \ell^{\pm}\ell^{\pm}$ channel comparing the VBS production $W^{\pm}W^{\pm}jj \rightarrow \ell^{\pm}\ell^{\pm}\nu\nu jj$ and QCD production $t\bar{t}$.

[1]The leading lepton is a lepton with the highest p_T in the event

Chapter 8

Summary and conclusion

As a contribution towards ssWW analysis, this thesis study was aimed at probing jets that fake leptons (non-prompt background) in $t\bar{t}$ events. In this thesis, the truth classification of leptonic/semileptonic decaying $t\bar{t}$ events has been performed. The classification was done on the events that passed the analysis selection cuts with two highest p_T leptons of the same electric charge using MC truth classification tools. These tools return the origin and type of the truth particle that is closest to the reconstructed lepton based on a specified cone size in $\eta - \phi$ space. The events that failed the tools were manually followed in the truth event chain to find the origin of the closest truth particle. According to the results of the study, it was found that out of 1456 $t\bar{t}$ events that fake the signal, 75.4% of them are still due to electron charge flip. Hence, probing jets in the non-prompt background, might not be a good approach to look for observables that can suppress the background events in the ssWW analysis. Nevertheless, the next dominant event class was $b-$jets with 20.0% of events, followed by $c-$jets with 1.03%. The other thing that was done to try and look for regions where the non-prompt background can be discriminated from the signal was to plot the η and ϕ kinematics distributions. Unfortunately, the statistics of the non-prompt events were too low, hence no strong arguments were drawn from the distributions. At the moment, the results of the study do not help in the optimisation of the fake background. However, if one wants to find optimal cuts for fake background rejection in the ssWW analysis, it might be worth investigating other areas such as plotting the invariant mass of the jets.

In the very big and background dominated dataset from the LHC, searching for a rare process like $W^{\pm}W^{\pm}jj$ is a difficult task. The ATLAS ssWW group hopes that finding the good optimal cuts for fake background rejection will make the measurements and the observation of this process possible. In summary, $W^{\pm}W^{\pm}jj$ production still remains the promising process in providing insight on electroweak symmetry breaking. The current ongoing ATLAS measurements are hoping to get a peek at something new, which will again confirm the Standard Model of particle physics.

Bibliography

[1] S. L. Glashow. In: *Nuclear Physics* 22.4 (1961), pp. 579 –588. ISSN: 0029-5582.

[2] S. Weinberg. In: *Phys. Rev. Lett.* 19 (21), pp. 1264–1266.

[3] Svartholm (ed) A. Salam. In: *Eighth Nobel Symposium. Stockholm: Almquvist and Wiksell* (1968), p. 367.

[4] F. Englert and R. Brout. In: *Phys. Rev. Lett.* 13 (9 1964), pp. 321–323.

[5] P. W. Higgs. In: *Phys. Rev. Lett.* 13 (16 1964), pp. 508–509.

[6] UA1 Collaboration. In: *Physics Letters B* 122.1 (1983), pp. 103 –116.

[7] UA2 Collaboration. In: *Physics Letters B* 122.5 (1983), pp. 476 –485.

[8] S. Holmes, R.S. Moore, and V. Shiltsev. In: *Journal of Instrumentation* 6.08 (2011), T08001.

[9] L. Evans and P. Bryant. In: *JINST* 3 (2008), S08001.

[10] ATLAS Collaboration. In: *Physics Letters B* 716.1 (2012), pp. 1 –29. ISSN: 0370-2693.

[11] CMS Collaboration. In: *Physics Letters B* 716.1 (2012), pp. 30 –61. ISSN: 0370-2693.

[12] B. W. Lee, C. Quigg, and H. B. Thacker. In: *Phys. Rev. Lett.* 38 (1977), p. 883.

[13] M. J. G. Veltman. In: *Phys. Polon. B* 8 (1977), p. 475.

[14] B.W. Lee, C. Quigg, and H.B. Thacker. In: *Phys. Rev. Lett. D* 16 (1977), p. 1519.

[15] Georges Aad et al. In: *Phys. Rev. Lett.* 113.14 (2014), p. 141803.

[16] J. Abdallah et al. In: (2014). arXiv: 1409.2893 [hep-ph].

[17] ATLAS Collaboration. In: *Phys. Rev. Lett.* 113 (2014), p. 141803.

[18] E. Torrence. *LuminosityPublicResultsRun2*. 2015. URL: https://twiki.cern.ch/twiki/bin/view/AtlasPublic/LuminosityPublicResultsRun2.

[19] CMS Collaboration. *Observation of electroweak production of same-sign W boson pairs in the two jet and two same-sign lepton final state in proton-proton collisions at 13 TeV*. Tech. rep. CMS-PAS-SMP-17-004. Geneva: CERN, 2017. URL: http://cds.cern.ch/record/2264525.

[20] CMS Collaboration. In: *Phys. Rev. Lett.* 114 (2014), p. 051801.

[21] M.E. Peskin and D.V. Schroeder. Frontiers in Physics. Avalon Publishing, 1995.

[22] S. Singh. NewYork : Harper Perennial, 2005.

[23] S. P. Martin. "A Supersymmetry primer". In: (1997). [Adv. Ser. Direct. High Energy Phys.18,1(1998)]. DOI: 10.1142/9789812839657_0001, 10.1142/9789814307505_0001. arXiv: hep-ph/9709356 [hep-ph].

[24] J. Beringer et al. In: *Phys. Rev.* D86 (2014), p. 010001.

[25] D. Griffiths. *Introduction to elementary particles*. John Wiley & Sons, 2008.

[26] A. Bettini. *Introduction to elementary particle physics*. New York: Cambridge University press, 2008.
[27] R. Mann. *Introduction to particle physics and the standard model*. Boca Raton: CRC Press, Taylor: Francis group, 2010.
[28] F. R. Villatoro. 2012.
[29] P. W. Higgs. In: *Phys. Rev.* 145 (1966), pp. 1156–1163.
[30] T. W. B. Kibble. In: *Phys. Rev.* 155 (1967), pp. 1554–1561.
[31] Sood Alexander. "Evidence for the production of two W bosons with the same electric charge and two jets in 20.3 fb$^{-}1$ of pp collisions at $\sqrt{s} = 8$ 8 TeV using the ATLAS detector." PhD thesis. University of California, 2014.
[32] C.A. Palmer. In: *UC San Diego Physics* (2014), b8201569.
[33] G. Altarelli and G. Parisi. In: *Nuclear Physics B* 126.2 (1977), pp. 298 – 318.
[34] V. N. Gribov and L. N. Lipatov. In: *Sov. J. Nucl. Phys.* 15.4 (1972), pp. 438–450.
[35] Y. L. Dokshitzer. In: *Sov. Phys. JETP* 46 (1977). [Zh. Eksp. Teor. Fiz.73,1216(1977)], pp. 641–653.
[36] C. Patrignani et al. In: *Chin. Phys.* C40.10 (2016), p. 100001.
[37] V. Chekelian. "Standard model physics at HERA". In: 2001, pp. 187–200. eprint: hep-ex/0107053.
[38] *The Durham HepData Project*. URL: http://hepdata.cedar.ac.uk/pdf/pdf3.html (visited on 11/03/2017).
[39] M. Beneke et al. "Top quark physics". In: 2000, pp. 419–529. eprint: hep-ph/0003033.
[40] N. Cabibbo. In: *Phys. Rev. Lett.* 10.531 (1963).
[41] M. Kobayashi and T. Maskawa. In: *Prog. Theor. Phys* 49.652 (1973).
[42] L.L. Chau and W.Y. Keung. In: *Phys. Rev. Lett* 53.1802 (1984).
[43] B. Abbott et al. In: *Phys. Rev.* D60 (1999), p. 012001.
[44] ATLAS Collaboration. In: *JINST* 3 (2008), S08003.
[45] CMS Collaboration. In: *JINST* 3 (2008), S08004.
[46] LHCb Collaboration. In: *JINST* 3 (2008), S08005.
[47] ALICE Collaboration. In: *JINST* 3.08 (2008), S08002.
[48] C. Mwewa. "Statistical Interpretation of Exotics Monojet Data in Search of an Invisibly Decaying Diggs Boson". MA thesis. University of Cape Town, 2014.
[49] J. Pequenao. *Computer generated image of the ATLAS inner detector*. 2008. URL: https://cds.cern.ch/record/1095926#03 (visited on 05/22/2017).
[50] ATLAS Collaboration. Tech. rep. ATLAS-CONF-2012-042. Geneva: CERN, 2012.
[51] W. Lampl et al. Tech. rep. Geneva: CERN, 2008.
[52] G. Sciolla. *ATLAS Muon Combined Performance*. 2016. URL: https://twiki.cern.ch/twiki/bin/view/AtlasProtected/MuonPerformance.
[53] M. Cacciari, G. P. Salam, and G. Soyez. In: *Journal of High Energy Physics* 2008.04 (2008), p. 063.
[54] ATLAS collaboration. In: *JINST* 11.04 (2016), P04008.

[55] B. Claudia. In: *Journal of Physics: Conference Series* 664.8 (2015), p. 082005.
[56] C. Pizio. "Missing transverse energy measurement in ATLAS detector: first LHC data results and importance for physics study". PhD thesis. Universita Degli Studi di Milano, 2010.
[57] J Poveda et al. In: *IEEE Transactions on Nuclear Science* 54 (2007), pp. 2629 –2636.
[58] J. Beringer et al. In: *Phys. Rev. D* 86 (2012), p. 010001.
[59] M. A. Dobbs et al. In: *Physics at TeV colliders. Proceedings, Workshop, Les Houches, France*. 2004, pp. 411–459. arXiv: hep-ph/0403045 [hep-ph].
[60] A. Buckley et al. In: *Phys. Rept.* 504 (2011), pp. 145–233.
[61] J. C. Collins, D. E. Soper, and G. F. Sterman. In: *Adv. Ser. Direct. High Energy Phys.* 5 (1989), pp. 1–91.
[62] R. Brock et al. In: *Submitted to: Rev. Mod. Phys.* (1994).
[63] U. Schnoor. "Vector Boson Scattering and Electroweak Production of Two Like-Charge W Bosons and Two Jets at the Current and Future ATLAS Detector". PhD thesis. der Technischen Universität Dresden, 2014.
[64] D.P. Landau and K. Binder. *A Guid to Monte Carlo Simulations in Statistical Physics*. New York: Cambridge University press, 2003.
[65] S. Höche. In: *Theoretical Advanced Study Institute in Elementary Particle Physics: Journeys Through the Precision Frontier: Amplitudes for Colliders (TASI 2014) Boulder, Colorado, June 2-27, 2014*. 2014. arXiv: 1411.4085 [hep-ph]. URL: https://inspirehep.net/record/1328513/files/arXiv:1411.4085.pdf.
[66] V. V. Sudakov. In: *Sov. Phys. JETP* 3 (1956), pp. 65–71.
[67] B. R. Webber. *Parton shower Monte Carlo event generators*. URL: http://www.scholarpedia.org/article/Parton_shower_Monte_Carlo_event_generators (visited on 08/10/2017).
[68] J. C. Winter, F. Krauss, and G. Soff. In: *The European Physical Journal C - Particles and Fields* 36.3 (2004), pp. 381–395.
[69] B. R. Webber. In: *Int. J. Mod. Phys.* A15S1 (2000), pp. 577–606.
[70] D.R. Yennie, S.C Frautschi, and H. Suura. In: *Ann. of Phys.* 13 (1961), pp. 379–452.
[71] S. Jadach. *Yennie-Frautschi-Suura soft photons in Monte Carlo event generators*. Tech. rep. MPI-PAE/PTh 6/87.
[72] S. Jadach and B. F. L. Ward. In: *Phys. Rev.* D38 (1988), p. 2897.
[73] W. Placzek and S. Jadach. In: *Eur. Phys. J.* C29 (2003), pp. 325–339.
[74] T. Gleisberg et al. In: *JHEP* 0902 (2009), p. 007.
[75] S. Hoeche et al. In: *JHEP* 0905 (2009), p. 053.
[76] T. Sjostrand, S. Mrenna, and P. Z. Skands. In: *Comput. Phys. Commun.* 2008.11 (2008), p. 010.
[77] B. Jager and G. Zanderighi. In: *JHEP* 1111 (2011), p. 055.
[78] T. Melia et al. In: *Eur. Phys. J. C* 71 (2011), p. 1670.
[79] G.L. Kane, W.W. Repko, and W.B. Rolnick. In: *Physics Letters B* 148.4 (1984), pp. 367 –372.
[80] A. Alboteanu, W. Kilian, and J. Reuter. In: *JHEP* 11 (2008), p. 010.
[81] S. Agostinelli. Tech. rep. 2003, A506.

[82] G. Aad et al. In: *The European Physical Journal C* C70.3 (2010), pp. 823–874.
[83] M. Dobbs and J. B. Hansen. In: *Computer Physics Communications* 134.1 (2001), pp. 41 –46.
[84] H. Lai et al. In: *Phys. Rev.* D82 (2010), p. 074024.
[85] ATLAS. *ATLAS Physics Activity*. URL: https://twiki.cern.ch/twiki/bin/view/AtlasProtected/AtlasPhysics (visited on 08/10/2017).
[86] D. A. et. al. *Recommendations of the Physics Objects and Analysis Harmonisation Study Groups 2014*. Tech. rep. ATL-COM-PHYS-2014-45. Geneva: CERN, 2016.
[87] K. Arnold et al. In: *Comput. Phys. Commun.* 180 (2009), pp. 1661–1670. DOI: 10.1016/j.cpc.2009.03.006. arXiv: 0811.4559 [hep-ph].
[88] ATLAS collaboration. In: *JHEP* 07 (2015), p. 162.
[89] J. Catmore. *DerivationFramework*. 2013. URL: https://twiki.cern.ch/twiki/bin/view/AtlasProtected/DerivationFramework#Generic_skimming_tool (visited on 03/17/2017).
[90] C. Anastopoulos. *MCTruthClassifier*. 2009. URL: https://twiki.cern.ch/twiki/bin/viewauth/AtlasProtected/MCTruthClassifier.

Appendix A

MC generated samples

A.1 Sample used specifically for this thesis

Process	Sample name	Production tag
$t\bar{t}$	mc15_13TeV.410000.PowhegPythiaEvtGen_P2012_ttbar_hdamp172p5_nonallhad.merge.DAOD_STDM3	p2823 (*reduced* data)
$t\bar{t}$	mc15_13TeV.410000.PowhegPythiaEvtGen_P2012_ttbar_hdamp172p5_nonallhad.merge.AOD	No tag for *full* data
$W^{\pm}W^{\pm}jj$	mc15_13TeV.361069.Sherpa_CT10_llvvjj_ss_EW4	p2823 (*reduced* data)

A.2 Information about truth classification and matching

Definitions. The following naming conventions are used in MC Truth Classifiers:

- `truthType`

  As returned by the MC Truth Classifiers, this variable denotes the type of the reconstructed muon or electron, and

- `truthOrigin`

  denotes the origin of the reconstructed muon or electron.

Classification.

```
enum ParticleType {
   Unknown          =  0, // failed to classify
   IsoElectron      =  2, // prompt electron
   NonIsoElectron   =  3, // non-prompt (fake) electron
   BkgElectron      =  4, // electron charge is flipped
   IsoMuon          =  6, // prompt muon
   NonIsoMuon       =  7, // non-prompt (fake) muon
   BkgMuon          =  8,
   IsoTau           =  10,
   NonIsoTau        =  11,
   BkgTau           =  12,
   IsoPhoton        =  14,
```

```
   NonIsoPhoton    =  15,
   BkgPhoton       =  16,
   Hadron          =  17,
   Neutrino        =  18,
   NuclFrag        =  19, // nucleus as a results of fragmentation
   NonPrimary      =  20,
   GenParticle     =  21,
   SUSYParticle    =  22
  };
enum ParticleOrigin {
        NonDefined    = 0, // failed to classify
    SingleElec    = 1,
    SingleMuon    = 2,
    SinglePhot    = 3,
    SingleTau     = 4,
    PhotonConv    = 5, // photon from W boson decays
    DalitzDec     = 6,
    Mu            = 8,
    TauLep        = 9, // hadronic tau lepton
    top           = 10,
    QuarkWeakDec  = 11,
    WBoson        = 12,
    ZBoson        = 13,
    Higgs         = 14,
    HiggsMSSM     = 15,
    HeavyBoson    = 16,
    WBosonLRSM    = 17,
    NuREle        = 18,
    NuRMu         = 19,
    NuRTau        = 20,
    LQ            = 21,
    SUSY          = 22,
    LightMeson    = 23,
    StrangeMeson  = 24,
    CharmedMeson  = 25,
    BottomMeson   = 26,
    CCbarMeson    = 27,
    JPsi          = 28,
    BBbarMeson    = 29,
    LightBaryon   = 30,
    StrangeBaryon = 31,
    CharmedBaryon = 32,
    BottomBaryon  = 33,
    PionDecay     = 34,
    KaonDecay     = 35,
    BremPhot      = 36,
    PromptPhot    = 37,
```

```
    ISRPhot       = 39,
    FSRPhot       = 40, // final state radiated photon that undergo con
    NucReact      = 41,
    PiZero        = 42,
    DiBoson       = 43,
    ZorHeavyBoson = 44
  };
```

A.3 MC truth record for the abnormal event

TABLE A.1: MC truth record of event number 36677173 in $t\bar{t}$ sample. The variables q, nP and nC denotes the electric charge of the particle, the number of its parents and the number of its children, respectively.

pdgId	q	nP	nC	p_T (GeV)	η	ϕ	Energy (GeV)	mass (GeV)	status	barcode	ΔR
2212	1	0	4	0.000000	9.999999$\times 10^{10}$	0.000000	6500.000000	0.938270	3	1	10.000000$\times 10^{10}$
2212	1	0	7	0.000000	-9.999999$\times 10^{10}$	0.000000	6500.000000	0.938270	3	2	9.999999$\times 10^{10}$
2	0	1	30	1.674607	8.760460	1.905951	5339.522461	0.000000	3	3	11.190445
21	0	1	12	2.181317	-4.415326	0.006722	90.220207	0.000000	3	4	2.620793
21	0	1	3	3.818619	7.859158	-1.843671	4943.850586	0.000000	3	5	10.885871
21	0	1	3	12.471814	-1.839323	-2.948675	40.229095	0.000000	3	6	4.701406
6	0	2	2	140.004044	3.905779	0.979425	3483.983154	172.228607	3	7	6.376793
-6	0	2	2	148.386368	2.978667	-2.260961	1472.477051	170.869400	3	8	6.711909
21	0	2	0	8.476918	-1.849889	-1.190010	27.619370	0.000000	3	9	2.962718
24	1	1	2	42.365635	4.047510	2.118639	1215.892334	81.077133	3	10	6.488402
5	0	1	0	128.193970	3.565495	0.674547	2268.090820	4.950000	3	11	6.083613
-24	-1	1	2	141.333389	3.025323	-2.219854	1461.678467	84.907608	3	12	6.725415
-5	0	1	0	9.229115	0.281539	-2.941640	10.798647	4.950000	3	13	5.388345
-13	1	1	0	24.191145	2.728614	-1.800728	185.993210	0.105700	3	14	6.241764
14	0	1	0	61.971424	3.502784	1.841179	1029.899170	0.000000	3	15	5.932479
11	-1	1	0	30.521629	2.114797	-3.040472	128.321457	0.000510	3	16	6.577337
-12	0	1	0	122.575562	3.077755	-2.036669	1333.357056	0.000000	3	17	6.663148
24	1	1	1	42.308105	4.046433	2.121170	1212.948242	81.077133	2	18	6.487485
-24	-1	1	1	140.957886	3.027946	-2.220239	1461.605713	84.907608	2	19	6.727767
-13	1	1	0	20.186802	2.687436	-1.778730	148.998932	0.105700	1	20	6.195351
14	0	1	0	61.660332	3.505770	1.823171	1027.788696	0.000000	1	21	5.935111
11	-1	1	2	30.449358	2.115371	-3.041774	128.089066	0.000510	1	22	6.578675
-12	0	1	0	122.045395	3.080557	-2.036330	1331.299683	0.000000	1	23	6.665273
24	1	1	4	41.738171	4.061303	2.090094	1214.517334	81.077133	2	24	6.500462
-24	-1	1	3	140.760986	3.027901	-2.220280	1459.506348	84.907608	2	25	6.727754
1	0	1	0	0.166208	0.872199	2.925063	0.233539	0.000000	10902	26	3.515158
2101	0	1	0	0.958015	7.792138	-1.184989	1159.911865	0.000000	10902	27	10.624154
1	0	1	0	0.383560	-4.557197	-3.012889	18.281700	0.000000	10902	28	5.185684
21	0	1	0	0.278135	-1.519494	-0.967380	0.665957	0.000000	10902	29	2.832823
-3	0	1	0	0.567710	-4.836314	1.159299	35.772644	0.500000	10902	30	2.471391
-1	0	1	1	3.684657	-1.704905	-1.322782	10.474515	0.330000	2	31	3.123408
21	0	1	1	2.867169	-1.963226	-0.982766	10.411651	0.000000	2	32	2.738246
21	0	1	1	0.223851	-3.035698	-2.300314	2.335163	0.000000	10902	33	4.061661
21	0	1	1	2.476821	-2.278961	-0.390950	12.221774	0.000000	2	34	2.111926
21	0	1	1	4.446801	-2.609898	-0.413480	30.396582	0.000000	2	35	2.136889
21	0	1	1	0.281890	-0.017296	-0.074678	0.281932	0.000000	10902	36	3.003109
21	0	1	1	0.924745	1.492365	-0.307104	2.160407	0.000000	2	37	4.411782
21	0	1	1	1.068815	2.585242	-0.340380	7.130003	0.000000	2	38	5.418827
21	0	1	1	1.837544	3.482748	0.552425	29.933380	0.000000	2	39	6.024488
21	0	1	1	0.730559	4.486555	1.433702	32.446384	0.000000	10902	40	6.920670
21	0	1	1	6.039605	3.867629	1.102912	144.496796	0.000000	2	41	6.325746
21	0	1	1	1.110415	3.304819	0.767056	15.146240	0.000000	2	42	5.811138
21	0	1	1	6.029214	3.722140	0.614372	124.735329	0.000000	2	43	6.248330
5	0	1	1	111.812218	3.532554	0.657884	1914.256836	4.950000	2	44	6.054050
-1	0	1	1	0.925546	-0.405681	-2.143534	1.055663	0.330000	2	45	4.357158

Continued on next page

pdgId	q	nP	nC	p_T (GeV)	η	ϕ	Energy (GeV)	mass (GeV)	status	barcode	ΔR
21	0	1	1	0.766142	-3.530753	-1.319842	13.092965	0.000000	10902	46	3.229500
21	0	1	1	0.319069	-4.970143	2.045324	22.981668	0.000000	10902	47	2.563061
3	0	1	1	0.216754	-6.623474	2.584167	81.561325	0.500000	10902	48	4.284061
2203	1	1	1	0.855157	-9.386441	-3.039248	5099.125000	0.000000	10902	49	8.427584
21	0	1	1	0.493159	-6.954978	-0.146779	258.503143	0.000000	10902	50	4.894790
21	0	1	1	0.861621	-6.668473	1.936513	339.131622	0.000000	10902	51	4.245852
21	0	1	1	0.229206	-7.696159	-2.422364	252.112717	0.000000	10902	52	6.698737
21	0	1	1	0.920243	-5.616899	-2.562236	126.551254	0.000000	10902	53	5.335479
21	0	1	1	1.260644	-5.417302	-1.314200	141.995850	0.000000	2	54	4.256046
21	0	1	1	0.494241	-3.752040	1.438855	10.535087	0.000000	10902	55	1.352310
21	0	1	1	0.724457	-3.128098	0.102810	8.285724	0.000000	2	56	1.758120
21	0	1	1	1.352197	-2.430627	-0.894816	7.744026	0.000000	2	57	2.610502
1	0	1	1	0.919410	-1.749667	-0.715922	2.744363	0.330000	2	58	2.524549
2	0	1	1	0.350749	5.448823	1.811845	40.773930	0.330000	10902	59	7.877777
21	0	1	1	2.102073	4.900000	0.184610	141.151291	0.000000	2	60	7.486599
21	0	1	1	0.195453	3.298326	-1.854745	2.648807	0.000000	10902	61	6.748555
21	0	1	1	0.921029	4.061687	-2.673866	26.751028	0.000000	10902	62	7.835111
21	0	1	1	2.059656	4.135794	2.069060	64.421120	0.000000	2	63	6.573667
21	0	1	1	2.173494	4.498519	1.448440	97.693207	0.000000	2	64	6.932040
21	0	1	1	0.674968	3.139016	1.785368	7.804142	0.000000	2	65	5.567820
21	0	1	1	1.627493	1.319242	-2.547551	3.261431	0.000000	2	66	5.676244
21	0	1	1	0.104184	-0.626870	-1.503955	0.125334	0.000000	10902	67	3.689373
-5	0	1	1	7.877325	0.247504	-3.017363	9.509689	4.950000	2	68	5.437097
21	0	1	1	0.526357	-0.545557	-3.051117	0.606649	0.000000	2	69	5.125170
21	0	1	1	0.857502	0.018777	-1.334056	0.857653	0.000000	2	70	3.910171
21	0	1	1	5.332404	1.037812	0.994065	8.471222	0.000000	2	71	3.540499
21	0	1	1	3.997077	0.753888	1.014140	5.187766	0.000000	2	72	3.258668
92	0	0	6	0.874636	7.883335	-1.342224	1160.145508	12.702854	2	73	10.755558
313	0	1	2	0.568045	3.813326	-2.579304	12.905107	0.913600	10902	74	7.576653
-321	-1	1	49	0.508242	4.038993	0.860885	14.439136	0.493600	1	75	6.523606
221	0	1	3	0.276443	5.625542	-1.818346	38.350124	0.547450	10902	76	8.795159
211	1	1	0	0.531721	7.570512	-0.809943	515.804871	0.139570	1	77	10.312924
111	0	1	2	0.425115	6.016698	0.426725	87.196388	0.134980	10902	78	8.542865
2112	0	1	0	0.568922	7.454516	-2.207794	491.449829	0.939570	1	79	10.633206
92	0	0	4	0.242116	-6.112394	1.552142	54.720306	2.812966	2	80	3.687655
-213	-1	1	2	0.496840	-4.491700	-2.394796	22.192284	0.738884	10902	81	4.599281
111	0	1	2	0.691192	-3.575133	1.105607	12.347977	0.134980	10902	82	1.298948
211	1	1	7	0.320839	-2.706846	0.558003	2.418133	0.139570	1	83	1.190704
311	0	1	1	0.297824	-4.780993	-2.368187	17.761909	0.497670	10902	84	4.713051
92	0	14	27	130.031784	3.523446	0.570090	2336.427002	769.640137	2	85	6.061062
211	1	1	0	3.968315	-1.727462	-1.118806	11.517076	0.139570	1	86	2.919864
113	0	1	2	1.517543	-2.136836	-1.584597	6.567702	0.803919	2	87	3.313133
-211	-1	1	0	2.704282	-2.270289	-0.716804	13.232089	0.139570	1	88	2.437620
223	0	1	3	1.802497	-2.519499	-0.381410	11.295766	0.788815	2	89	2.099073
211	1	1	0	0.076965	-3.739969	0.052333	1.626905	0.139570	1	90	2.118262
-211	-1	1	0	1.209403	-2.310727	-0.496913	6.158012	0.139570	1	91	2.215723
111	0	1	2	0.214127	-2.114640	1.585546	0.910176	0.134980	10902	92	0.339648
211	1	1	0	1.077475	-1.920850	-0.655243	3.759336	0.139570	1	93	2.424638
221	0	1	3	0.473880	-2.576364	0.371994	3.181062	0.547450	2	94	1.351816
111	0	1	2	0.326839	-1.866699	-1.790162	1.090477	0.134980	2	95	3.550553
111	0	1	2	1.088614	-2.274246	0.104621	5.348681	0.134980	2	96	1.618419
-323	-1	1	2	0.525358	-1.213483	-1.293986	1.267163	0.824753	2	97	3.245621
323	1	1	2	0.847476	1.133907	-0.907977	1.700126	0.882355	2	98	4.424183
111	0	1	2	0.728274	1.780009	1.357089	2.224805	0.134980	2	99	4.223627
111	0	1	2	0.343068	2.466098	0.421490	2.039092	0.134980	2	100	5.062680
111	0	1	2	0.252531	0.612355	-0.461071	0.330223	0.134980	10902	101	3.739553
-211	-1	1	6	0.424804	2.217115	-1.602980	1.978089	0.139570	1	102	5.709119
211	1	1	26	0.768134	2.814988	1.296282	6.435747	0.139570	1	103	5.260102
-2112	0	1	0	0.225141	4.200331	-0.500515	7.569643	0.939570	1	104	6.989363
113	0	1	2	0.649952	3.484530	0.790377	10.646654	0.923827	2	105	5.984860
1114	-1	1	2	0.944322	3.437365	0.398022	14.748940	1.179660	2	106	6.011909
113	0	1	2	0.696784	4.031630	1.609332	19.655548	0.806326	10902	107	6.460873
213	1	1	2	3.563444	3.760418	0.815921	76.598625	0.674514	2	108	6.253851
111	0	1	2	0.696029	4.539141	1.287435	32.581779	0.134980	10902	109	6.980657
-213	-1	1	2	7.289633	3.698309	0.791943	147.266296	0.776556	2	110	6.195924
211	1	1	0	0.743006	3.255188	0.270015	9.646362	0.139570	1	111	5.864534
-523	-1	1	2	112.559975	3.537734	0.657779	1937.050659	5.324800	2	112	6.059169
92	0	4	7	1.291801	-5.207785	-2.090074	118.691628	12.772232	2	113	4.712638
213	1	1	2	0.929886	-0.993581	-1.961233	1.568175	0.648276	2	114	3.946940
113	0	1	3	0.078849	-4.558003	2.720055	3.844206	0.794355	10902	115	2.354593

Continued on next page

pdgId	q	nP	nC	p_T (GeV)	η	ϕ	Energy (GeV)	mass (GeV)	status	barcode	ΔR
-211	-1	1	7	0.248297	-2.019161	-0.620758	0.961752	0.139570	1	116	2.372006
213	1	1	2	0.322146	-4.241675	2.953749	11.235726	0.885267	10902	117	2.195652
-213	-1	1	2	0.165672	-5.596510	2.668781	22.341181	0.893427	10902	118	3.308402
213	1	1	2	0.227968	-6.066412	-0.459694	49.148666	0.791726	10902	119	4.238825
-323	-1	1	2	0.242137	-5.498246	-2.279024	29.591915	1.055397	10902	120	5.038040
92	0	10	11	2.541861	-8.500008	-1.152795	6246.728516	66.333183	10902	121	6.715131
111	0	1	2	0.496884	-9.235618	2.800011	2548.018066	0.134980	10902	122	6.893070
2224	2	1	2	0.885759	-8.679552	-2.537347	2604.758789	1.250413	10902	123	7.560793
223	0	1	3	0.648148	-7.313092	1.342508	486.049377	0.777140	10902	124	4.898958
-211	-1	1	0	0.710106	-6.294217	-1.607835	192.237778	0.139570	1	125	5.098095
211	1	1	0	0.358519	-4.789955	0.361685	21.566143	0.139570	1	126	2.722207
111	0	1	2	0.610057	-6.742421	2.098196	258.545715	0.134980	10902	127	4.330978
111	0	1	2	0.978160	-5.430242	-1.427689	111.612526	0.134980	10902	128	4.346498
-211	-1	1	2	0.665553	-2.300423	-1.040639	3.356833	0.139570	1	129	2.759291
211	1	1	0	0.270539	-3.632130	2.323375	5.117750	0.139570	1	130	1.348455
-213	-1	1	2	0.615952	-3.284472	-0.640891	8.274871	0.832133	2	131	2.507262
113	0	1	2	1.548704	-2.212735	-0.580053	7.190953	0.635445	2	132	2.305842
92	0	10	13	9.332361	4.415233	2.841515	394.140015	79.907860	2	133	6.935587
211	1	1	0	0.785134	4.913756	-0.200879	53.450996	0.139570	1	134	7.588148
-213	-1	1	2	0.257617	6.002604	0.981634	52.106403	0.752923	10902	135	8.462867
213	1	1	2	0.538149	4.917000	1.210840	36.764336	0.807587	10902	136	7.362696
2114	0	1	2	0.639347	5.316408	1.635486	65.114128	1.180407	10902	137	7.745191
211	1	1	17	0.581362	4.609441	2.245493	29.195765	0.139570	1	138	7.057723
-2224	-2	1	2	0.519887	5.209347	1.189005	47.579071	1.178878	10902	139	7.655852
113	0	1	2	0.116971	5.060016	-2.671464	9.236300	0.592739	10902	140	8.678880
211	1	1	0	1.891078	4.111716	1.964069	57.742165	0.139570	1	141	6.544799
-211	-1	1	19	0.911197	3.798191	1.243694	20.339670	0.139570	1	142	6.244422
221	0	1	2	0.528843	2.259048	-2.610130	2.617082	0.547450	2	143	6.378443
111	0	1	2	0.626564	3.230462	-2.503500	7.936848	0.134980	2	144	7.058602
3212	0	1	2	0.366132	1.835532	-2.596461	1.675385	1.192550	2	145	6.064275
-5132	1	1	7	8.073796	0.353504	-3.004604	10.381849	5.840000	2	146	5.479045
92	0	2	2	0.938508	-0.299713	-1.922246	1.464302	1.087136	2	147	4.214938
111	0	1	2	0.503420	-0.382615	-3.127701	0.557313	0.134980	2	148	5.257707
111	0	1	2	0.892545	-0.098618	-1.367411	0.906989	0.134980	2	149	3.864352
92	0	2	2	9.329021	0.923212	1.002666	13.658988	1.318464	2	150	3.426585
-211	-1	1	0	5.013229	0.788541	1.003121	6.655750	0.139570	1	151	3.294882
211	1	1	10	4.315792	1.064683	1.002136	7.003238	0.139570	1	152	3.565186
321	1	1	0	0.596514	3.367740	-3.026902	8.677630	0.493600	1	153	7.489125
-211	-1	1	0	0.259944	3.480550	-1.125311	4.227476	0.139570	1	154	6.556414
211	1	1	0	0.038011	6.385853	-2.740541	11.278569	0.139570	1	155	9.876661
-211	-1	1	35	0.142913	4.634550	-2.438391	7.360730	0.139570	1	156	8.193970
111	0	1	2	0.177935	5.400611	-1.127815	19.710831	0.134980	10902	157	8.329370
22	0	1	2	0.217108	5.850175	0.135420	37.700562	0.000000	1	158	8.428019
22	0	1	0	0.225929	6.082564	0.706342	49.495831	0.000000	1	159	8.570574
-211	-1	1	0	0.054662	-3.595962	-0.571464	1.006715	0.139570	1	160	2.567941
111	0	1	2	0.513234	-4.413323	-2.498107	21.185568	0.134980	10902	161	4.657906
22	0	1	2	0.233393	-3.576301	0.831326	4.174128	0.000000	1	162	1.449083
22	0	1	0	0.470786	-3.546607	1.240291	8.173848	0.000000	1	163	1.215097
130	0	1	2	0.297824	-4.780993	-2.368187	17.761909	0.497670	1	164	4.713051
211	1	1	0	1.168909	-1.788596	-1.437220	3.596081	0.139570	1	165	3.217160
-211	-1	1	0	0.400004	-2.692859	-2.028107	2.971621	0.139570	1	166	3.753123
-211	-1	1	0	0.392006	-2.273947	-0.586946	1.929916	0.139570	1	167	2.307803
211	1	1	15	1.278996	-2.394410	-0.278696	7.069723	0.139570	1	168	1.994669
111	0	1	2	0.155155	-3.384823	-0.717258	2.296128	0.134980	10902	169	2.614195
22	0	1	0	0.117613	-1.712705	1.039662	0.336626	0.000000	1	170	0.984469
22	0	1	2	0.128977	-2.172471	2.078728	0.573549	0.000000	1	171	0.444166
111	0	1	2	0.105453	-1.896792	-0.069168	0.383823	0.134980	10902	172	1.862330
111	0	1	2	0.228904	-2.779049	0.296054	1.855122	0.134980	10902	173	1.462302
111	0	1	2	0.162717	-2.431188	0.765520	0.942117	0.134980	10902	174	0.950169
22	0	1	2	0.332409	-1.826289	-1.840915	1.059023	0.000000	1	175	3.607200
22	0	1	0	0.017630	-1.182232	0.076587	0.031454	0.000000	1	176	2.059003
22	0	1	2	0.248880	-2.433457	0.259282	1.429311	0.000000	1	177	1.456411
22	0	1	0	0.843576	-2.217395	0.059157	3.919371	0.000000	1	178	1.669908
-311	0	1	1	0.565030	-1.149646	-1.143036	1.100380	0.497670	2	179	3.131679
-211	-1	1	20	0.091240	-0.038034	3.045429	0.166783	0.139570	1	180	2.735309
321	1	1	0	0.529824	1.221161	-1.427037	1.094136	0.493600	1	181	4.816198
111	0	1	2	0.468173	0.708749	-0.311913	0.605990	0.134980	2	182	3.735325
22	0	1	2	0.342506	1.571097	1.388559	0.859647	0.000000	1	183	4.012821
22	0	1	2	0.386088	1.935484	1.329172	1.365158	0.000000	1	184	4.380936
22	0	1	2	0.182148	2.203947	0.099342	0.835247	0.000000	1	185	4.906211

Continued on next page

pdgId	q	nP	nC	p_T (GeV)	η	ϕ	Energy (GeV)	mass (GeV)	status	barcode	ΔR
22	0	1	0	0.179790	2.589011	0.748021	1.203844	0.000000	1	186	5.109840
22	0	1	0	0.153388	0.774058	-0.842546	0.201681	0.000000	1	187	4.098790
22	0	1	0	0.124090	0.267085	0.017137	0.128542	0.000000	1	188	3.185990
-211	-1	1	2	0.239366	2.085079	-0.436044	0.987666	0.139570	1	189	5.000114
211	1	1	5	0.612116	3.450759	1.167328	9.658989	0.139570	1	190	5.904645
2112	0	1	0	0.848094	3.486386	0.321588	13.897401	0.939570	1	191	6.076826
-211	-1	1	11	0.118052	2.650473	0.978675	0.851539	0.139570	1	192	5.132038
-211	-1	1	2	0.568205	3.373978	2.238811	8.305116	0.139570	1	193	5.825880
211	1	1	0	0.410243	4.013006	0.655899	11.350434	0.139570	1	194	6.527974
211	1	1	0	0.715164	4.020947	1.003069	19.943468	0.139570	1	195	6.488565
111	0	1	2	2.863861	3.677317	0.769441	56.655151	0.134980	2	196	6.178573
22	0	1	2	0.544846	4.507580	1.390474	24.712341	0.000000	1	197	6.943568
22	0	1	2	0.163948	4.564229	0.938581	7.869438	0.000000	1	198	7.035644
-211	-1	1	0	4.193374	3.640170	0.859079	79.935349	0.139570	1	199	6.128696
111	0	1	2	3.118421	3.764902	0.701610	67.330948	0.134980	2	200	6.275742
211	1	1	0	0.929594	-0.960421	-1.864484	1.399291	0.139570	1	203	3.869428
111	0	1	2	0.089917	-0.502293	2.802773	0.168884	0.134980	10902	204	2.211679
211	1	1	4	0.192648	-1.391161	0.213923	0.434184	0.139570	1	205	1.825126
-211	-1	1	2	0.260345	-3.263311	-3.108401	3.410017	0.139570	1	206	4.895808
211	1	1	0	0.250517	-2.541730	-1.238801	1.606922	0.139570	1	207	2.956659
111	0	1	2	0.496703	-3.656905	2.500673	9.628805	0.134980	10902	208	1.457913
-211	-1	1	0	0.369270	-3.667776	-1.614914	7.237231	0.139570	1	209	3.553733
111	0	1	2	0.463323	-4.177158	1.857919	15.103951	0.134980	10902	210	1.754566
211	1	1	0	0.292243	-5.493419	1.190598	35.521091	0.139570	1	211	3.109704
22	0	1	2	0.384651	-4.260462	-1.318957	13.627578	0.000000	1	212	3.544802
-321	-1	1	19	0.446034	-4.749093	-1.782327	25.760530	0.493600	1	213	4.197839
111	0	1	2	0.260145	-3.381114	1.818809	3.831384	0.134980	10902	214	0.958311
22	0	1	0	0.414990	-9.317547	2.839333	2309.760010	0.000000	1	215	6.980213
22	0	1	0	0.083817	-8.645617	2.604126	238.257828	0.000000	1	216	6.280407
2212	1	1	0	0.505996	-8.811910	-2.862385	1698.559570	0.938270	1	217	7.855465
211	1	1	0	0.437214	-8.329739	-2.158786	906.199158	0.139570	1	218	7.059582
-211	-1	1	0	0.186360	-7.226740	2.915460	128.190720	0.139570	1	219	4.946094
211	1	1	0	0.387950	-7.022352	0.745277	217.528046	0.139570	1	220	4.695358
111	0	1	2	0.329295	-6.747948	1.439248	140.330597	0.134980	10902	221	4.328417
22	0	1	0	0.308581	-6.640353	2.303865	118.088760	0.000000	1	222	4.252855
22	0	1	0	0.314361	-6.795259	1.896360	140.456985	0.000000	1	223	4.370628
22	0	1	2	0.607329	-5.335307	-1.361858	63.022881	0.000000	1	224	4.233387
22	0	1	2	0.374286	-5.559279	-1.534636	48.589645	0.000000	1	225	4.513002
-211	-1	1	9	0.191244	-2.905045	1.961025	1.757428	0.139570	1	226	0.536110
111	0	1	2	0.786182	-2.804322	-0.766218	6.517443	0.134980	2	227	2.510216
-211	-1	1	16	1.512757	-2.123984	-0.612435	6.418595	0.139570	1	228	2.347933
211	1	1	0	0.061226	-3.209792	0.347166	0.772358	0.139570	1	229	1.575902
-211	-1	1	0	0.451085	5.279475	1.014572	44.267899	0.139570	1	230	7.739664
111	0	1	2	0.193794	4.392856	-2.083229	7.838503	0.134980	10902	231	7.807742
211	1	1	0	0.260446	3.865131	-0.280482	6.217169	0.139570	1	232	6.602485
111	0	1	2	0.578949	4.658861	1.675859	30.547165	0.134980	10902	233	7.087340
2212	1	1	0	0.557678	5.404489	1.641759	62.022873	0.938270	1	234	7.833205
-211	-1	1	0	0.081755	4.324563	1.592683	3.091258	0.139570	1	235	6.754051
-2212	-1	1	0	0.247986	5.591188	1.259504	33.250469	0.938270	1	236	8.032519
-211	-1	1	0	0.273077	4.653269	1.124994	14.328598	0.139570	1	237	7.106229
-211	-1	1	0	0.074420	5.398946	-1.234596	8.231208	0.139570	1	238	8.364867
211	1	1	9	0.129984	2.724546	3.008369	1.005093	0.139570	1	239	5.312584
22	0	1	2	0.568110	1.841521	-2.947720	1.836331	0.000000	1	240	6.322918
22	0	1	2	0.188304	2.100476	-1.001085	0.780751	0.000000	1	241	5.281217
22	0	1	2	0.476772	3.173713	-2.621531	5.706463	0.000000	1	242	7.084825
22	0	1	0	0.163078	3.307512	-2.152038	2.230386	0.000000	1	243	6.918063
3122	0	1	2	0.412637	1.647920	-2.538241	1.575047	1.115680	1	244	5.891689
22	0	1	0	0.051717	1.281687	1.027928	0.100337	0.000000	1	245	3.773263
22	0	1	0	0.442618	-0.473391	-3.119039	0.493146	0.000000	1	252	5.215025
22	0	1	0	0.060939	0.324062	3.092534	0.064167	0.000000	1	253	3.077594
22	0	1	2	0.408553	-0.146138	-1.525154	0.412923	0.000000	1	254	3.963787
22	0	1	0	0.493258	-0.057233	-1.236928	0.494066	0.000000	1	255	3.786846
22	0	1	0	0.006359	2.742676	1.482321	0.049580	0.000000	1	256	5.176306
22	0	1	2	0.183445	5.367615	-1.145384	19.661247	0.000000	1	257	8.304400
22	0	1	2	0.506584	-4.361682	-2.539600	19.858534	0.000000	1	258	4.673880
22	0	1	0	0.022176	-4.784759	-1.252533	1.327036	0.000000	1	259	3.789840
22	0	1	0	0.051020	-3.584294	0.516650	0.919788	0.000000	1	260	1.665488
22	0	1	2	0.146434	-2.930915	-1.052328	1.376339	0.000000	1	261	2.813262
22	0	1	0	0.012189	0.811808	0.633302	0.016430	0.000000	1	262	3.416180
22	0	1	0	0.096472	-2.012625	-0.150890	0.367392	0.000000	1	263	1.912313

Continued on next page

pdgId	q	nP	nC	p_T (GeV)	η	ϕ	Energy (GeV)	mass (GeV)	status	barcode	ΔR
22	0	1	0	0.050382	-2.950641	1.421526	0.482927	0.000000	1	264	0.599415
22	0	1	0	0.212132	-2.554078	0.080037	1.372195	0.000000	1	265	1.640471
22	0	1	0	0.104801	-1.918543	0.135311	0.364593	0.000000	1	266	1.660573
22	0	1	0	0.099529	-2.443943	1.434937	0.577524	0.000000	1	267	0.281179
310	0	1	2	0.565030	-1.149646	-1.143036	1.100380	0.497670	1	268	3.131679
22	0	1	2	0.271644	0.927555	-0.322726	0.397122	0.000000	1	269	3.926492
22	0	1	0	0.196566	0.351965	-0.296970	0.208868	0.000000	1	270	3.432350
22	0	1	0	0.713370	3.734968	0.712509	14.948875	0.000000	1	271	6.244443
22	0	1	2	2.152030	3.656721	0.788305	41.706276	0.000000	1	272	6.155350
22	0	1	0	0.899932	3.700125	0.678403	18.213310	0.000000	1	273	6.215655
22	0	1	2	2.218829	3.789875	0.711021	49.117630	0.000000	1	274	6.298880
22	0	1	0	0.059563	0.481248	-2.631579	0.066594	0.000000	1	280	5.231115
22	0	1	0	0.067484	-0.976404	2.078729	0.102290	0.000000	1	281	1.496663
22	0	1	2	0.425480	-3.733178	2.474216	8.900118	0.000000	1	282	1.509272
22	0	1	0	0.072254	-3.001730	2.657083	0.728687	0.000000	1	283	1.102260
22	0	1	2	0.377469	-4.256111	1.779798	13.315092	0.000000	1	284	1.828868
22	0	1	0	0.091857	-3.661586	2.184386	1.788860	0.000000	1	285	1.319283
22	0	1	0	0.066163	-3.988509	1.385921	1.786179	0.000000	1	286	1.594612
22	0	1	2	0.202000	-3.005684	1.956647	2.045205	0.000000	1	287	0.625586
22	0	1	0	0.171551	-7.041319	1.541900	98.032417	0.000000	1	288	4.616224
22	0	1	0	0.159618	-6.272860	1.328891	42.298176	0.000000	1	289	3.863900
22	0	1	0	0.620474	-2.876394	-0.744039	5.524230	0.000000	1	290	2.500194
22	0	1	0	0.166431	-2.472417	-0.848992	0.993213	0.000000	1	291	2.565055
22	0	1	0	0.154921	3.898606	-2.331996	3.822972	0.000000	1	292	7.510946
22	0	1	0	0.057961	4.931249	-1.364965	4.015531	0.000000	1	293	7.978368
22	0	1	0	0.117310	4.895684	1.295366	7.843279	0.000000	1	294	7.336103
22	0	1	2	0.472044	4.566259	1.768283	22.703886	0.000000	1	295	6.994825
22	0	1	2	0.399353	2.691910	-1.800159	2.960720	-0.000000	1	10001	6.211151
22	0	1	2	3.494617	2.988112	-1.878518	34.768898	0.000000	1	10002	6.500503
22	0	1	0	0.045810	1.596248	-2.930843	0.117666	0.000000	1	10003	6.147174
22	0	1	0	0.000004	-0.543613	2.093735	0.000005	0.000000	1	10004	1.922296
-521	-1	1	3	111.128128	3.538087	0.657687	1913.084473	5.279170	2	10005	6.059533
223	0	1	3	20.916603	3.505342	0.629245	348.501556	0.779711	2	10006	6.032352
-211	-1	1	24	9.187181	3.510425	0.661941	153.850296	0.139570	1	10007	6.031553
211	1	1	17	3.717312	3.503016	0.587779	61.792297	0.139570	1	10008	6.037672
111	0	1	2	8.021550	3.499391	0.611014	132.858978	0.134977	2	10009	6.029810
22	0	1	2	2.025185	3.505450	0.582730	33.746117	0.000000	1	10010	6.041008
22	0	1	2	5.997448	3.497155	0.620564	99.112862	0.000000	1	10011	6.025870
4212	1	1	2	63.167183	3.537730	0.654521	1087.042480	2.444978	2	10012	6.059736
4122	1	1	3	59.409519	3.539032	0.654792	1023.706421	2.286460	2	10013	6.060970
211	1	1	0	4.592052	3.536231	0.622970	78.906242	0.139570	1	10014	6.063865
223	0	1	3	28.471060	3.535643	0.664837	488.937134	0.770690	2	10015	6.055882
-211	-1	1	0	8.410881	3.563131	0.657662	148.459747	0.139570	1	10016	6.084198
211	1	1	0	4.227034	3.502835	0.657699	70.252541	0.139570	1	10017	6.024823
111	0	1	2	15.833728	3.529400	0.670554	270.224823	0.134977	2	10018	6.048743
22	0	1	2	12.932989	3.526765	0.667464	220.139847	0.000005	1	10019	6.046682
22	0	1	2	2.901076	3.540947	0.684330	50.084988	0.000000	1	10020	6.057756
3212	0	1	2	26.350542	3.543011	0.649483	455.863129	1.192640	2	10021	6.065818
22	0	1	2	2.014821	3.505979	0.648990	33.591164	0.000000	1	10022	6.029453
3122	0	1	0	24.335722	3.546017	0.649524	422.271973	1.115683	1	10023	6.068770
111	0	1	2	3.757695	3.516911	0.650236	63.335953	0.134977	2	10024	6.039993
22	0	1	2	1.991638	3.530784	0.680793	34.037098	-0.000001	1	10025	6.048345
22	0	1	0	1.768034	3.499916	0.615813	29.298855	-0.000001	1	10026	6.029450
-2224	-2	1	2	27.064796	3.562756	0.687059	477.540558	1.133028	2	10027	6.078785
-2212	-1	1	0	21.979559	3.557394	0.688136	385.744446	0.938272	1	10028	6.073318
-211	-1	1	0	5.085305	3.585593	0.682403	91.796150	0.139570	1	10029	6.102081
22	0	1	2	1.431885	3.509899	0.664901	23.966021	-0.000000	1	10030	6.030519
211	1	1	0	0.781069	0.252630	3.094754	0.818120	0.139570	1	10031	3.014894
113	0	1	2	1.065388	0.256198	-2.954379	1.314739	0.719263	2	10032	5.386686
211	1	1	0	0.095483	-1.328678	-3.100552	0.238111	0.139570	1	10033	4.940187
-211	-1	1	0	0.971023	0.442256	-2.940056	1.076628	0.139570	1	10034	5.469588
211	1	1	10	0.258806	1.026360	2.897776	0.430754	0.139570	1	10035	3.651367
-211	-1	1	2	0.325058	0.325536	-3.035500	0.369785	0.139570	1	10036	5.491606
111	0	1	2	0.700677	0.004760	2.371370	0.713568	0.134980	2	10037	2.519927
22	0	1	0	0.023543	-0.123650	-2.835463	0.023723	0.000000	1	10038	5.101437
22	0	1	0	0.689816	0.009065	2.341323	0.689845	0.000000	1	10039	2.516446
331	0	1	3	1.857273	0.135880	-3.083017	2.105006	0.957865	2	10040	5.440855
211	1	1	3	0.372687	0.542300	3.043840	0.450986	0.139570	1	10041	3.254054
-211	-1	1	0	0.523944	0.050260	-3.017189	0.542855	0.139570	1	10042	5.342629
221	0	1	3	0.966608	0.015142	-3.058642	1.111165	0.547853	2	10043	5.363295

Continued on next page

pdgId	q	nP	nC	p_T (GeV)	η	ϕ	Energy (GeV)	mass (GeV)	status	barcode	ΔR
22	0	1	0	0.321400	0.427987	3.043154	0.351288	0.000000	1	10044	3.149752
-211	-1	1	2	0.326829	0.174118	-2.955098	0.359956	0.139570	1	10045	5.346882
211	1	1	6	0.326301	-0.538556	-2.984412	0.399921	0.139570	1	10046	5.065796
-4112	0	1	2	3.509055	0.482505	-2.747292	4.629879	2.454812	2	10047	5.328353
-4122	-1	1	5	3.354115	0.475353	-2.770185	4.383764	2.286460	2	10048	5.343652
-3122	0	1	2	1.083057	0.484740	-2.482635	1.647927	1.115683	1	10049	5.109998
-211	-1	1	2	0.246470	0.098633	-2.674915	0.284289	0.139570	1	10050	5.065875
-211	-1	1	4	0.448518	0.735217	-2.465793	0.591987	0.139570	1	10051	5.243379
211	1	1	0	1.706841	0.412756	-3.046124	1.859557	0.139570	1	10052	5.544980
22	0	1	0	0.000005	-0.220853	-2.803119	0.000005	0.000000	1	10053	5.029185
211	1	1	0	0.173708	0.570127	-2.289472	0.246114	0.139570	1	10054	5.003224
1000030060	0	1	0	0.083626	-0.578290	1.362731	5.602430	5.601573	1	200001	1.883444
22	0	1	0	0.000240	-0.367251	2.390635	0.000256	-0.000000	1	200002	2.168815
2112	0	1	0	0.040641	2.882726	-2.179592	1.007655	0.939565	1	200003	6.586417
-211	-1	1	0	0.455186	0.077967	-1.104837	0.477426	0.139570	1	200004	3.773202
13	-1	1	0	0.111545	0.186447	-2.845997	0.155060	0.105658	1	200005	5.257965
-14	0	1	0	0.025261	0.495386	1.858185	0.028425	0.000000	1	200006	2.927224
-2212	-1	1	5	0.781440	0.553739	-2.498338	1.303143	0.938272	1	200007	5.162456
211	1	1	2	0.301962	0.295820	-2.441987	0.344784	0.139570	1	200008	4.970657
111	0	1	0	0.165151	0.795587	2.962190	0.258305	0.134977	1	200009	3.456538
211	1	1	0	0.324610	-0.671608	-0.519721	0.424229	0.139570	1	200010	2.843104
-211	-1	1	4	0.444150	0.684463	-1.104537	0.569677	0.139570	1	200011	4.200400
211	1	1	0	0.239172	0.404271	2.321497	0.294198	0.139570	1	200012	2.896697
-211	-1	1	0	0.621450	0.294519	-2.897534	0.663445	0.139570	1	200013	5.356855
1000280610	0	1	0	0.048030	0.603171	-2.041501	56.742714	56.742687	1	200016	4.827698
2112	0	1	0	0.048017	0.319985	0.418598	0.940921	0.939565	1	200017	3.039058
2212	1	1	0	0.608857	0.182340	0.345159	1.124066	0.938272	1	200018	2.948581
-211	-1	1	0	0.273304	0.516299	-2.232115	0.340470	0.139570	1	200019	4.925056
1000220480	0	1	0	0.280385	0.442515	2.544516	44.653130	44.652065	1	200021	2.988131
22	0	1	0	0.000906	-0.020770	-0.473407	0.000906	0.000000	1	200022	3.254021
22	0	1	0	0.002472	-0.058728	-0.084984	0.002476	-0.000000	1	200023	2.976171
22	0	1	0	0.002521	-0.090885	-0.871937	0.002531	0.000000	1	200024	3.487063
2212	1	1	0	0.101223	0.255794	-1.815899	0.944079	0.938272	1	200025	4.435854
2212	1	1	0	0.051547	-1.357489	-2.809128	0.944331	0.938272	1	200026	4.649808
2112	0	1	0	0.109863	0.009370	0.246650	0.945967	0.939565	1	200027	2.846160
2212	1	1	0	0.108507	-0.252349	-2.558909	0.944931	0.938272	1	200028	4.796583
2112	0	1	0	0.077150	0.987949	1.621262	0.946942	0.939565	1	200029	3.417621
2212	1	1	0	0.042539	1.803984	0.748396	0.947608	0.938272	1	200030	4.341480
2212	1	1	0	0.087739	0.986207	-1.761112	0.947789	0.938272	1	200031	4.873134
2112	0	1	2	0.426175	-0.498892	0.023543	1.055220	0.939565	1	200032	2.566363
-13	1	1	0	0.206701	0.164138	0.779944	0.234628	0.105658	1	200033	2.756210
14	0	1	0	0.064717	0.695361	0.948517	0.081004	0.000000	1	200034	3.216555
1000050100	0	1	0	0.163565	0.016918	-2.165637	9.325899	9.324465	1	200035	4.587383
22	0	1	0	0.000104	-1.043682	1.989602	0.000166	0.000000	1	200036	1.411519
22	0	1	0	0.000394	-1.230343	1.774210	0.000731	-0.000000	1	200037	1.199453
22	0	1	0	0.000769	-1.341331	-2.798170	0.001570	0.000000	1	200038	4.642901
2212	1	1	0	0.396101	-0.881392	-3.102598	1.092774	0.938272	1	200039	5.060531
2212	1	1	2	0.604706	0.350756	0.835256	1.137052	0.938272	1	200040	2.915250
1000080160	0	1	0	0.062540	-0.199942	0.475561	14.895218	14.895082	1	200041	2.550253
1000040080	0	1	0	0.409535	-0.244075	-3.016821	7.466774	7.454851	1	200042	5.212268
1000020040	0	1	0	0.207507	1.013396	-0.425674	3.741391	3.727379	1	200043	4.053536
22	0	1	0	0.000537	-0.354648	-0.825145	0.000571	-0.000000	1	200044	3.279654
22	0	1	0	0.000796	0.214074	2.577660	0.000814	-0.000000	1	200045	2.779478
2212	1	1	0	0.015831	-1.947903	-0.302805	0.939981	0.938272	1	200046	2.074884
1000070140	0	1	0	0.059814	1.540091	-2.591376	13.041020	13.040204	1	200047	5.856572
1000060120	0	1	0	0.027904	1.195712	-2.420623	11.175034	11.174920	1	200050	5.499363
22	0	1	0	0.001568	0.145778	-0.769549	0.001584	0.000000	1	200051	3.578074
211	1	1	10	0.362324	0.436397	1.522223	0.421174	0.139570	1	200052	2.871290
1000080160	0	1	0	0.161567	0.125153	0.212946	14.895988	14.895099	1	200053	2.962885
1000020040	0	1	0	0.243197	-0.274958	0.350567	3.735918	3.727379	1	200054	2.549650
1000010020	0	1	0	0.149808	-0.973228	-2.233247	1.889244	1.875613	1	200055	4.208502
22	0	1	0	0.000083	1.273822	-2.471359	0.000160	0.000000	1	200056	5.589055
22	0	1	0	0.000250	2.505415	2.148173	0.001542	0.000000	1	200057	4.952702
2212	1	1	0	0.049209	-0.882824	1.921538	0.940855	0.938272	1	200058	1.559192
2212	1	1	0	0.099703	-0.066043	-1.358105	0.943578	0.938272	1	200059	3.876694
2112	0	1	0	0.216429	1.045512	1.517800	1.001212	0.939565	1	200060	3.479511
2112	0	1	0	0.424996	0.090416	0.105942	1.031933	0.939565	1	200061	2.989237
2212	1	1	0	0.519066	0.231867	-2.501039	1.079134	0.938272	1	200062	4.985740
13	-1	1	0	0.184000	0.391814	-1.525259	0.224697	0.105658	1	200063	4.296177
-14	0	1	0	0.123463	0.195216	-1.712478	0.125823	0.000000	1	200064	4.316884

Continued on next page

pdgId	q	nP	nC	p_T (GeV)	η	ϕ	Energy (GeV)	mass (GeV)	status	barcode	ΔR
1000280580	0	1	0	0.451254	0.185042	1.439319	53.954159	53.952206	1	200065	2.627981
22	0	1	0	0.000110	0.360039	-1.468647	0.000118	-0.000000	1	200066	4.232632
22	0	1	0	0.000914	-0.160687	2.543555	0.000926	0.000000	1	200067	2.414073
2112	0	1	0	0.059561	0.175533	0.563572	0.941510	0.939565	1	200068	2.847396
2112	0	1	0	0.064299	-0.916860	-1.221488	0.944184	0.939565	1	200069	3.303277
22	0	1	0	0.005605	-0.089941	0.241364	0.005628	0.000000	1	200070	2.764392
2212	1	1	0	0.115169	0.115682	-0.502626	0.945408	0.938272	1	200071	3.375365
2112	0	1	0	0.082297	0.958173	3.037975	0.947589	0.939565	1	200072	3.635535
2112	0	1	0	0.143398	0.507009	-0.399092	0.953468	0.939565	1	200073	3.617833
211	1	1	0	0.273654	0.348328	-2.844955	0.322220	0.139570	1	200074	5.339426
-11	1	1	0	0.757436	3.530434	0.681755	12.940076	0.000511	1	200079	6.047837
11	-1	1	2	1.234203	3.530997	0.680203	21.097021	0.000511	1	200080	6.048657
22	0	1	0	0.156482	3.528916	0.680533	2.669294	0.000000	1	200081	6.046550
22	0	1	0	0.112487	3.526165	0.682229	1.913558	0.000000	1	200082	6.043549
-11	1	1	0	0.347217	3.507573	0.647944	5.798022	0.000511	1	200088	6.031207
11	-1	1	2	1.667605	3.505647	0.649208	27.793140	0.000511	1	200089	6.029088
22	0	1	0	0.387569	3.505068	0.670806	6.455683	-0.000000	1	200090	6.024735
22	0	1	0	0.499517	3.502264	0.672444	8.297138	0.000000	1	200091	6.021689
-11	1	1	0	0.508557	3.541292	0.684850	8.782907	0.000511	1	200095	6.058008
11	-1	1	2	2.392519	3.540874	0.684219	41.302086	0.000511	1	200096	6.057703
22	0	1	0	1.242155	3.541541	0.684190	21.457630	-0.000000	1	200098	6.058365
-11	1	1	2	6.420698	3.526743	0.667489	109.288048	0.000511	1	200099	6.046657
11	-1	1	2	6.512290	3.526786	0.667439	110.851791	0.000511	1	200100	6.046708
22	0	1	0	0.499721	3.526588	0.666819	8.504536	-0.000000	1	200101	6.046620
22	0	1	0	4.420402	3.526621	0.666336	75.231400	0.000001	1	200102	6.046737
22	0	1	0	0.547200	3.526685	0.667500	9.313466	0.000000	1	200103	6.046598
22	0	1	0	1.652664	3.526447	0.667805	28.122028	0.000000	1	200104	6.046311
22	0	1	0	0.124423	3.526780	0.667981	2.117912	0.000000	1	200105	6.046608
22	0	1	0	0.194745	3.525439	0.668649	3.310488	0.000000	1	200106	6.045171
22	0	1	0	0.128135	3.525251	0.668648	2.177766	-0.000000	1	200107	6.044987
22	0	1	0	0.281940	3.525489	0.668519	4.792955	0.000000	1	200108	6.045243
22	0	1	2	1.722242	3.526221	0.679488	29.299347	-0.000000	1	200109	6.044074
-11	1	1	0	0.712639	3.527889	0.682361	12.143865	0.000511	1	200110	6.045225
11	-1	1	0	1.009608	3.525036	0.677459	17.155485	0.000511	1	200111	6.043255
-11	1	1	2	1.785811	3.496849	0.620695	29.503010	0.000511	1	200115	6.025545
11	-1	1	2	4.211637	3.497285	0.620508	69.609840	0.000511	1	200116	6.026008
22	0	1	0	1.265878	3.497192	0.619470	20.920444	0.000000	1	200117	6.026105
22	0	1	0	1.354883	3.495934	0.621469	22.363291	-0.000000	1	200118	6.024505
-11	1	1	2	1.044589	3.505198	0.582477	17.401852	0.000511	1	200119	6.040808
11	-1	1	0	0.980595	3.505718	0.583001	16.344265	0.000511	1	200120	6.041221
22	0	1	0	0.301622	3.517706	0.539104	5.087859	0.000000	1	200123	6.061364
22	0	1	0	0.149692	3.492579	0.624737	2.462513	0.000000	1	200128	6.020613
22	0	1	0	0.777477	3.499587	0.623454	12.879678	0.000000	1	200129	6.027737
1000100200	0	1	0	0.215475	0.771010	1.596831	18.619879	18.617733	1	200130	3.201585
22	0	1	0	0.000074	0.182669	0.890289	0.000076	-0.000000	1	200131	2.738392
22	0	1	0	0.000950	1.141596	-0.724512	0.001639	-0.000000	1	200132	4.324257
22	0	1	0	0.001172	-1.431242	0.084943	0.002592	-0.000000	1	200133	1.911433
22	0	1	0	0.003485	-1.278730	-1.605260	0.006745	0.000000	1	200134	3.514304
2212	1	1	0	0.088036	0.653647	-0.430870	0.944413	0.938272	1	200135	3.755863
2112	0	1	0	0.108166	-0.202469	-2.381415	0.946028	0.939565	1	200136	4.662709
2212	1	1	0	0.103129	-0.011541	-1.770772	0.943923	0.938272	1	200137	4.242220
2112	0	1	0	0.149117	0.054468	-2.689411	0.951360	0.939565	1	200138	5.056614
1000010020	0	1	0	0.177154	-0.157040	0.164166	1.884168	1.875613	1	200139	2.750662
2212	1	1	0	0.985469	1.330705	1.294366	2.204254	0.938272	1	200140	3.782609
-211	-1	1	0	0.107019	2.413450	2.615290	0.618572	0.139570	1	200141	4.924681
310	0	1	0	0.207166	1.319052	-0.987785	0.648008	0.497614	1	200142	4.620812
310	0	1	0	0.103359	1.984028	0.937645	0.627890	0.497614	1	200143	4.480467
-211	-1	1	0	0.692414	3.282152	1.028699	9.234594	0.139570	1	200144	5.751694
211	1	1	0	1.574302	3.682426	0.306408	31.303629	0.139570	1	200145	6.271193
211	1	1	0	0.944765	3.636899	0.089442	17.951189	0.139570	1	200146	6.279500
1000020030	0	1	0	0.527294	0.186542	-0.026138	2.859176	2.808391	1	200161	3.141925
1000010030	0	1	0	0.238265	-1.389246	-3.097373	2.854423	2.808921	1	200162	4.923951
1000010020	0	1	0	0.130627	1.701987	-2.809510	1.911787	1.875613	1	200163	6.126762
2112	0	1	0	0.105257	0.545083	-2.785359	0.947361	0.939565	1	200164	5.394516
2212	1	1	0	0.133985	0.755085	-2.948407	0.954275	0.938272	1	200165	5.646957
2212	1	1	8	0.296144	2.239192	0.811422	1.689940	0.938272	1	200166	4.754346
-211	-1	1	0	0.329009	1.096844	-0.284489	0.565081	0.139570	1	200167	4.053123
211	1	1	0	0.414143	2.535665	-2.688362	2.634345	0.139570	1	200168	6.636056
-211	-1	1	7	0.309153	3.096517	0.953462	3.429185	0.139570	1	200169	5.577215
-211	-1	1	0	0.326755	2.503846	-1.202816	2.016213	0.139570	1	200170	5.731002

Continued on next page

pdgId	q	nP	nC	p_T (GeV)	η	ϕ	Energy (GeV)	mass (GeV)	status	barcode	ΔR
111	0	1	2	0.854268	1.966816	0.154148	3.115785	0.134977	1	200171	4.664336
211	1	1	0	0.152315	2.788524	2.692461	1.250591	0.139570	1	200172	5.307547
-211	-1	1	0	1.087606	2.351271	0.800207	5.762825	0.139570	1	200173	4.866523
-211	-1	1	27	3.285259	3.251164	0.513436	42.477177	0.139570	1	200174	5.805384
111	0	1	0	0.700544	3.704779	0.610274	14.244693	0.134977	1	200175	6.231968
2212	1	1	0	0.085478	0.999994	-0.629996	0.947497	0.938272	1	200176	4.154019
211	1	1	0	0.363127	2.539911	2.730187	2.320483	0.139570	1	200177	5.070800
111	0	1	0	0.146137	2.999005	1.134878	1.475983	0.134977	1	200178	5.458362
-211	-1	1	0	0.278099	2.337183	-0.000391	1.459563	0.139570	1	200179	5.065115
111	0	1	2	0.413472	2.503908	-0.246363	2.548902	0.134977	1	200180	5.308198
111	0	1	0	0.124834	0.850483	-2.257767	0.219244	0.134977	1	200181	5.151619
211	1	1	0	0.366217	2.539667	1.279821	2.339593	0.139570	1	200182	4.987118
211	1	1	18	1.475128	3.862957	1.401950	35.128189	0.139570	1	200183	6.299143
-211	-1	1	0	1.423083	3.801208	0.778944	31.861383	0.139570	1	200184	6.299610
1000040080	0	1	0	0.179564	-0.656545	2.163848	7.458169	7.454933	1	200185	1.827623
22	0	1	0	0.000490	0.148689	-0.858623	0.000495	0.000000	1	200186	3.642564
22	0	1	0	0.001602	0.003495	-0.570275	0.001602	0.000000	1	200187	3.337599
2212	1	1	0	0.073524	0.285891	2.718517	0.941390	0.938272	1	200188	2.893592
2212	1	1	0	0.020849	-2.306491	-2.435852	0.944206	0.938272	1	200189	4.153325
2212	1	1	0	0.025041	2.326157	1.025311	0.947155	0.938272	1	200190	4.804385
2112	0	1	0	0.466328	0.652662	-0.188168	1.098544	0.939565	1	200191	3.621794
2112	0	1	0	0.069046	3.467753	2.271597	1.452772	0.939565	1	200192	5.922270
1000120250	0	1	0	0.123735	0.901306	2.075083	23.268728	23.268051	1	200193	3.349013
22	0	1	0	0.000051	-2.687310	0.309015	0.000375	-0.000000	1	200194	1.430304
2112	0	1	0	0.091129	-0.688460	-1.417011	0.946407	0.939565	1	200195	3.583442
-211	-1	1	0	0.247942	-0.119571	2.531262	0.286073	0.139570	1	200196	2.448613
2212	1	1	0	0.300418	1.493967	-0.718745	1.172334	0.938272	1	200197	4.616400
211	1	1	0	0.322544	1.188176	0.398710	0.594904	0.139570	1	200198	3.848871
-211	-1	1	5	0.247444	2.896366	2.302732	2.251548	0.139570	1	200199	5.356996
1000060110	0	1	0	0.090320	0.235195	1.388093	10.254478	10.254058	1	200200	2.683633
22	0	1	0	0.000152	-0.734993	-2.147561	0.000195	0.000000	1	200201	4.218078
22	0	1	0	0.001092	0.441962	1.763424	0.001200	-0.000000	1	200202	2.870726
2112	0	1	0	0.372587	0.227574	1.598854	1.014356	0.939565	1	200203	2.658510
-211	-1	1	0	0.330557	2.560088	-2.128468	2.155497	0.139570	1	200204	6.297793
22	0	1	0	0.356455	1.818337	0.281082	1.127092	-0.000000	1	200205	4.482475
22	0	1	0	0.502710	2.051994	0.064264	1.988692	0.000000	1	200206	4.775021
1000240500	0	1	0	0.366394	-0.144542	-1.534097	46.513680	46.512207	1	200207	3.972020
22	0	1	0	0.000778	0.005559	1.892125	0.000778	0.000000	1	200208	2.440314
22	0	1	0	0.001043	-0.341797	-2.264463	0.001104	0.000000	1	200209	4.493924
22	0	1	0	0.001192	-0.386665	0.138497	0.001282	0.000000	1	200210	2.579936
22	0	1	0	0.000728	1.405042	1.588412	0.001574	0.000000	1	200211	3.835522
22	0	1	0	0.001504	0.364025	-2.259496	0.001604	0.000000	1	200212	4.857934
22	0	1	0	0.001586	1.945583	-0.450862	0.005662	0.000000	1	200213	4.881124
2212	1	1	0	0.073604	0.489659	-3.119099	0.941901	0.938272	1	200214	5.647124
2112	0	1	0	0.083494	0.100569	-1.477161	0.943305	0.939565	1	200215	4.073055
2112	0	1	0	0.135266	0.287305	2.358078	0.950070	0.939565	1	200216	2.790618
2212	1	1	0	0.068601	-0.980783	-2.834159	0.944054	0.938272	1	200217	4.774576
2212	1	1	0	0.116302	0.507882	-0.252568	0.947460	0.938272	1	200218	3.534909
2112	0	1	0	0.093501	0.778438	2.872150	0.947620	0.939565	1	200219	3.408961
1000010020	0	1	0	0.071672	1.519566	-0.697661	1.883448	1.875613	1	200220	4.627139
1000010020	0	1	0	0.230930	0.165678	0.934833	1.890167	1.875613	1	200221	2.709023
2112	0	1	0	0.126968	-1.276654	0.791643	0.971053	0.939565	1	200222	1.476583
2112	0	1	0	0.128306	1.431597	0.996929	0.981501	0.939565	1	200223	3.926313
2112	0	1	0	0.848561	1.746368	0.638301	2.677010	0.939565	1	200224	4.311517
-211	-1	1	0	0.348048	2.334533	-1.903505	1.818950	0.139570	1	200225	5.981952
211	1	1	0	0.127721	4.475141	2.865305	5.609839	0.139570	1	200226	6.998575
130	0	1	0	0.484894	1.277375	-0.187831	1.061199	0.497614	1	200227	4.166041
310	0	1	2	0.595561	1.799802	2.401080	1.916086	0.497614	1	200228	4.283361
-211	-1	1	0	1.115121	2.374048	-0.296622	6.042157	0.139570	1	200229	5.206973
-211	-1	1	0	0.297824	2.250006	2.497548	1.435341	0.139570	1	200230	4.743257
211	1	1	0	0.650522	2.941068	1.398723	6.177913	0.139570	1	200231	5.378783
111	0	1	2	1.224720	2.174499	0.169281	5.458676	0.134977	1	200232	4.855692
331	0	1	0	0.495307	3.782667	0.975551	10.927865	0.957780	1	200233	6.254978
111	0	1	2	0.322793	2.138479	2.096643	1.395258	0.134977	1	200254	4.582709
111	0	1	2	0.303451	1.091868	2.725610	0.520828	0.134977	1	200255	3.662241
22	0	1	0	0.293676	2.200535	2.151637	1.342187	-0.000000	1	200256	4.649386
22	0	1	0	0.033681	1.027268	1.596830	0.053071	-0.000000	1	200257	3.457679
22	0	1	2	0.308982	1.019756	2.798973	0.484051	0.000000	1	200258	3.614287
22	0	1	0	0.023130	1.038914	0.950198	0.036777	0.000000	1	200259	3.550777
-11	1	1	0	0.072909	1.023068	2.794702	0.114513	0.000511	1	200260	3.616170

Continued on next page

pdgId	q	nP	nC	p_T (GeV)	η	ϕ	Energy (GeV)	mass (GeV)	status	barcode	ΔR
11	-1	1	0	0.236072	1.018729	2.800292	0.369538	0.000511	1	200261	3.613703
22	0	1	0	0.272058	1.990203	0.066964	1.013918	-0.000000	1	200262	4.716147
22	0	1	2	0.954489	2.219719	0.198398	4.444757	0.000000	1	200263	4.889465
113	0	0	2	0.406027	3.806573	0.573034	9.172153	0.775490	1	200264	6.338780
211	1	1	0	0.170471	4.460824	1.557181	7.380196	0.139570	1	200266	6.891014
-211	-1	1	2	0.342471	2.335665	0.145595	1.791957	0.139570	1	200267	5.016093
-11	1	1	0	0.156239	2.229053	0.189236	0.734224	0.000511	1	200270	4.901185
11	-1	1	0	0.798256	2.217872	0.200191	3.710533	0.000511	1	200271	4.887153
1000130270	0	1	0	0.103946	-0.145022	-0.268730	25.126724	25.126507	1	200272	3.025156
22	0	1	2	0.328662	2.298434	-0.177843	1.653004	0.000000	1	200279	5.091964
22	0	1	0	0.088490	3.005635	-0.503476	0.895898	-0.000000	1	200280	5.869672
-11	1	1	0	0.221877	2.298542	-0.179858	1.116046	0.000511	1	200283	5.092814
11	-1	1	0	0.106787	2.298197	-0.173658	0.536958	0.000511	1	200284	5.090189
2212	1	1	0	0.113702	0.659060	-0.340429	0.948557	0.938272	1	200285	3.709422
1000020040	0	1	0	0.654383	0.579862	-0.641308	3.805579	3.727379	1	200286	3.821630
1000010020	0	1	6	0.332482	1.353749	2.884613	1.997336	1.875613	1	200287	3.958636
2112	0	1	0	0.186356	-0.473477	0.666582	0.962235	0.939565	1	200288	2.218607
2112	0	1	0	0.259503	-0.917681	2.698249	1.012252	0.939565	1	200289	1.802112
211	1	1	0	0.302496	1.132440	-0.070276	0.536566	0.139570	1	200290	3.983592
111	0	1	0	0.243622	0.929015	2.753033	0.381230	0.134977	1	200291	3.513988
-211	-1	1	0	0.081066	1.895621	-2.465765	0.309198	0.139570	1	200292	6.015097
2112	0	1	0	0.083824	-1.084210	-2.685897	0.949662	0.939565	1	200293	4.602247
2212	1	1	0	0.249890	-0.305019	2.795632	0.974059	0.938272	1	200294	2.382204
2112	0	1	0	0.208385	2.771469	0.629748	1.917676	0.939565	1	200295	5.312021
211	1	1	4	0.324430	0.767059	-0.023528	0.446994	0.139570	1	200296	3.638078
111	0	1	0	0.228367	1.623692	-1.119428	0.616583	0.134977	1	200297	4.945407
111	0	1	2	0.445016	2.730602	-1.722675	3.430905	0.134977	1	200298	6.199780
211	1	1	0	0.706015	1.883941	2.561087	2.380322	0.139570	1	200299	4.394395
-211	-1	1	5	0.435272	2.361475	0.035238	2.333071	0.139570	1	200300	5.076071
111	0	1	0	0.853464	3.554395	2.668928	14.934212	0.134977	1	200301	6.058228
211	1	1	0	1.180041	2.646414	0.840933	8.364274	0.139570	1	200302	5.149621
1000070130	0	1	0	0.108046	1.923786	-0.158893	12.117083	12.111193	1	200303	4.738700
2212	1	1	0	0.111273	-0.066804	-2.150595	0.944876	0.938272	1	200304	4.530464
2112	0	1	0	0.169552	-0.062971	-2.254369	0.954801	0.939565	1	200305	4.621301
2212	1	1	0	0.153097	0.677092	2.252093	0.957227	0.938272	1	200306	3.151447
2112	0	1	0	0.192663	0.151061	2.268071	0.959560	0.939565	1	200307	2.637913
2112	0	1	0	0.065753	1.017735	1.889186	0.945178	0.939565	1	200308	3.450468
1000120260	0	1	0	0.139616	-0.784629	-0.471124	24.197220	24.196516	1	200331	2.735691
22	0	1	0	0.000240	0.124611	1.726087	0.000242	0.000000	1	200332	2.553000
2212	1	1	0	0.074875	0.591588	-1.987311	0.942424	0.938272	1	200333	4.778317
211	1	1	0	0.206555	1.292231	0.129190	0.427797	0.139570	1	200334	4.044727
22	0	1	0	0.224883	2.978349	-1.774988	2.215795	-0.000000	1	200337	6.435634
22	0	1	0	0.220755	2.390330	-1.669382	1.215110	0.000000	1	200338	5.888847
1000070150	0	1	0	0.367188	-0.103183	-1.925396	13.973871	13.968994	1	200343	4.320179
22	0	1	0	0.000279	2.341550	2.850836	0.001463	-0.000000	1	200344	4.903130
22	0	1	0	0.007468	-0.650224	1.769670	0.009103	0.000000	1	200345	1.778963
2212	1	1	0	0.161788	0.682333	0.302640	0.959546	0.938272	1	200346	3.416600
-211	-1	1	0	0.556054	2.085372	0.781059	2.276278	0.139570	1	200347	4.609487
-11	1	1	0	0.402419	3.509236	0.663800	6.730992	0.000511	1	200352	6.030058
11	-1	1	2	1.029466	3.510158	0.665331	17.235031	0.000511	1	200353	6.030699
-11	1	1	0	0.229378	4.566860	1.769839	11.039042	0.000511	1	200354	6.995437
11	-1	1	0	0.242666	4.565689	1.766813	11.664845	0.000511	1	200355	6.994244
-11	1	1	0	0.114909	-3.006649	1.951685	1.164540	0.000511	1	200356	0.624584
11	-1	1	0	0.087095	-3.004373	1.963194	0.880665	0.000511	1	200357	0.626931
-11	1	1	0	0.090318	-4.255079	1.779698	3.182657	0.000511	1	200358	1.827833
11	-1	1	0	0.287151	-4.256435	1.779829	10.132435	0.000511	1	200359	1.829193
-11	1	1	0	0.414333	-3.732949	2.473995	8.664966	0.000511	1	200360	1.508962
11	-1	1	0	0.011147	-3.741654	2.482441	0.235153	0.000511	1	200361	1.520736
-11	1	1	2	1.855634	3.790042	0.710681	41.084538	0.000511	1	200362	6.299100
11	-1	1	0	0.363196	3.789018	0.712757	8.033090	0.000511	1	200363	6.297757
-11	1	1	2	1.143362	3.656717	0.787079	22.158249	0.000511	1	200364	6.155531
11	-1	1	2	1.008669	3.656723	0.789694	19.548029	0.000511	1	200365	6.155143
-11	1	1	0	0.164290	0.925351	-0.318341	0.239794	0.000511	1	200366	3.922332
11	-1	1	0	0.107354	0.930895	-0.329438	0.157328	0.000511	1	200367	3.932832
211	1	1	0	0.457780	-0.788070	-1.508111	0.623272	0.139570	1	200368	3.617103
-211	-1	1	6	0.213531	-1.392412	-0.271375	0.477082	0.139570	1	200369	2.240895
1000110240	0	1	0	0.485970	-0.817040	0.164956	22.351589	22.341921	1	200370	2.236322
22	0	1	0	0.005272	-0.480337	-2.632885	0.005892	0.000000	1	200371	4.764964
2212	1	1	0	0.124594	-0.304529	3.010347	0.947292	0.938272	1	200372	2.487336
2112	0	1	0	0.072963	1.451566	-0.782384	0.953825	0.939565	1	200373	4.614567

Continued on next page

pdgId	q	nP	nC	p_T (GeV)	η	ϕ	Energy (GeV)	mass (GeV)	status	barcode	ΔR
2212	1	1	0	0.029100	2.610887	-0.315424	0.959166	0.938272	1	200374	5.433184
-211	-1	1	0	0.233963	-0.932650	-2.931221	0.370597	0.139570	1	200375	4.881691
22	0	1	0	0.140313	3.664064	0.783544	2.739286	0.000000	1	200376	6.163328
22	0	1	0	0.174048	3.508136	0.700459	2.907983	-0.000000	1	200381	6.022687
22	0	1	0	0.729979	3.659950	0.794653	14.192666	-0.000000	1	200382	6.157590
22	0	1	0	0.198533	3.789893	0.711096	4.394956	0.000000	1	200383	6.298886
22	0	1	0	0.115073	3.790390	0.689224	2.548641	0.000000	1	200384	6.302901
-11	1	1	0	0.122033	-2.927844	-1.054505	1.143494	0.000511	1	200388	2.814858
11	-1	1	0	0.024403	-2.946064	-1.041438	0.232845	0.000511	1	200389	2.805305
-11	1	1	0	0.460032	-4.362314	-2.539283	18.045025	0.000511	1	200390	4.673853
11	-1	1	0	0.046553	-4.355414	-2.542734	1.813508	0.000511	1	200391	4.674146
-11	1	1	0	0.016550	5.435020	-1.102766	1.897463	0.000511	1	200392	8.353235
11	-1	1	0	0.166912	5.360578	-1.149609	17.763786	0.000511	1	200393	8.299252
-11	1	1	0	0.258347	-0.143825	-1.529597	0.261024	0.000511	1	200394	3.968751
11	-1	1	0	0.150202	-0.150107	-1.517514	0.151899	0.000511	1	200395	3.955255
2112	0	1	0	0.269210	1.811353	-2.743918	1.264055	0.939565	1	200396	6.153315
111	0	1	0	0.158916	1.167849	-2.184965	0.310994	0.134977	1	200397	5.305454
-11	1	1	0	0.465611	3.173606	-2.620467	5.572283	0.000511	1	200400	7.084089
11	-1	1	0	0.011172	3.177189	-2.665885	0.134180	0.000511	1	200401	7.114802
-11	1	1	0	0.116028	2.100452	-1.002190	0.481066	0.000511	1	200402	5.281766
11	-1	1	0	0.072276	2.100512	-0.999309	0.299685	0.000511	1	200403	5.280335
-11	1	1	2	0.313295	1.843380	-2.945724	1.014470	0.000511	1	200404	6.322702
11	-1	1	0	0.254817	1.839225	-2.950174	0.821861	0.000511	1	200405	6.323178
1000020040	0	1	0	0.070531	0.420523	-0.751336	3.728236	3.727444	1	200406	3.768603
1000020040	0	1	0	0.241076	0.097492	2.994197	3.735241	3.727379	1	200407	2.831000
22	0	1	0	0.000193	-0.394562	1.436755	0.000208	-0.000000	1	200408	2.052843
22	0	1	0	0.001689	0.345907	2.845929	0.001791	0.000000	1	200409	2.995673
22	0	1	0	0.002766	0.312603	-1.285298	0.002903	0.000000	1	200410	4.064335
2212	1	1	0	0.092076	-0.098568	0.138005	0.942823	0.938272	1	200411	2.813723
2112	0	1	0	0.079502	-2.467343	-1.631961	1.051493	0.939565	1	200412	3.347872
2212	1	1	0	0.623114	0.949687	-1.001378	1.318179	0.938272	1	200413	4.335168
2212	1	1	0	0.734539	0.856879	2.068940	1.386732	0.938272	1	200414	3.304185
22	0	1	0	0.172386	1.980558	3.076128	0.636517	0.000000	1	200416	4.614047
1000010020	0	1	0	0.525406	0.316278	-1.761040	1.955127	1.875613	1	200422	4.429525
2212	1	1	0	0.114201	-1.518690	-1.313966	0.977249	0.938272	1	200423	3.163273
2112	0	1	0	0.983455	-0.421430	0.907925	1.425536	0.939565	1	200424	2.163394
2112	0	1	0	0.278957	0.943910	-2.247296	1.026222	0.939565	1	200425	5.203601
2112	0	1	0	0.864485	-1.269104	-0.284457	1.906820	0.939565	1	200426	2.311808
211	1	1	0	0.517997	-1.117674	-0.828141	0.887693	0.139570	1	200427	2.861636
2112	0	1	0	0.455817	-0.645508	-0.215773	1.090797	0.939565	1	200428	2.628520
2112	0	1	0	0.127975	-1.546571	-0.769188	0.990668	0.939565	1	200429	2.636694
2212	1	1	0	0.223286	-1.482101	2.662742	1.071201	0.938272	1	200430	1.338783
2212	1	1	0	0.107096	-1.364855	1.797573	0.964484	0.938272	1	200431	1.066660
-211	-1	1	0	0.171604	0.825995	-1.907520	0.272075	0.139570	1	200432	4.870163
2112	0	1	2	0.368045	0.101673	0.067131	1.009775	0.939565	1	200433	3.019741
2212	1	1	0	0.362240	-0.300216	2.578789	1.011809	0.938272	1	200434	2.296515
111	0	1	0	0.277690	-0.609988	2.543384	0.357439	0.134977	1	200435	1.997896
-211	-1	1	0	0.068031	-2.593523	0.589861	0.478378	0.139570	1	200436	1.137872
211	1	1	0	0.534273	-2.061007	-2.369675	2.136634	0.139570	1	200437	4.101843
1000020040	0	1	0	0.095688	-1.343897	1.352677	3.732547	3.727402	1	200452	1.143613
1000010020	0	1	0	0.129082	0.290710	1.156700	1.880435	1.875613	1	200453	2.775940
22	0	1	0	0.000552	-0.829706	1.574792	0.000754	-0.000000	1	200454	1.604858
22	0	1	0	0.001810	0.304378	-2.257268	0.001895	0.000000	1	200455	4.822058
2112	0	1	0	0.146328	0.141966	-1.458467	0.951120	0.939565	1	200456	4.084343
2112	0	1	0	0.194115	-0.602676	-1.992057	0.967414	0.939565	1	200457	4.132856
2212	1	1	0	0.188134	-1.029351	-2.095481	0.984133	0.938272	1	200458	4.059832
111	0	1	2	0.548386	-0.561988	1.234135	0.651425	0.134977	1	200459	1.927502
-211	-1	1	0	0.194723	-2.289013	-2.767370	0.980348	0.139570	1	200460	4.485220
22	0	1	0	0.209469	-0.710158	1.502318	0.264547	0.000000	1	200461	1.731406
22	0	1	2	0.350823	-0.449574	1.075253	0.386877	0.000000	1	200462	2.079850
-11	1	1	0	0.037654	-0.447639	1.074302	0.041493	0.000511	1	200465	2.081984
11	-1	1	0	0.313165	-0.449806	1.075367	0.345384	0.000511	1	200466	2.079594
-11	1	1	0	0.016102	-5.526841	-1.561804	2.023604	0.000511	1	200467	4.510262
11	-1	1	0	0.358190	-5.560695	-1.533415	46.566044	0.000511	1	200468	4.513106
-11	1	1	0	0.284637	-5.334707	-1.363359	29.519268	0.000511	1	200472	4.234067
11	-1	1	0	0.322692	-5.335834	-1.360533	33.503613	0.000511	1	200473	4.232786
1000060120	0	1	0	0.151588	0.412200	-1.280095	11.176076	11.174863	1	200480	4.128380
1000020040	0	1	0	0.041075	2.091675	-2.277896	3.731241	3.727417	1	200481	6.031540
1000020040	0	1	0	0.278288	0.114492	0.283676	3.737889	3.727379	1	200482	2.918353
22	0	1	0	0.000138	-1.827912	3.061045	0.000441	-0.000000	1	200483	1.473276

Continued on next page

pdgId	q	nP	nC	p_T (GeV)	η	ϕ	Energy (GeV)	mass (GeV)	status	barcode	ΔR
22	0	1	0	0.001023	-0.048240	0.408640	0.001024	0.000000	1	200484	2.715396
2112	0	1	0	0.107350	-0.967503	-2.599789	0.953368	0.939565	1	200485	4.556033
2112	0	1	0	0.249380	-0.395403	0.795991	0.977350	0.939565	1	200486	2.231318
1000290620	0	1	0	0.154077	-0.621572	-1.597536	57.675354	57.675060	1	200487	3.773849
22	0	1	0	0.000032	0.720369	-0.743709	0.000041	0.000000	1	200488	3.995392
22	0	1	0	0.000349	-0.000319	0.419669	0.000349	0.000000	1	200489	2.752285
22	0	1	0	0.000682	-0.906931	-0.127135	0.000982	0.000000	1	200490	2.389718
22	0	1	0	0.000447	1.355040	3.120734	0.000923	0.000000	1	200491	4.035881
22	0	1	0	0.000585	-0.209602	-2.307858	0.000598	0.000000	1	200492	4.594759
22	0	1	0	0.000092	2.768753	-1.468430	0.000734	-0.000000	1	200493	6.094969
22	0	1	0	0.001028	0.791990	1.917761	0.001368	0.000000	1	200494	3.226692
22	0	1	0	0.000433	-0.784443	-2.104903	0.000573	-0.000000	1	200495	4.159252
2112	0	1	0	0.050713	-1.118527	-0.906427	0.943482	0.939565	1	200496	2.931066
2112	0	1	0	0.266684	0.871011	2.470337	1.011416	0.939565	1	200497	3.384583
2112	0	1	2	0.533663	-2.162374	-1.767385	2.530804	0.939565	1	200498	3.493211
211	1	1	0	0.155330	-2.158871	2.027897	0.695792	0.139570	1	200499	0.412438
211	1	1	14	0.703893	-2.023399	-3.016523	2.712241	0.139570	1	200500	4.749504
-211	-1	1	0	0.221466	-1.958870	-0.835105	0.812928	0.139570	1	200501	2.593638
331	0	1	3	0.601086	-2.467153	-0.202437	3.694844	0.957780	1	200502	1.918514
111	0	1	2	0.943557	-2.658391	2.926422	6.768237	0.134977	1	200503	1.232395
-211	-1	1	0	0.273001	-2.024384	-0.937693	1.060757	0.139570	1	200504	2.683954
-321	-1	1	0	0.681686	-3.177622	0.490513	8.205770	0.493677	1	200505	1.436115
1000070150	0	1	0	0.069032	1.090506	-1.032177	13.969451	13.968984	1	200506	4.464663
1000020040	0	1	0	0.218035	1.352528	1.967294	3.754418	3.727379	1	200507	3.789258
22	0	1	0	0.000354	0.321564	1.978699	0.000372	0.000000	1	200508	2.762481
22	0	1	0	0.001544	0.156674	1.079015	0.001563	0.000000	1	200509	2.662290
2212	1	1	0	0.052013	0.503721	-0.458019	0.940110	0.938272	1	200510	3.649949
2212	1	1	0	0.049109	-0.703453	1.873596	0.940303	0.938272	1	200511	1.732127
2212	1	1	0	0.093642	-0.548371	2.009133	0.944476	0.938272	1	200512	1.902761
2212	1	1	0	0.199416	0.397733	1.559850	0.962679	0.938272	1	200513	2.830394
2112	0	1	0	0.253732	-0.722356	-0.452134	0.993490	0.939565	1	200514	2.758607
2212	1	1	0	0.244966	-0.903081	0.754111	1.002069	0.938272	1	200515	1.803087
2112	0	1	0	0.437358	-0.811570	-2.314046	1.109171	0.939565	1	200516	4.341977
2212	1	1	5	0.368217	-1.331926	2.547078	1.198735	0.938272	1	200517	1.376008
-211	-1	1	0	0.364528	-0.757721	-0.708278	0.494387	0.139570	1	200518	2.943918
111	0	1	2	0.757835	-1.303351	-2.915344	1.504018	0.134977	1	200519	4.765720
1000130270	0	1	0	0.392650	0.116446	-2.192684	25.129616	25.126507	1	200521	4.663842
1000060120	0	1	0	0.091918	0.284947	1.986003	11.175364	11.174954	1	200522	2.726747
22	0	1	0	0.000150	-0.141171	0.059378	0.000151	0.000000	1	200523	2.823937
22	0	1	0	0.000995	-1.590306	2.194039	0.002542	0.000000	1	200524	0.964972
22	0	1	0	0.002785	-1.360109	1.447450	0.005784	-0.000000	1	200525	1.101420
2212	1	1	0	0.231907	-1.697333	2.643775	1.143865	0.938272	1	200526	1.181424
22	0	1	0	0.120147	-1.500523	-2.562239	0.282770	-0.000000	1	200532	4.377388
22	0	1	0	0.646437	-1.250484	-2.979662	1.221249	0.000000	1	200533	4.840835
221	0	1	2	0.457255	-2.324608	-0.148839	2.422314	0.547853	1	200534	1.867408
-211	-1	1	11	0.153831	-2.071602	-1.446824	0.635721	0.139570	1	200535	3.182568
211	1	1	0	0.154105	-2.071619	0.702775	0.636809	0.139570	1	200536	1.073897
22	0	1	2	0.455005	-1.508290	0.148431	1.078426	-0.000000	1	200537	1.817368
22	0	1	0	0.135113	-2.987820	-1.554530	1.343889	0.000000	1	200538	3.317724
1000110230	0	1	0	0.582796	-0.165901	-1.877823	21.417383	21.409233	1	200539	4.246416
22	0	1	0	0.000209	0.123067	1.208268	0.000211	0.000000	1	200540	2.601401
22	0	1	0	0.000053	2.070904	-2.186750	0.000213	0.000000	1	200541	5.955874
22	0	1	0	0.000190	-0.900525	2.479200	0.000273	-0.000000	1	200542	1.707998
22	0	1	0	0.000923	0.214055	0.109381	0.000944	-0.000000	1	200543	3.092347
2112	0	1	0	0.057900	0.857750	-0.428911	0.943011	0.939565	1	200544	3.924010
2212	1	1	0	0.111509	-0.397589	1.802177	0.945970	0.938272	1	200545	2.032620
22	0	1	0	0.005021	-1.080913	1.934026	0.008251	-0.000000	1	200546	1.365030
2112	0	1	0	0.160052	0.002658	1.665352	0.953100	0.939565	1	200547	2.431546
2212	1	1	0	0.137040	-0.907572	-0.861249	0.958825	0.938272	1	200548	2.992224
-211	-1	1	0	0.343059	-0.863867	1.100103	0.499138	0.139570	1	200549	1.681250
-11	1	1	0	0.231674	-1.511707	0.147902	0.550806	0.000511	1	200550	1.816097
11	-1	1	0	0.223330	-1.504733	0.148980	0.527620	0.000511	1	200551	1.818699
22	0	1	0	0.241878	-2.837599	3.078835	2.072080	0.000000	1	200557	1.423253
22	0	1	2	0.705439	-2.583137	2.874342	4.696157	0.000000	1	200558	1.168949
-11	1	1	2	0.508562	-2.582764	2.874429	3.384289	0.000511	1	200562	1.168986
11	-1	1	0	0.196877	-2.584097	2.874118	1.311868	0.000511	1	200563	1.168854
22	0	1	2	0.436876	-2.576376	2.877866	2.888938	0.000000	1	200564	1.171568
-11	1	1	0	0.429093	-2.574608	2.878144	2.832515	0.000511	1	200565	1.171622
11	-1	1	0	0.007783	-2.669249	2.862525	0.056423	0.000511	1	200566	1.171864
-11	1	1	0	0.033020	-4.266478	-1.333903	1.176918	0.000511	1	200567	3.560707

Continued on next page

pdgId	q	nP	nC	p_T (GeV)	η	ϕ	Energy (GeV)	mass (GeV)	status	barcode	ΔR
11	-1	1	0	0.351635	-4.259884	-1.317554	12.450660	0.000511	1	200568	3.543301
1000040090	0	1	0	0.126593	-0.102003	-0.053103	8.393715	8.392750	1	200582	2.922428
1000020040	0	1	0	0.267747	-0.383567	-2.696060	3.738564	3.727479	1	200583	4.862581
1000020030	0	1	0	0.148751	0.672303	-2.513974	2.814390	2.808391	1	200584	5.244442
1000010020	0	1	0	0.124594	-1.129768	-0.426183	1.887661	1.875613	1	200585	2.504787
22	0	1	0	0.000077	0.614354	-1.222063	0.000092	0.000000	1	200586	4.229482
22	0	1	0	0.000656	-0.292646	0.485582	0.000684	-0.000000	1	200587	2.464642
2212	1	1	0	0.057616	0.494413	1.473465	0.940507	0.938272	1	200588	2.932801
2112	0	1	0	0.099691	-0.138245	1.840702	0.944941	0.939565	1	200589	2.293532
2112	0	1	0	0.282771	0.095641	-1.794006	0.981568	0.939565	1	200590	4.323025
-211	-1	1	0	0.321716	-3.003433	1.729839	3.253008	0.139570	1	200591	0.575240
2212	1	1	0	0.192467	-0.160017	2.670113	0.958308	0.938272	1	200592	2.460965
2212	1	1	0	0.232471	-0.314537	-2.768795	0.969496	0.938272	1	200593	4.957705
2212	1	1	0	0.268909	0.856042	-1.979704	1.009918	0.938272	1	200594	4.944010
2112	0	1	0	0.479353	-0.848996	0.678689	1.149786	0.939565	1	200595	1.889384
-11	1	1	0	0.135727	4.563300	0.936177	6.508778	0.000511	1	200603	7.034987
11	-1	1	0	0.028224	4.568602	0.950138	1.360660	0.000511	1	200604	7.038725
-11	1	1	0	0.396332	4.506886	1.391692	17.963774	0.000511	1	200605	6.942818
11	-1	1	0	0.148515	4.509423	1.387223	6.748568	0.000511	1	200606	6.945562
1000060120	0	1	0	0.105382	0.052522	0.045156	11.175362	11.174863	1	200607	2.990899
1000100200	0	1	0	0.377240	-0.106899	2.702732	18.621630	18.617764	1	200608	2.522594
2112	0	1	0	0.041904	-0.493471	-3.035477	0.940746	0.939565	1	200609	5.130045
2212	1	1	0	0.054204	-0.953825	2.802280	0.941744	0.938272	1	200610	1.831657
22	0	1	0	0.004565	-0.097298	-2.434666	0.004586	0.000000	1	200611	4.760178
2212	1	1	0	0.095532	-0.087436	2.147248	0.943160	0.938272	1	200612	2.380379
2112	0	1	0	0.191233	0.906790	0.348004	0.979093	0.939565	1	200613	3.604695
2212	1	1	0	0.283472	0.383565	0.221540	0.986470	0.938272	1	200614	3.184247
111	0	1	0	0.123434	-0.395970	2.612500	0.189661	0.134977	1	200615	2.221467
2112	0	1	7	0.110280	1.824402	1.823803	1.002888	0.939565	1	200616	4.254144
2112	0	1	0	0.293210	0.948251	-1.241720	1.035468	0.939565	1	200617	4.488629
-211	-1	1	20	0.217699	-0.100207	-1.523084	0.259519	0.139570	1	200618	3.988728
1000010020	0	1	0	0.129287	-0.416413	-1.161033	1.880880	1.875613	1	200619	3.510479
1000010020	0	1	0	0.116104	0.913276	0.555382	1.883121	1.875613	1	200620	3.537356
2112	0	1	0	0.087534	-1.032231	-1.074631	0.949713	0.939565	1	200621	3.120105
1000020040	0	1	0	0.305074	-0.431037	-1.901832	3.742301	3.727379	1	200622	4.132282
2112	0	1	0	0.189610	0.222690	1.419588	0.959452	0.939565	1	200623	2.667542
1000010020	0	1	0	0.264794	0.487684	2.046377	1.898968	1.875613	1	200624	2.934743
22	0	1	0	0.000073	-0.029192	-2.064469	0.000073	0.000000	1	200625	4.477232
22	0	1	0	0.000007	-1.267595	1.885051	0.000014	-0.000000	1	200626	1.173064
22	0	1	0	0.000004	0.486790	1.229621	0.000005	0.000000	1	200627	2.955402
22	0	1	0	0.000002	-0.310840	0.353885	0.000002	0.000000	1	200628	2.517622
22	0	1	0	0.000001	-0.458318	0.759776	0.000001	0.000000	1	200629	2.189716
22	0	1	0	0.000001	0.507918	-1.797922	0.000001	0.000000	1	200630	4.578996
22	0	1	0	0.000000	0.522673	2.451628	0.000000	-0.000000	1	200631	3.041423
11	-1	1	0	0.000018	-0.291619	-0.684938	0.000511	0.000511	1	200632	3.213827
11	-1	1	0	0.000015	-0.247265	-3.018216	0.000511	0.000511	1	200633	5.212199
11	-1	1	0	0.000004	1.811206	-2.181521	0.000511	0.000511	1	200634	5.758663
11	-1	1	0	0.000008	-0.906590	-1.476118	0.000511	0.000511	1	200635	3.536016
22	0	1	0	0.000000	1.410523	-0.143507	0.000000	0.000000	1	200636	4.265405
11	-1	1	0	0.000004	-1.597153	-2.051730	0.000511	0.000511	1	200637	3.858022
11	-1	1	0	0.000022	0.340357	2.319493	0.000512	0.000511	1	200638	2.833800
1000120250	0	1	0	0.401247	0.774092	1.499088	23.274012	23.268032	1	200645	3.209776
22	0	1	0	0.000067	1.592216	0.398645	0.000172	0.000000	1	200646	4.230802
22	0	1	0	0.000181	-0.405854	-1.333300	0.000196	0.000000	1	200647	3.658807
2112	0	1	0	0.020036	0.609540	1.306004	0.939869	0.939565	1	200648	3.065407
22	0	1	0	0.000676	-0.922087	-0.546832	0.000984	0.000000	1	200649	2.718062
2112	0	1	0	0.107149	-0.220508	-1.154726	0.945955	0.939565	1	200650	3.621312
2212	1	1	0	0.238876	0.007652	-2.028632	0.968204	0.938272	1	200651	4.467001
1000020040	0	1	0	0.353737	-0.010641	1.067600	3.744128	3.727379	1	200658	2.503081
1000010030	0	1	0	0.271165	0.345038	-1.793870	2.823592	2.808921	1	200659	4.473114
2212	1	1	0	0.163399	-1.273383	3.024062	0.989664	0.938272	1	200660	1.745234
2112	0	1	2	0.281613	1.108274	0.541311	1.051911	0.939565	1	200661	3.726525
211	1	1	12	0.388294	3.883432	1.330320	9.438767	0.139570	1	200662	6.323553
1000010030	0	1	0	0.174777	-1.366302	-0.204805	2.832526	2.808921	1	200663	2.194599
1000010020	0	1	0	0.163443	1.119929	1.602761	1.895974	1.875613	1	200664	3.550093
1000010020	0	1	0	0.646409	0.761441	2.566020	2.056362	1.875613	1	200665	3.301205
2112	0	1	0	0.493669	0.739601	-1.190480	1.133999	0.939565	1	200666	4.299048
211	1	1	0	0.216663	1.124892	2.259048	0.394348	0.139570	1	200667	3.594565
-211	-1	1	0	0.363179	2.882930	-2.958143	3.257532	0.139570	1	200668	7.074923
2212	1	1	0	0.021045	-2.988327	0.910169	0.961360	0.938272	1	200669	0.981025

Continued on next page

pdgId	q	nP	nC	p_T (GeV)	η	ϕ	Energy (GeV)	mass (GeV)	status	barcode	ΔR
2212	1	1	0	0.214357	0.374962	1.774347	0.965957	0.938272	1	200670	2.803943
2212	1	1	0	0.065324	-1.839536	2.907001	0.961650	0.938272	1	200671	1.328894
2112	0	1	0	0.219134	2.120036	-0.791757	1.319189	0.939565	1	200672	5.193769
221	0	1	3	0.558751	1.114327	-0.159345	1.090657	0.547853	1	200673	4.008294
211	1	1	0	0.438334	2.826175	1.633350	3.715314	0.139570	1	200674	5.255188
111	0	1	0	0.191123	1.028318	-0.334904	0.330241	0.134977	1	200680	4.019153
111	0	1	0	0.135867	0.346416	-0.598318	0.197443	0.134977	1	200681	3.613036
111	0	1	0	0.263819	1.357397	0.193332	0.562973	0.134977	1	200682	4.080389
13	-1	1	0	0.169458	2.391757	0.650642	0.940023	0.105658	1	200691	4.936387
-14	0	1	0	0.008420	0.372051	0.942053	0.009010	0.000000	1	200692	2.905314
-11	1	1	0	0.033205	2.134869	0.113241	0.142352	0.000511	1	200693	4.836420
11	-1	1	0	0.148943	2.218708	0.096243	0.692895	0.000511	1	200694	4.921169
-11	1	1	2	0.353162	1.929912	1.331749	1.242084	0.000511	1	200696	4.375158
11	-1	1	0	0.032933	1.993060	1.301530	0.123074	0.000511	1	200697	4.440782
-11	1	1	0	0.091989	1.565549	1.389236	0.229709	0.000511	1	200698	4.007236
11	-1	1	0	0.250517	1.573128	1.388311	0.629938	0.000511	1	200699	4.014865
22	0	1	0	0.171376	1.924148	1.416808	0.599415	0.000000	1	200700	4.362765
2112	0	1	0	0.066862	-0.121304	-1.811280	0.941976	0.939565	1	200701	4.214501
2112	0	1	0	0.040504	-1.434845	1.548733	0.943853	0.939565	1	200702	1.007452
1000020040	0	1	0	0.160078	0.671482	-1.829283	3.732610	3.727379	1	200703	4.709125
1000020040	0	1	0	0.102028	-1.331661	0.726618	3.733104	3.727379	1	200704	1.476827
2112	0	1	0	0.245100	0.156735	-2.666833	0.971774	0.939565	1	200705	5.088145
2212	1	1	0	0.298354	0.372601	0.846534	0.991116	0.938272	1	200706	2.932720
22	0	1	0	0.000042	1.162715	-0.900294	0.000073	0.000000	1	200707	4.442884
22	0	1	0	0.000014	-0.061104	-2.156863	0.000014	0.000000	1	200708	4.538784
22	0	1	0	0.000003	-1.158733	-1.514267	0.000005	0.000000	1	200709	3.470527
22	0	1	0	0.000002	-0.769322	-1.342057	0.000002	-0.000000	1	200710	3.478824
22	0	1	0	0.000001	-0.797762	-0.574849	0.000001	-0.000000	1	200711	2.811658
22	0	1	0	0.000001	0.858584	-2.480356	0.000001	0.000000	1	200712	5.330179
22	0	1	0	0.000000	-0.411737	-0.485860	0.000000	-0.000000	1	200713	2.985565
22	0	1	0	0.000000	0.118289	-1.623960	0.000000	-0.000000	1	200714	4.199843
11	-1	1	0	0.000015	0.314665	-2.372756	0.000511	0.000511	1	200715	4.923370
11	-1	1	0	0.000011	0.629347	2.870375	0.000511	0.000511	1	200716	3.268475
11	-1	1	0	0.000002	-2.450648	1.680389	0.000511	0.000511	1	200717	0.041739
11	-1	1	0	0.000006	-1.160959	-3.055627	0.000511	0.000511	1	200718	4.936774
11	-1	1	0	0.000005	-1.332934	-1.829081	0.000511	0.000511	1	200719	3.710167
11	-1	1	0	0.000015	0.974988	-0.129137	0.000512	0.000511	1	200720	3.871201
1000080160	0	1	0	0.092053	0.582534	-1.660500	14.895473	14.895082	1	200727	4.523732
-11	1	1	0	0.205461	-2.414455	0.264940	1.158089	0.000511	1	200728	1.450811
11	-1	1	0	0.043432	-2.518425	0.232513	0.271222	0.000511	1	200729	1.485903
-11	1	1	0	0.078265	-1.823305	-1.838512	0.248639	0.000511	1	200730	3.605331
11	-1	1	0	0.254144	-1.827205	-1.841654	0.810384	0.000511	1	200731	3.607777
-11	1	1	0	0.109004	-2.184423	2.075044	0.490414	0.000511	1	200732	0.434337
11	-1	1	0	0.019974	-2.104428	2.098831	0.083136	0.000511	1	200733	0.501735
1000070160	0	1	0	0.009430	-2.639489	-0.020876	14.906160	14.906013	1	200734	1.749347
22	0	1	0	0.000271	0.949957	-2.805512	0.000403	0.000000	1	200735	5.643961
22	0	1	0	0.001232	-0.584450	2.083792	0.001448	0.000000	1	200736	1.880302
1000020040	0	1	0	0.182839	0.277828	-1.234087	3.732215	3.727379	1	200737	4.003079
2112	0	1	0	0.047504	-1.300591	-2.721168	0.944223	0.939565	1	200738	4.577940
1000010020	0	1	0	0.135191	-0.269400	2.164487	1.880840	1.875613	1	200739	2.205122
2212	1	1	0	0.060182	0.576126	-2.925773	0.940913	0.938272	1	200740	5.529024
2212	1	1	0	0.065132	-0.302592	-0.344483	0.940743	0.938272	1	200741	2.960272
2212	1	1	0	0.162789	-0.451244	-2.648369	0.955315	0.938272	1	200742	4.791031
2112	0	1	7	0.542791	-1.647693	-2.112874	1.737994	0.939565	1	200743	3.907341
111	0	1	0	0.147027	-0.499929	2.062071	0.213785	0.134977	1	200744	1.959301
331	0	1	3	0.655744	-1.755375	0.181186	2.175762	0.957780	1	200745	1.675591
211	1	1	0	0.103242	-0.950874	1.067033	0.207496	0.139570	1	200746	1.613609
-211	-1	1	0	0.129944	-3.169895	-1.272790	1.555660	0.139570	1	200747	3.079097
211	1	1	12	0.660407	-1.763636	-0.477679	1.987787	0.139570	1	200748	2.291879
221	0	1	2	0.524876	-1.639767	0.499265	1.506652	0.547853	1	200751	1.449679
111	0	1	0	0.143836	-0.939218	-0.920379	0.251390	0.134977	1	200752	3.027606
111	0	1	0	0.098886	-2.062836	-0.189927	0.417720	0.134977	1	200753	1.940353
22	0	1	0	0.100645	-0.031219	-1.117945	0.100694	0.000000	1	200754	3.711574
22	0	1	2	0.539005	-1.612945	0.686886	1.405958	0.000000	1	200755	1.312760
-11	1	1	0	0.184292	-1.614625	0.685066	0.481460	0.000511	1	200759	1.313145
11	-1	1	2	0.354713	-1.612070	0.687832	0.924498	0.000511	1	200760	1.312563
22	0	1	0	0.138957	-1.619660	0.664624	0.364717	0.000000	1	200761	1.326173
1000060120	0	1	0	0.648715	-0.378310	2.922728	11.196527	11.174892	1	200762	2.379010
22	0	1	0	0.000162	-0.470359	2.826185	0.000180	-0.000000	1	200763	2.251001
22	0	1	0	0.000157	0.541499	2.614734	0.000181	0.000000	1	200764	3.102966

Continued on next page

pdgId	q	nP	nC	p_T (GeV)	η	ϕ	Energy (GeV)	mass (GeV)	status	barcode	ΔR
22	0	1	0	0.000758	0.448344	-2.294976	0.000835	0.000000	1	200765	4.935673
22	0	1	0	0.003472	0.549006	1.525557	0.004008	-0.000000	1	200766	2.983438
22	0	1	0	0.004267	-0.395173	0.369044	0.004604	-0.000000	1	200767	2.438713
2212	1	1	0	0.093920	-0.779663	1.645423	0.946423	0.938272	1	200768	1.650201
2212	1	1	0	0.248739	-0.391099	0.134438	0.975798	0.938272	1	200769	2.578916
2112	0	1	0	0.326576	-0.255554	-2.317844	0.998275	0.939565	1	200770	4.581536
211	1	1	0	0.365224	0.179901	-2.905796	0.396525	0.139570	1	200771	5.306708
-211	-1	1	0	0.466418	-0.947513	-0.186761	0.705865	0.139570	1	200772	2.410856
2212	1	1	0	0.939806	-0.816248	-0.336930	1.579534	0.938272	1	200773	2.610011
1000120260	0	1	0	0.017042	-1.164658	-1.169093	24.196615	24.196596	1	200774	3.149428
22	0	1	0	0.000119	-0.589651	2.630429	0.000141	0.000000	1	200775	2.053688
22	0	1	0	0.001950	-1.000371	-0.010611	0.003010	0.000000	1	200776	2.240373
22	0	1	0	0.002603	-0.921778	0.083624	0.003789	-0.000000	1	200777	2.221134
2212	1	1	0	0.325074	-1.077897	-1.085114	1.079058	0.938272	1	200778	3.109380
2112	0	1	0	0.286969	-1.521603	2.918432	1.164782	0.939565	1	200779	1.506262
111	0	1	0	0.278322	-0.885160	-2.196626	0.417107	0.134977	1	200780	4.205670
1000130270	0	1	0	0.121146	-0.019806	1.359054	25.126799	25.126507	1	200785	2.434821
2112	0	1	0	0.045260	-0.210051	1.958548	0.940704	0.939565	1	200786	2.231572
1000020040	0	1	0	0.148071	0.507414	2.817135	3.731143	3.727379	1	200787	3.135603
1000010020	0	1	0	0.354590	-0.657354	1.867976	1.925170	1.875613	1	200788	1.777549
1000010020	0	1	4	0.502641	0.572751	-0.360125	1.965431	1.875613	1	200789	3.649068
2212	1	1	0	0.218933	-0.017519	-2.068212	0.963484	0.938272	1	200790	4.486654
2112	0	1	0	0.179657	0.214213	2.655366	0.957373	0.939565	1	200791	2.804681
2112	0	1	0	0.087708	-3.379505	-0.078397	1.594995	0.939565	1	200792	2.030613
211	1	1	0	0.511924	-1.932397	1.339096	1.810137	0.139570	1	200793	0.622741
111	0	1	2	0.545321	-1.425484	-2.020833	1.207347	0.134977	1	200794	3.868764
130	0	1	0	0.358062	-4.346996	-1.423625	13.840698	0.497614	1	200795	3.679185
1000140280	0	1	0	0.211031	1.170010	-1.114078	26.055859	26.053194	1	200796	4.577759
22	0	1	0	0.001745	-0.218505	-1.532143	0.001787	-0.000000	1	200797	3.928342
22	0	1	0	0.008968	-0.830406	-3.063527	0.012242	-0.000000	1	200798	5.039280
2112	0	1	0	0.273282	-0.284389	0.228788	0.981667	0.939565	1	200799	2.609120
22	0	1	0	0.028573	-0.419147	-2.215793	0.031120	0.000000	1	200800	4.415142
22	0	1	0	0.517319	-1.462255	-2.010132	1.176227	0.000000	1	200801	3.849037
-11	1	1	0	0.159300	-3.559261	0.835471	2.800937	0.000511	1	200802	1.433072
11	-1	1	0	0.074098	-3.611926	0.822415	1.373190	0.000511	1	200803	1.482816
-11	1	1	0	0.077169	5.860746	0.139748	13.542648	0.000511	1	200804	8.437594
11	-1	1	0	0.139940	5.844290	0.133034	24.157913	0.000511	1	200805	8.422686
2212	1	1	0	0.096774	0.417018	-0.465349	0.944164	0.938272	1	200806	3.585126
1000020040	0	1	0	0.325788	-0.146740	-0.907983	3.741897	3.727379	1	200807	3.476989
1000020030	0	1	0	0.519801	0.206858	1.399954	2.858143	2.808391	1	200808	2.654072
2112	0	1	0	0.126358	-0.429807	-2.882237	0.949676	0.939565	1	200809	5.013495
1000020040	0	1	0	0.422216	-0.272339	3.127384	3.753022	3.727379	1	200810	2.577083
1000010020	0	1	0	0.244540	1.053978	-2.564290	1.916429	1.875613	1	200811	5.517690
1000010020	0	1	0	0.168240	1.130497	-0.649110	1.897549	1.875613	1	200812	4.272911
1000020040	0	1	0	0.183736	-0.757031	0.527784	3.735030	3.727379	1	200813	2.050481
2212	1	1	0	0.164255	-0.973088	-3.005409	0.970584	0.938272	1	200814	4.940299
1000020030	0	1	0	0.361343	0.191314	-0.672302	2.832396	2.808391	1	200815	3.544744
2212	1	1	0	0.105202	0.998574	-2.388087	0.952182	0.938272	1	200816	5.346482
2212	1	1	0	0.087573	0.131113	0.086340	0.942420	0.938272	1	200817	3.034090
2112	0	1	0	0.125826	0.943607	0.650470	0.957823	0.939565	1	200818	3.536226
2212	1	1	0	0.099371	-0.390589	-3.073841	0.944359	0.938272	1	200819	5.205006
2212	1	1	0	0.087351	1.406024	-1.185289	0.957096	0.938272	1	200820	4.808140
2112	0	1	0	0.207502	0.348002	-0.121100	0.965022	0.939565	1	200821	3.328965
2112	0	1	0	0.185402	-0.549240	-3.042562	0.963645	0.939565	1	200822	5.115860
2212	1	1	0	0.222571	0.561902	-2.286228	0.973268	0.938272	1	200823	4.995700
1000010030	0	1	0	0.576100	-0.396762	2.263693	2.876973	2.808921	1	200824	2.104218
2212	1	1	0	0.322298	1.183126	0.432256	1.100677	0.938272	1	200825	3.832763
2112	0	1	0	0.183209	0.597528	-0.557301	0.964276	0.939565	1	200826	3.784509
211	1	1	0	0.459807	2.108509	1.619232	1.926452	0.139570	1	200827	4.537902
111	0	1	2	0.487287	1.916935	-0.108331	1.697999	0.134977	1	200828	4.712610
2112	0	1	0	0.347805	-0.183771	-0.037230	1.003934	0.939565	1	200829	2.847969
2112	0	1	0	0.224131	1.361510	-2.967192	1.048784	0.939565	1	200830	6.024326
2112	0	1	0	0.183542	0.487605	0.764085	0.961840	0.939565	1	200831	3.067318
2112	0	1	0	0.258161	0.701025	-2.462296	0.993938	0.939565	1	200832	5.220021
2212	1	1	0	0.423078	0.188341	-1.952367	1.032364	0.938272	1	200833	4.505748
2112	0	1	0	0.242705	1.173866	1.207538	1.033300	0.939565	1	200834	3.637898
-211	-1	1	0	0.155887	-0.782390	2.850912	0.248898	0.139570	1	200835	1.999496
2112	0	1	0	0.206593	-0.740241	-1.032476	0.976446	0.939565	1	200836	3.225237
2212	1	1	0	0.095510	2.639251	1.579901	1.154160	0.938272	1	200837	5.069438
-211	-1	1	0	0.533995	1.067793	-2.426286	0.879610	0.139570	1	200838	5.420245

Continued on next page

pdgId	q	nP	nC	p_T (GeV)	η	ϕ	Energy (GeV)	mass (GeV)	status	barcode	ΔR
111	0	1	2	0.335810	0.339502	1.838456	0.380121	0.134977	1	200839	2.770591
-211	-1	1	0	0.146299	1.971838	-1.808967	0.553562	0.139570	1	200840	5.637817
22	0	1	2	0.411612	1.900240	0.014886	1.407102	0.000000	1	200867	4.650759
22	0	1	0	0.093638	1.799709	-0.679085	0.290897	0.000000	1	200868	4.859172
-11	1	1	2	0.344046	1.898643	0.017079	1.174333	0.000511	1	200869	4.648471
11	-1	1	0	0.067570	1.908262	0.003721	0.232769	0.000511	1	200870	4.662314
22	0	1	0	0.123320	1.935604	-0.673013	0.436093	0.000000	1	200871	4.974950
1000120250	0	1	0	0.128082	-0.504409	1.729015	23.268572	23.268124	1	200873	1.924005
22	0	1	0	0.000916	0.230358	-0.177893	0.000940	0.000000	1	200874	3.264117
2212	1	1	0	0.065272	0.050600	1.253779	0.940545	0.938272	1	200875	2.521634
2112	0	1	0	0.344732	0.163322	2.709123	1.002408	0.939565	1	200876	2.775568
2112	0	1	2	0.458330	-0.232632	-0.582785	1.050916	0.939565	1	200877	3.178714
22	0	1	0	0.019692	1.442626	0.745645	0.043994	0.000000	1	200883	3.990685
22	0	1	0	0.327219	0.232812	1.891917	0.336127	0.000000	1	200884	2.667008
2212	1	1	3	0.339412	0.412097	-0.706973	1.008093	0.938272	1	200886	3.733297
1000040080	0	1	0	0.286406	0.207373	-0.750719	7.465276	7.459540	1	200888	3.609747
1000020040	0	1	0	0.223183	0.426051	2.363006	3.735340	3.727379	1	200889	2.926898
2212	1	1	0	0.244469	-0.119879	-0.752980	0.970043	0.938272	1	200890	3.379856
1000070130	0	1	0	0.339998	-0.068785	1.717284	12.115986	12.111193	1	200891	2.359583
2212	1	1	0	0.032537	1.369316	1.137406	0.940741	0.938272	1	200892	3.841459
2112	0	1	2	0.341349	0.528903	-0.973377	1.017375	0.939565	1	200893	3.997062
2112	0	1	5	0.227860	1.592780	0.272657	1.105961	0.939565	1	200894	4.272231
111	0	1	2	0.381124	0.659384	0.516562	0.486137	0.134977	1	200895	3.312417
211	1	1	6	0.559683	1.317211	0.097247	1.128278	0.139570	1	200896	4.080282
-211	-1	1	0	0.630966	0.405423	1.725613	0.697639	0.139570	1	200897	2.833808
111	0	1	2	0.485457	0.745307	1.067028	0.641019	0.134977	1	200898	3.239285
111	0	1	2	0.596237	1.483796	1.173317	1.388780	0.134977	1	200899	3.949581
211	1	1	0	1.715180	0.824383	0.866044	2.335942	0.139570	1	200900	3.361885
22	0	1	0	0.131300	0.634360	1.013885	0.158616	-0.000000	1	200901	3.142105
22	0	1	0	0.273012	0.621846	0.285060	0.327521	-0.000000	1	200902	3.369049
1000060110	0	1	0	0.049086	1.088342	0.083917	10.254416	10.254094	1	200903	3.876843
22	0	1	0	0.000758	-1.861870	2.791635	0.002497	-0.000000	1	200904	1.215972
22	0	1	0	0.005066	0.361317	-1.123091	0.005401	0.000000	1	200905	3.980074
211	1	1	9	0.181997	0.948783	-1.696246	0.304159	0.139570	1	200906	4.800668
111	0	1	2	0.303850	0.686671	2.827687	0.401700	0.134977	1	200907	3.307569
2112	0	1	0	0.810069	0.562824	0.044543	1.330323	0.939565	1	200908	3.426359
1000020040	0	1	0	0.225849	0.363099	-2.781519	3.735193	3.727417	1	200909	5.293121
1000020040	0	1	0	0.176865	0.523602	0.920500	3.732831	3.727379	1	200910	3.057195
22	0	1	0	0.000427	-0.276994	-1.194797	0.000443	0.000000	1	200911	3.619297
2112	0	1	0	0.072820	0.278280	-2.806172	0.942607	0.939565	1	200912	5.270022
22	0	1	0	0.006587	-0.106228	0.155095	0.006625	0.000000	1	200913	2.797816
22	0	1	0	0.005158	-1.555355	-3.108174	0.012760	0.000000	1	200914	4.902220
2212	1	1	0	0.141450	0.548051	-2.192363	0.952365	0.938272	1	200915	4.912424
2212	1	1	0	0.258603	0.304817	2.664017	0.976544	0.938272	1	200916	2.893032
2212	1	1	0	0.541054	-0.332350	0.251366	1.098470	0.938272	1	200917	2.556857
22	0	1	0	0.270743	0.649251	2.646406	0.329839	0.000000	1	200918	3.215273
22	0	1	0	0.061580	0.570098	-2.540337	0.071861	0.000000	1	200919	5.206200
22	0	1	0	0.059105	1.136658	1.692028	0.101579	-0.000000	1	200920	3.565104
22	0	1	2	0.438890	0.664607	0.988151	0.539440	0.000000	1	200921	3.177389
22	0	1	0	0.584478	1.462910	1.214170	1.329706	-0.000000	1	200922	3.923462
22	0	1	0	0.026829	1.426350	0.076548	0.059073	0.000000	1	200923	4.188749
-11	1	1	0	0.334895	0.662992	0.987666	0.411234	0.000511	1	200924	3.175928
11	-1	1	0	0.103992	0.669798	0.989713	0.128205	0.000511	1	200925	3.182085
1000240510	0	1	0	0.368543	-1.381662	0.987104	47.448921	47.442513	1	200926	1.275313
22	0	1	0	0.001322	0.455245	-2.295060	0.001461	-0.000000	1	200927	4.939767
22	0	1	0	0.000516	-1.175356	2.636451	0.000916	0.000000	1	200928	1.554944
22	0	1	0	0.001046	0.515033	-0.223765	0.001188	0.000000	1	200929	3.524921
2212	1	1	0	0.073886	0.371726	-1.085019	0.941596	0.938272	1	200930	3.960361
2112	0	1	0	0.115912	-0.018181	2.058552	0.946691	0.939565	1	200931	2.434452
1000020040	0	1	0	0.130690	1.547791	-2.791052	3.741183	3.727379	1	200932	6.010034
2112	0	1	0	0.053928	0.918514	-0.353045	0.942824	0.939565	1	200933	3.934623
2112	0	1	0	0.039444	0.541184	-0.647188	0.940660	0.939565	1	200934	3.794918
2112	0	1	0	0.123517	0.188934	2.586930	0.947940	0.939565	1	200935	2.758503
2212	1	1	0	0.366719	0.549804	-1.390387	1.029443	0.938272	1	200936	4.303160
2212	1	1	0	0.433200	1.140315	-2.191188	1.199145	0.938272	1	200937	5.291422
111	0	1	2	0.291258	0.838525	-0.858818	0.421966	0.134977	1	200938	4.159405
211	1	1	0	0.380590	2.012147	0.628248	1.455437	0.139570	1	200939	4.571727
-211	-1	1	0	0.634061	2.205028	2.244651	2.913922	0.139570	1	200940	4.663492
2212	1	1	0	0.188869	1.644441	-0.533028	1.066600	0.938272	1	200941	4.652363
111	0	1	2	0.296034	1.468014	1.582040	0.689915	0.134977	1	200942	3.898673

Continued on next page

pdgId	q	nP	nC	p_T (GeV)	η	ϕ	Energy (GeV)	mass (GeV)	status	barcode	ΔR
-211	-1	1	0	0.553232	2.513933	-0.259438	3.442379	0.139570	1	200943	5.322353
-211	-1	1	0	0.871781	3.206401	2.066440	10.780726	0.139570	1	200944	5.645675
22	0	1	0	0.015350	1.019288	1.836280	0.024038	0.000000	1	200945	3.449764
22	0	1	0	0.305175	0.761150	-0.880539	0.397927	-0.000000	1	200946	4.112590
22	0	1	0	0.013301	0.721235	-1.827870	0.016913	0.000000	1	200947	4.740968
22	0	1	2	0.308878	1.414563	1.570624	0.673003	-0.000000	1	200948	3.845668
-11	1	1	0	0.086125	1.408464	1.561906	0.186641	0.000511	1	200949	3.839912
11	-1	1	0	0.222756	1.416894	1.573994	0.486361	0.000511	1	200950	3.847871
1000070140	0	1	0	0.071897	-0.520379	0.132247	13.040461	13.040204	1	200953	2.479455
1000260540	0	1	0	0.044816	-0.722533	-0.184164	50.231304	50.231274	1	200954	2.553291
22	0	1	0	0.000173	1.230570	0.384366	0.000322	-0.000000	1	200955	3.893614
2112	0	1	0	0.021543	-1.301779	-0.964669	0.940527	0.939565	1	200956	2.907489
22	0	1	0	0.001099	-0.513865	-1.607991	0.001248	0.000000	1	200957	3.835640
2112	0	1	0	0.145357	0.363557	-1.617005	0.952276	0.939565	1	200958	4.347605
2112	0	1	0	0.139054	1.336886	-1.034857	0.981250	0.939565	1	200959	4.662898
1000050110	0	1	0	0.087965	-0.476472	-2.759254	10.253058	10.252589	1	200961	4.882107
22	0	1	0	0.000084	1.151799	-0.672054	0.000146	0.000000	1	200962	4.303358
22	0	1	0	0.003986	0.144041	0.813636	0.004027	0.000000	1	200963	2.725981
2212	1	1	0	0.032533	2.934064	2.911335	0.987138	0.938272	1	200964	5.494111
2112	0	1	0	0.340430	0.738487	0.249050	1.036454	0.939565	1	200965	3.489984
2212	1	1	0	0.442924	-0.121913	0.032533	1.038974	0.938272	1	200967	2.855299
1000020030	0	1	0	0.311833	0.977507	-1.009462	2.847955	2.808391	1	200974	4.361927
1000010030	0	1	0	0.511597	-0.321081	2.436118	2.860016	2.808921	1	200975	2.227035
2212	1	1	0	0.193198	-0.765233	2.766539	0.971674	0.938272	1	200976	1.967311
2112	0	1	0	0.579171	0.451161	-1.277063	1.136336	0.939565	1	200977	4.153098
2212	1	1	0	0.300828	0.138788	0.783164	0.986208	0.938272	1	200978	2.731278
2212	1	1	0	0.312482	1.487102	-0.384019	1.186697	0.938272	1	200979	4.442933
-211	-1	1	0	0.355133	0.733486	0.513315	0.475949	0.139570	1	200980	3.382751
2212	1	1	0	0.115166	0.929182	1.912235	0.953293	0.938272	1	200981	3.363298
2112	0	1	0	0.174150	1.566673	-1.099390	1.035515	0.939565	1	200982	4.887228
2112	0	1	0	0.119754	-0.562976	-2.392746	0.949827	0.939565	1	200983	4.512082
331	0	1	0	0.152949	4.553846	2.356591	7.328532	0.957780	1	200984	7.011567
221	0	1	2	0.722498	2.479003	2.423712	4.374200	0.547853	1	200985	4.958185
211	1	1	0	0.121681	4.006680	0.015564	3.348068	0.139570	1	200986	6.655843
111	0	1	2	0.369164	1.226734	-0.952228	0.696767	0.134977	1	200987	4.525210
-211	-1	1	16	0.223561	1.144223	1.817447	0.411013	0.139570	1	200988	3.574040
211	1	1	9	0.124358	2.221053	2.791018	0.596413	0.139570	1	200989	4.772154
221	0	1	0	0.468424	3.856992	-2.622183	11.102030	0.547853	1	200990	7.636939
22	0	1	0	0.264213	3.126693	2.201977	3.017614	0.000000	1	200995	5.576305
22	0	1	2	0.468372	1.725382	2.548093	1.356587	-0.000000	1	200996	4.236335
-11	1	1	0	0.088007	1.738748	2.545520	0.258123	0.000511	1	200999	4.248939
11	-1	1	2	0.380364	1.722264	2.548688	1.098464	0.000511	1	201000	4.233396
22	0	1	0	0.266778	1.360939	-1.087800	0.554402	0.000000	1	201001	4.713637
22	0	1	0	0.110861	0.737076	-0.620957	0.142364	0.000000	1	201002	3.934454
1000040090	0	1	0	0.596509	-0.103820	2.328396	8.414169	8.392769	1	201003	2.403942
1000010020	0	1	0	0.098033	-1.004740	0.368875	1.881748	1.875613	1	201004	1.959748
1000020040	0	1	0	0.210190	0.236566	1.085407	3.733638	3.727379	1	201005	2.738452
2212	1	1	0	0.037454	-0.390973	1.553119	0.939139	0.938272	1	201006	2.043870
22	0	1	0	0.001508	0.405695	3.086010	0.001634	-0.000000	1	201007	3.147968
2112	0	1	0	0.006366	3.042426	-1.110570	0.941941	0.939565	1	201008	6.157702
2212	1	1	0	0.093236	-0.475663	2.997266	0.944017	0.938272	1	201009	2.335703
2212	1	1	0	0.058889	1.175501	-2.344708	0.944071	0.938272	1	201010	5.429056
2112	0	1	0	0.079234	-0.945570	-2.666276	0.946868	0.939565	1	201011	4.626042
2112	0	1	0	0.059107	-1.567892	-1.717265	0.951137	0.939565	1	201012	3.539146
2212	1	1	0	0.120326	-0.767533	-1.772616	0.951406	0.938272	1	201013	3.863498
2212	1	1	0	0.143191	0.623594	-1.728819	0.953897	0.938272	1	201014	4.602073
2112	0	1	0	0.120868	1.283508	-3.010242	0.968476	0.939565	1	201015	6.009359
2112	0	1	0	0.202884	0.589345	0.821747	0.969523	0.939565	1	201016	3.147334
2112	0	1	0	0.216945	0.455703	-1.203389	0.969700	0.939565	1	201017	4.103517
2112	0	1	0	0.284268	0.450454	-0.760577	0.990519	0.939565	1	201018	3.797300
1000100220	0	1	0	0.203205	-0.231210	-2.547458	20.480808	20.479746	1	201019	4.796028
22	0	1	0	0.000412	0.766566	2.115231	0.000539	0.000000	1	201020	3.219820
22	0	1	0	0.001190	-0.009500	1.434982	0.001190	-0.000000	1	201021	2.435101
2112	0	1	0	0.049041	-0.683559	-0.025984	0.941540	0.939565	1	201022	2.465312
22	0	1	0	0.001675	-0.659863	2.813977	0.002053	0.000000	1	201023	2.081791
2212	1	1	0	0.082065	0.111625	-1.831410	0.941899	0.938272	1	201024	4.362733
2212	1	1	0	0.029941	1.785314	-0.815125	0.942748	0.938272	1	201025	4.915293
2212	1	1	0	0.574932	-0.392030	1.943687	1.124437	0.938272	1	201026	2.049063
2212	1	1	0	0.350595	1.506058	-0.746402	1.252223	0.938272	1	201027	4.641290
22	0	1	0	0.189644	1.705147	2.541952	0.538963	0.000000	1	201028	4.215289

Continued on next page

pdgId	q	nP	nC	p_T (GeV)	η	ϕ	Energy (GeV)	mass (GeV)	status	barcode	ΔR
-211	-1	0	9	0.064693	4.337215	-2.484225	2.478675	0.139570	1	201031	7.963187
1000270610	0	1	0	0.249857	-0.267829	2.621475	56.745098	56.744507	1	201035	2.342729
22	0	1	0	0.000286	-0.394363	2.363169	0.000308	0.000000	1	201036	2.134575
2112	0	1	0	0.077557	-0.030177	-2.155413	0.942764	0.939565	1	201037	4.553758
2212	1	1	0	0.058699	1.497017	2.191757	0.948324	0.938272	1	201038	3.954148
2212	1	1	0	0.296284	0.997690	-0.234844	1.043380	0.938272	1	201039	3.942389
-211	-1	1	0	0.160189	-0.982630	-0.693971	0.281055	0.139570	1	201040	2.810088
111	0	1	0	0.283938	-0.333775	-1.497678	0.328876	0.134977	1	201041	3.835755
-211	-1	1	0	0.141432	1.812293	3.098655	0.466036	0.139570	1	201042	4.460472
2212	1	1	0	0.387840	2.277399	1.790410	2.128783	0.938272	1	201043	4.706360
1000060120	0	1	0	0.058415	0.029818	-2.365630	11.175015	11.174863	1	201070	4.764431
1000120250	0	1	0	0.092099	0.809103	-3.128374	23.268377	23.268047	1	201071	5.826330
22	0	1	0	0.000068	0.809775	2.648956	0.000092	0.000000	1	201072	3.369950
22	0	1	0	0.000300	-0.881954	1.916646	0.000424	0.000000	1	201073	1.559417
22	0	1	0	0.000581	-1.466421	-1.032717	0.001327	0.000000	1	201074	2.911881
22	0	1	0	0.000898	-2.386080	-1.566259	0.004920	-0.000000	1	201075	3.282216
2112	0	1	0	0.967511	-0.168277	-0.802078	1.358535	0.939565	1	201076	3.383362
2112	0	1	2	0.710483	-0.974520	2.104401	1.428037	0.939565	1	201077	1.504917
1000060120	0	1	0	0.067280	-0.576625	-0.133741	11.175140	11.174863	1	201078	2.617121
1000190420	0	1	0	0.415651	0.819643	0.421489	39.082092	39.078033	1	201079	3.496357
22	0	1	0	0.000822	-0.219395	0.330147	0.000842	-0.000000	1	201080	2.607541
22	0	1	0	0.001720	-0.297496	0.994001	0.001796	0.000000	1	201081	2.249765
22	0	1	0	0.003076	0.409036	2.917561	0.003337	-0.000000	1	201082	3.081455
2112	0	1	0	0.015377	-0.793738	0.423005	0.939789	0.939565	1	201083	2.083995
1000010020	0	1	0	0.087746	-0.701200	-0.491912	1.878849	1.875613	1	201084	2.802961
2112	0	1	0	0.067656	-0.895046	2.509153	0.944520	0.939565	1	201085	1.726461
2112	0	1	0	0.047944	0.891904	-2.359654	0.942045	0.939565	1	201086	5.256671
2212	1	1	0	0.056313	1.734205	1.695054	0.952577	0.938272	1	201087	4.162624
1000010030	0	1	0	0.238207	0.024327	0.760577	2.819009	2.808921	1	201088	2.632098
2212	1	1	0	0.086064	-0.772137	0.835899	0.945054	0.938272	1	201089	1.875399
2112	0	1	0	0.144783	0.809272	-1.771175	0.959554	0.939565	1	201090	4.758203
1000010020	0	1	0	0.203141	-0.249528	2.791676	1.887277	1.875613	1	201091	2.430041
2212	1	1	0	0.181278	-0.479271	-0.755612	0.959875	0.938272	1	201092	3.147425
2112	0	1	0	0.332736	-0.168114	-1.989687	0.998326	0.939565	1	201093	4.340337
2112	0	1	0	0.158168	0.300460	1.901419	0.954006	0.939565	1	201094	2.735141
2212	1	1	0	0.279391	0.905117	1.816749	1.020710	0.938272	1	201095	3.335016
2212	1	1	0	0.374928	2.014230	-3.069044	1.710377	0.938272	1	201096	6.529188
-211	-1	1	0	0.255594	1.176250	1.492314	0.474739	0.139570	1	201097	3.611532
2212	1	1	0	0.240799	-0.169838	-2.706050	0.969550	0.938272	1	201098	4.965148
2112	0	1	0	0.111020	-1.170739	0.419078	0.959832	0.939565	1	201099	1.806327
2212	1	1	0	0.211857	0.383135	1.737870	0.965482	0.938272	1	201100	2.811591
211	1	1	10	0.364216	1.827907	0.797748	1.170493	0.139570	1	201101	4.354134
111	0	1	0	0.141999	3.192542	-3.125240	1.737021	0.134977	1	201102	7.418165
221	0	1	3	0.537411	0.609155	0.199684	0.842646	0.547853	1	201103	3.394820
211	1	1	0	0.193781	2.194711	2.548564	0.891608	0.139570	1	201104	4.697504
1000100210	0	1	0	0.211042	0.045841	-2.134027	19.551722	19.550581	1	201108	4.576242
22	0	1	0	0.001335	-0.913493	2.641608	0.001932	-0.000000	1	201109	1.775438
2212	1	1	0	0.079616	0.052517	-1.020596	0.941653	0.938272	1	201110	3.693510
2212	1	1	0	0.069106	0.631780	-0.326058	0.941968	0.938272	1	201111	3.678752
2212	1	1	0	0.024608	1.953670	1.195160	0.942441	0.938272	1	201112	4.412845
2112	0	1	0	0.461999	0.106767	0.041706	1.048174	0.939565	1	201113	3.037945
111	0	1	0	0.176977	-0.645287	0.520231	0.253959	0.134977	1	201114	2.146739
111	0	1	0	0.243074	0.298699	-0.384496	0.287635	0.134977	1	201115	3.442042
2212	1	1	0	0.548953	0.571529	3.048849	1.136369	0.938272	1	201116	3.282790
2112	0	1	0	0.332517	1.392075	1.622923	1.177790	0.939565	1	201117	3.821569
111	0	1	0	0.093895	1.250978	0.650104	0.222959	0.134977	1	201122	3.830541
111	0	1	0	0.106525	0.777577	0.916849	0.194747	0.134977	1	201123	3.303970
111	0	1	2	0.388747	0.269331	-0.089584	0.424939	0.134977	1	201124	3.246008
22	0	1	0	0.245731	0.340887	0.167511	0.260147	0.000000	1	201127	3.172635
22	0	1	0	0.163503	0.125502	-0.481705	0.164792	0.000000	1	201128	3.369090
1000130260	0	1	0	0.084164	0.579080	1.114622	24.200211	24.200010	1	201129	3.066923
22	0	1	0	0.000133	-1.344291	0.599628	0.000272	-0.000000	1	201130	1.555894
22	0	1	0	0.000742	0.220726	-2.999873	0.000761	0.000000	1	201131	5.408713
22	0	1	0	0.002454	-1.298969	-1.457010	0.004833	0.000000	1	201132	3.367719
2112	0	1	0	0.288162	0.503762	1.607024	0.994353	0.939565	1	201133	2.934142
-211	-1	1	8	0.785676	1.522315	-1.555936	1.891183	0.139570	1	201134	5.129463
1000050110	0	1	0	0.123763	0.594553	-2.434848	10.253665	10.252621	1	201135	5.134683
22	0	1	0	0.000364	0.541410	-0.610881	0.000419	-0.000000	1	201136	3.772597
22	0	1	0	0.000677	-0.669974	0.032219	0.000834	0.000000	1	201137	2.434338
22	0	1	0	0.003188	-0.873220	-0.316509	0.004483	0.000000	1	201138	2.558963

Continued on next page

pdgId	q	nP	nC	p_T (GeV)	η	ϕ	Energy (GeV)	mass (GeV)	status	barcode	ΔR
22	0	1	0	0.005120	-0.059370	-0.137125	0.005129	0.000000	1	201139	3.007499
211	1	1	0	0.068588	-1.723417	-1.662042	0.242486	0.139570	1	201140	3.450506
-211	-1	1	5	0.544431	0.272215	-1.997304	0.581719	0.139570	1	201141	4.591234
2112	0	1	0	0.449077	2.022933	-0.276836	1.966314	0.939565	1	201142	4.876906
1000060130	0	1	0	0.099043	0.466089	-1.025300	12.110044	12.109545	1	201143	3.986336
1000010020	0	1	0	0.120578	0.631786	-0.489004	1.881245	1.875613	1	201144	3.771630
22	0	1	0	0.000282	0.143058	0.989257	0.000285	0.000000	1	201145	2.672064
2212	1	1	0	0.051009	-0.625331	0.686289	0.940273	0.938272	1	201146	2.076198
-211	-1	1	0	0.515507	0.116124	-2.205586	0.537426	0.139570	1	201147	4.674484
1000040080	0	1	0	0.134618	-0.041679	-0.616495	7.456088	7.454870	1	201148	3.336966
1000020030	0	1	0	0.102660	-0.626981	2.261317	2.811106	2.808391	1	201149	1.882208
22	0	1	0	0.000837	-0.713986	-0.430673	0.001059	0.000000	1	201150	2.746990
211	1	1	0	0.173645	0.147155	2.051336	0.224255	0.139570	1	201151	2.597302
111	0	1	2	0.317762	-0.760915	0.457096	0.435712	0.134977	1	201152	2.089125
2112	0	1	0	0.469698	-1.640987	3.117842	1.569657	0.939565	1	201153	1.608109
111	0	1	2	0.581843	-1.192005	-0.395072	1.055197	0.134977	1	201154	2.446199
22	0	1	0	0.022858	0.380041	1.454012	0.024529	0.000000	1	201156	2.820573
22	0	1	2	0.305955	-0.807276	0.394312	0.411183	0.000000	1	201157	2.091403
22	0	1	0	0.034229	-0.744905	0.450297	0.044172	-0.000000	1	201158	2.106003
22	0	1	2	0.559720	-1.197112	-0.440844	1.011025	0.000000	1	201159	2.483265
1000100200	0	1	0	0.466739	-0.346046	2.238007	18.624311	18.617733	1	201160	2.146831
22	0	1	0	0.001237	0.706122	0.602975	0.001558	-0.000000	1	201161	3.326131
22	0	1	0	0.001015	1.596351	3.123826	0.002608	0.000000	1	201162	4.263945
22	0	1	0	0.002785	0.132160	1.632921	0.002810	-0.000000	1	201163	2.561864
2112	0	1	0	0.074191	1.066587	1.889959	0.947267	0.939565	1	201164	3.499297
2112	0	1	0	0.150212	-0.147204	1.870525	0.951756	0.939565	1	201165	2.286413
2112	0	1	0	0.068829	-0.429072	-0.255103	0.942575	0.939565	1	201166	2.807345
2112	0	1	0	0.054843	0.266929	-1.444083	0.941281	0.939565	1	201167	4.153162
2112	0	1	0	0.048950	-0.675966	-2.243976	0.941515	0.939565	1	201168	4.330107
2112	0	1	0	0.066682	-0.934947	1.543709	0.944664	0.939565	1	201169	1.503289
2212	1	1	0	0.153191	-0.766566	0.790615	0.959445	0.938272	1	201170	1.901931
1000020030	0	1	0	0.255874	-0.104606	0.435490	2.820151	2.808391	1	201171	2.653067
2112	0	1	0	0.049326	-1.641235	3.116424	0.948803	0.939565	1	201172	1.606752
2112	0	1	0	0.176206	0.018242	-0.215624	0.955951	0.939565	1	201173	3.117026
2212	1	1	0	0.286163	-0.048385	0.713968	0.981038	0.938272	1	201174	2.582199
1000010030	0	1	0	0.434611	-0.358171	-0.101620	2.846789	2.808921	1	201175	2.754688
2112	0	1	0	0.130699	-0.251734	2.306204	0.949195	0.939565	1	201176	2.255316
2212	1	1	0	0.129737	-0.960641	-2.413392	0.958189	0.938272	1	201177	4.382179
2112	0	1	0	0.077956	1.377129	-2.349414	0.953827	0.939565	1	201178	5.568378
1000010030	0	1	0	0.193743	0.107419	-2.001043	2.815672	2.808921	1	201179	4.499364
2212	1	1	0	0.180136	0.043624	-2.870212	0.955440	0.938272	1	201180	5.209721
1000010020	0	1	0	0.173094	1.034454	-1.705096	1.895560	1.875613	1	201181	4.867532
2112	0	1	0	0.157324	-1.132436	1.004478	0.977440	0.939565	1	201182	1.478260
2212	1	1	0	0.123176	1.256362	-1.673205	0.966979	0.938272	1	201183	5.006176
2212	1	1	0	0.221716	-0.597912	-1.831667	0.974312	0.938272	1	201184	3.991775
2112	0	1	0	0.304817	0.021453	-0.957186	0.987795	0.939565	1	201185	3.625722
2212	1	1	0	0.049329	2.819724	-0.748736	1.026015	0.938272	1	201186	5.797916
2112	0	1	7	0.459428	0.259167	1.759968	1.052785	0.939565	1	201187	2.687900
2212	1	1	5	0.413304	0.271816	1.459716	1.031557	0.938272	1	201188	2.712289
2112	0	1	0	0.455920	1.073801	-0.253815	1.199097	0.939565	1	201189	4.017974
2112	0	1	0	0.340062	0.693706	-1.558116	1.031307	0.939565	1	201190	4.523839
2212	1	1	0	0.331758	1.115287	-0.687934	1.092879	0.938272	1	201191	4.281924
2112	0	1	0	0.064790	-1.417323	-0.227195	0.950163	0.939565	1	201192	2.190203
2112	0	1	0	0.340446	0.728520	0.801360	1.035319	0.939565	1	201193	3.286628
2112	0	1	0	0.257594	0.176439	1.560162	0.975308	0.939565	1	201194	2.609445
2212	1	1	0	0.387638	-0.097455	0.927815	1.015898	0.938272	1	201195	2.460466
3112	-1	1	2	0.413507	0.410764	-1.661512	1.278821	1.197449	1	201196	4.412043
2112	0	1	0	0.224224	1.915365	1.291224	1.219664	0.939565	1	201197	4.364422
211	1	1	0	0.221546	0.563967	-1.620075	0.293088	0.139570	1	201198	4.481223
2212	1	1	0	0.406127	0.889131	0.792018	1.101763	0.938272	1	201199	3.443684
111	0	1	0	0.211061	0.184287	-1.349635	0.253565	0.134977	1	201200	4.027672
2112	0	1	0	0.415037	1.040147	-1.246097	1.148519	0.939565	1	201201	4.561002
2112	0	1	0	0.305348	-0.091430	-1.795064	0.988333	0.939565	1	201202	4.217420
2112	0	1	2	0.992378	1.078635	0.709674	1.879549	0.939565	1	201203	3.648441
211	1	1	0	0.504098	0.620146	-0.950445	0.620089	0.139570	1	201204	4.049899
111	0	1	2	0.512862	1.981503	2.855048	1.900210	0.134977	1	201205	4.554680
221	0	1	0	0.149949	4.185612	2.934540	4.959827	0.547853	1	201206	6.725350
211	1	1	0	0.187919	1.743198	2.249686	0.570800	0.139570	1	201207	4.205606
111	0	1	2	0.318847	2.509452	2.305810	1.978192	0.134977	1	201208	4.972958
-11	1	1	0	0.321704	-1.197555	-0.438574	0.581309	0.000511	1	201209	2.481074

Continued on next page

pdgId	q	nP	nC	p_T (GeV)	η	ϕ	Energy (GeV)	mass (GeV)	status	barcode	ΔR
11	-1	1	0	0.238017	-1.196507	-0.443912	0.429715	0.000511	1	201210	2.486230
-11	1	1	0	0.075435	-0.794933	0.408367	0.100552	0.000511	1	201212	2.092173
11	-1	1	0	0.230519	-0.811264	0.389712	0.310631	0.000511	1	201213	2.091226
1000120250	0	1	0	0.405142	-0.122786	0.760433	23.271677	23.268097	1	201214	2.495639
2112	0	1	0	0.017125	-0.527232	0.832218	0.939769	0.939565	1	201215	2.096384
22	0	1	0	0.000259	-1.092605	-0.441504	0.000429	0.000000	1	201216	2.537267
2212	1	1	0	0.124054	0.921663	1.155618	0.955491	0.938272	1	201217	3.396524
2212	1	1	0	0.236253	0.162345	-2.815755	0.968325	0.938272	1	201218	5.219745
1000240520	0	1	0	0.287587	0.957925	1.523482	48.372025	48.370113	1	201236	3.391743
2112	0	1	0	0.032709	1.303275	0.550119	0.941787	0.939565	1	201237	3.909438
2112	0	1	0	0.053949	-0.822199	2.382547	0.942415	0.939565	1	201238	1.739104
2212	1	1	0	0.086120	-0.457246	-1.846962	0.943097	0.938272	1	201239	4.071581
2112	0	1	0	0.106308	0.646711	0.764028	0.948424	0.939565	1	201240	3.218969
22	0	1	0	0.011222	-0.000649	2.261380	0.011222	0.000000	1	201241	2.488293
2212	1	1	0	0.174290	-1.118798	2.455641	0.983625	0.938272	1	201242	1.504164
2112	0	1	0	0.222203	0.924674	-2.153239	0.993913	0.939565	1	201244	5.119713
-211	-1	1	0	0.236543	-0.279458	-1.212550	0.282696	0.139570	1	201245	3.632130
22	0	1	2	0.365440	2.006620	3.015546	1.383660	0.000000	1	201267	4.621554
22	0	1	0	0.162945	1.821048	2.488485	0.516550	0.000000	1	201268	4.319115
-211	-1	0	12	0.109445	2.838455	2.840492	0.948695	0.139570	1	201270	5.385593
1000260540	0	1	0	0.614792	0.658835	0.842162	50.236835	50.231190	1	201272	3.208404
1000010020	0	1	0	0.204924	0.669741	-1.314439	1.892550	1.875613	1	201273	4.333582
2112	0	1	0	0.015748	0.742767	1.748122	0.939785	0.939565	1	201274	3.171301
2112	0	1	0	0.024839	-1.223873	0.734262	0.940685	0.939565	1	201275	1.553704
22	0	1	0	0.001102	-0.213668	-1.858985	0.001127	-0.000000	1	201276	4.205134
2112	0	1	0	0.065914	-0.499514	3.001431	0.942499	0.939565	1	201277	2.318107
2112	0	1	0	0.074265	-0.283027	-1.517294	0.942737	0.939565	1	201278	3.880030
2212	1	1	0	0.074828	-0.641200	-1.972222	0.942650	0.938272	1	201279	4.098125
2112	0	1	0	0.042185	-1.462109	3.116339	0.944447	0.939565	1	201280	1.701614
2112	0	1	0	0.141809	-0.172880	-2.492539	0.950526	0.939565	1	201281	4.774554
211	1	1	0	0.095208	0.288528	2.617223	0.171232	0.139570	1	201282	2.862568
-211	-1	1	0	0.280716	1.432217	-2.735695	0.636814	0.139570	1	201283	5.892274
1000060120	0	1	0	0.112001	-0.209476	1.930112	11.175449	11.174863	1	201288	2.229228
-11	1	1	0	0.069732	2.007927	3.018820	0.264361	0.000511	1	201289	4.623729
11	-1	1	0	0.295708	2.006310	3.014774	1.119300	0.000511	1	201290	4.621039
22	0	1	0	0.036857	2.963729	-2.896144	0.357917	-0.000000	1	201292	7.095327
22	0	1	2	0.303264	2.360018	2.198344	1.620275	0.000000	1	201293	4.812650
-11	1	1	0	0.022500	2.375623	2.178534	0.122069	0.000511	1	201294	4.826236
11	-1	1	0	0.280769	2.358740	2.199931	1.498206	0.000511	1	201295	4.811538
22	0	1	0	0.181144	2.115319	-3.040980	0.761966	-0.000000	1	201296	6.578066
22	0	1	0	2.489495	2.115614	-3.032917	10.474842	0.000000	1	201297	6.572441
22	0	1	0	0.523292	2.115732	-3.032872	2.202065	0.000000	1	201298	6.572490
22	0	1	0	6.284491	2.115851	-3.033030	26.448832	0.000000	1	201299	6.572687
22	0	1	2	0.619509	2.116013	-3.033140	2.607667	-0.000000	1	201300	6.572878
-11	1	1	0	0.146839	2.117902	-3.030602	0.619219	0.000511	1	201303	6.572351
11	-1	1	0	0.472670	2.115423	-3.033928	1.988448	0.000511	1	201304	6.573040
-11	1	1	2	0.938525	2.987815	-1.878300	9.334893	0.000511	1	201305	6.500135
11	-1	1	2	2.556091	2.988220	-1.878598	25.434004	0.000511	1	201306	6.500638
22	0	1	0	0.135015	2.989065	-1.853633	1.344573	0.000000	1	201307	6.487573
22	0	1	0	2.138770	2.989611	-1.851672	21.310982	-0.000000	1	201308	6.486951
22	0	1	0	0.528766	2.983256	-1.952573	5.235485	0.000000	1	201312	6.537720
22	0	1	0	0.121541	2.989517	-1.886916	1.210932	-0.000000	1	201313	6.506321
-11	1	1	0	0.104698	2.688446	-1.795577	0.773547	0.000511	1	201314	6.205702
11	-1	1	0	0.294657	2.693132	-1.801787	2.187173	0.000511	1	201315	6.213081
11	-1	1	2	30.268103	2.115320	-3.040978	127.320259	0.000511	1	1000022	6.578065
-211	-1	1	0	0.664521	-2.299830	-0.911500	3.349690	0.139570	1	1000129	2.630327
130	0	1	10	0.404365	-4.475102	-2.201821	17.761618	0.497614	1	1000164	4.419952
-211	-1	1	0	0.632795	3.264229	2.402403	8.290206	0.139570	1	1000193	5.733868
-211	-1	1	9	0.385252	-2.868657	-3.100707	3.406586	0.139570	1	1000206	4.836474
-211	-1	1	0	0.297208	-0.262522	-1.028106	0.337700	0.139570	1	1010045	3.495608
211	1	0	12	0.199973	0.648119	-2.065929	0.280633	0.139570	1	1200012	4.874974
2112	0	1	0	0.017199	-2.971405	-2.884416	0.954519	0.939565	1	1200032	4.632042
2212	1	1	5	0.450997	0.379559	-1.084022	1.055694	0.938272	1	1200040	3.965199
11	-1	1	2	1.063300	3.529295	0.680551	18.144821	0.000511	1	1200080	6.046921
11	-1	1	0	0.939296	3.526223	0.682261	15.979655	0.000511	1	1200081	6.043601
11	-1	1	2	1.249043	3.505083	0.670901	20.805468	0.000511	1	1200089	6.024733
11	-1	1	0	0.752230	3.503264	0.671919	12.507257	0.000511	1	1200090	6.022765
11	-1	1	0	1.150738	3.539823	0.685052	19.844381	0.000511	1	1200096	6.056525
-11	1	1	2	5.923036	3.526381	0.666953	100.780785	0.000511	1	1200099	6.046393
-11	1	1	0	1.501045	3.526544	0.665890	25.544497	0.000511	1	1200100	6.046738

Continued on next page

pdgId	q	nP	nC	p_T (GeV)	η	ϕ	Energy (GeV)	mass (GeV)	status	barcode	ΔR
11	-1	1	2	5.965547	3.526717	0.667516	101.538124	0.000511	1	1200101	6.046626
11	-1	1	2	4.298596	3.526527	0.667742	73.151497	0.000511	1	1200102	6.046400
11	-1	1	2	4.174295	3.526489	0.667878	71.033554	0.000511	1	1200103	6.046339
11	-1	1	2	3.983638	3.525446	0.668697	67.718575	0.000511	1	1200104	6.045170
11	-1	1	2	3.854995	3.525583	0.668556	65.540695	0.000511	1	1200105	6.045329
11	-1	1	2	3.572955	3.525583	0.668617	60.745617	0.000511	1	1200106	6.045319
11	-1	1	0	1.847492	3.526231	0.679507	31.430464	0.000511	1	1200107	6.044080
-11	1	1	2	1.641946	3.493486	0.624608	27.035337	0.000511	1	1200115	6.021528
11	-1	1	2	2.946420	3.496982	0.619618	48.683620	0.000511	1	1200116	6.025872
11	-1	1	0	1.592956	3.496930	0.621416	26.319004	0.000511	1	1200117	6.025494
-11	1	1	0	0.620445	3.517677	0.539586	10.465569	0.000511	1	1200119	6.061242
-11	1	1	0	0.852242	3.499162	0.623222	14.112247	0.000511	1	1200124	6.027361
-211	-1	1	0	0.253699	2.629167	0.359614	1.773071	0.139570	1	1200267	5.236180
11	-1	1	0	0.856675	3.508757	0.700205	14.322166	0.000511	1	1200353	6.023342
-11	1	1	2	1.657279	3.789897	0.711141	36.687572	0.000511	1	1200362	6.298883
-11	1	1	0	0.409466	3.658745	0.794572	7.951492	0.000511	1	1200364	6.156410
11	-1	1	0	0.828509	3.664294	0.784283	16.178381	0.000511	1	1200365	6.163443
-11	1	1	0	1.510606	3.789345	0.690334	33.422192	0.000511	1	1200366	6.301690
-11	1	1	0	0.042512	1.966316	3.073433	0.154836	0.000511	1	1200404	4.599644
2112	0	1	6	0.365646	-0.073187	0.483298	1.008562	0.939565	1	1200433	2.658130
2112	0	1	0	0.239205	-2.973936	-1.023347	2.527694	0.939565	1	1200498	2.792836
-11	1	1	0	0.063105	-2.560862	2.889466	0.410949	0.000511	1	1200562	1.181236
2112	0	1	0	0.344046	0.838145	0.759065	1.051519	0.939565	1	1200661	3.403707
-11	1	1	0	0.085138	1.917546	1.409670	0.295907	0.000511	1	1200696	4.356674
11	-1	1	0	0.171356	-1.619870	0.660599	0.449841	0.000511	1	1200760	1.329238
-211	-1	0	5	0.138962	-0.846335	-1.050027	0.237184	0.139570	1	1200835	3.186219
-11	1	1	0	0.038326	1.931136	-0.669446	0.134954	0.000511	1	1200869	4.969317
2112	0	1	0	0.128599	-1.423465	-0.249736	0.981095	0.939565	1	1200877	2.207421
2112	0	1	6	0.315706	0.671268	-1.178344	1.017118	0.939565	1	1200893	4.240654
11	-1	1	0	0.087772	1.694234	2.548464	0.246912	0.000511	1	1201000	4.205873
2112	0	1	0	0.753977	-0.892894	2.174549	1.427760	0.939565	1	1201077	1.602571
2112	0	1	0	0.959718	1.119935	0.599840	1.878963	0.939565	1	1201203	3.719618
11	-1	1	2	27.647930	2.115644	-3.032905	116.335266	0.000511	1	1201291	6.572453
11	-1	1	2	27.000269	2.115738	-3.032860	113.620476	0.000511	1	1201292	6.572486
11	-1	1	2	20.712973	2.115800	-3.032992	87.168007	0.000511	1	1201293	6.572624
11	-1	1	0	20.083214	2.116018	-3.033166	84.535652	0.000511	1	1201294	6.572901
-11	1	1	2	0.401858	2.984980	-1.957036	3.985752	0.000511	1	1201305	6.541651
11	-1	1	2	2.418354	2.989106	-1.853635	24.084681	0.000511	1	1201306	6.487608
11	-1	1	0	0.262982	2.985594	-1.851376	2.609935	0.000511	1	1201307	6.483433
-11	1	1	0	0.093984	2.984088	-1.893791	0.931335	0.000511	1	1201309	6.505612